POLITECNICO DI TORINO

Facoltà di Ingegneria
Corso di Laurea in Ingegneria Biomedica

Tesi di Laurea

A modular wearable device for vital signs monitoring in heavy industries

Relatore:
prof. Danilo Demarchi

Candidato:
Erika CONSOLI

ANNO ACCADEMICO 2019-2020

Abstract

This thesis deals with the design of a modular wearable prototype able to perform the monitoring of several physiological parameters. Wearable Health Devices (WHD) have drawn a lot of attention during the last decade in a wide range of domains. A variety of commercial devices have been produced with the aim to monitor the health condition of a person in everyday life or during sport activities.
The focus of this project is the experimentation of a wearable device intended to be used by workers in heavy industries in order to monitor their vital signs during working days. The main motivation behind this choice is the lack of WHD for this particular type of application. By its nature, the Oil&Gas industry is plenty with hazards to the health of employees. Despite standard and precaution, workers suffer injuries on the job every day. In this respect, WHD can certainly make a valid contribution to improve the workplace safety in dangerous environments.
The approach adopted in this work is to implement a single system which included different types of sensors in order to combine all the information extracted, thus providing a complete picture of the health condition of workers. Data measured from each sensor are managed by the Atmega328 microcontroller. A firmware based on the use of Interrupts events is designed to perform the following operations: data acquisition, data processing and data transmission.
A stressfull situation, due to the onset of a illness, triggers several body responses. Changes in the normal heart functioning is the first evidence. For this reason, an electrocardiogram (ECG) to measure Heart Rate (HR) parameter is included. A temperature sensor to monitor the skin temperature is also included in the prototype.
In response to events which pertubate the normal state of a person, the sympathetic nervous system actives the sweat secretion causing a phenomen known as Galvanic Skin Response (GSR). The proposed system extracts features from GSR signals in order to recognize the variation of the skin electrical conductance, thus identifying the onset of a stress event.
A reflectance pulse oximeter made it possible the measure of two important parameters: Peripheral Oxygen Saturation (SpO_2) and Pulse Transit Time (PTT). Regarding the extraction of the first parameter, this work proposes an algorithm which calculates the

differents portions of light absorbed by the pulsatile and non-pulsatile arterial blood. Furthermore, calibration and testing procedures are carried out taking as reference a commercial medical pulse oximeter.
The PTT measurement is performed combining the information given by the two synchronized ECG and PPG signals. Future works should include the implementation of a PTT-based system to estimate Blood Pressure values allowing a more complete health monitoring.
Finally, an accelerometer-based fall detection system is implemented to distinguish the different person's movements and detect a fall event which can be associated to injuries in hazardous environments.
Testing on different subjects are carried out to evaluate the accuracy of the algorithms implemented. In order to obtain a broader picture of the system behaviour, different simulations are taken into account during tests procedures. The good performance obtained by the proposed system provide solid basis for the continuation of the prototyping development.

Keywords: wearable systems, health monitoring, photoplethysmography, oxygen saturation, electrocardiogram, pulse transit time, fall detection, galvanic skin response

Contents

Acronyms

ECG Electrocardiogram
PPG Photoplethysmography
HR Heart rate
OSHA Occupational Safety and Health Amministration
HRA Health Risk Assesment
WDH Wearable Health Device
GSR Galvanic skin response
AHA American Heart Association
R Ratio of Ratios
SCR Phasic Skin Conductance Response
SCL Tonic Skin Conductance Level
BP Blood Pressure
SBP Systemic Blood Pressure
DBP Diastolic Blood Pressure
PWV Pulse Waves Velocity
PTT Pulse Transit Time
PAT Pulse Arrival Time
PEP Pre-ejection period
MEMS Micro-Electro-Mechanical Systems
SNS Sympathetic Nervous System
PGA Programmable Gain Amplifier
CMRR Common Mode Rejection Ratio
FIFO First In First Out
HPF High pass filter
LPF Low pass filter
INA Instrumentation Amplifier
MCM Multi-Chip Module
UART Universal Synchronous Asynchronous Receiver-Transmitter
FIR Finite Impulse Response

Chapter 1

Introduction

Wearable Health Devices (WHD) have been conquering enormous attention in the last years. Technological advancements have been enabled the deployment of WHD in a wide range of domains, including sport, medicine, and work.
In this thesis, the experimentation of a wearable device intended to be used by workers in heavy industries has been performed. By its nature, the Oil&Gas industry is plenty with hazards to the health of workers. The hazards that pose a potential threat to the safety of employees are: chemical exposures, temperature extremes, collision with moving parts and fatigue. In this respect, WHD can certainly make a valid contribution to monitoring vital signs during working days.
The state of the art is rich of wearable solutions which can monitor several parameters simultaneously. Most of these devices are intended to be used to monitor the lifestyle such as sleep quality, sport performance etc. Instead, regarding the application in heavy industries, less solutions have been implemented. The use of electronic devices in hazardous locations is more complicated in terms of certifications and norms. Moreover, the existing devices does not monitor all the parameters which are useful to obtain a complete overview of the health status of a person.
With the aim to enhance the workplace safety, WHD have to satisfy rigorous criteria. In addition to the accuracy and reliability of measurements, the comfort is an important requirement that cannot miss in this type of application. In this work, particular attention has been provided in finding a configuration that can continuoulsy and unobtrusively monitor the health status without any restriction by the person's movement. Among all the possible solutions, chest belt has been indicated as the most suitable configuration for our specific needs. This configuration allows to satisfy more requirements simultaneously. In fact in other configurations, such as wrist belt, only few parameters can be extracted because of the body region of application.

The general approach was to implement a single system which included different types of sensors in order to have a complete picture of the health status of workers. Data are

read and trasmitted by the Atmega328 microcontroller A firmware based on the use of interrupts was implemented and subsequently tested to ensuring a correct functioning.
When a subject is involved in a injury, a first evidence of illness is the heart rate (HR) variation. Since the electrocardiogram (ECG) is the most accurate method for heart monitoring, a single lead ECG sistem was included in the system. Heart deficiency, shocks and bleeding can induce changes in the normal range of the skin temperature. Thus, a simple temperature sensor was also included.
A stressful situation, due to the onset of illness, activates the sympathetic nervous system which drives cognitive and emotional states on a subconscious level. Changes in autonomic arousal trigger several body responses such as the increase of sweat secretion. The result is a measurable change in the electrical properties of the skin, such as the conductance. This phenomenon is called "galvanic skin response" (GSR). In this thesis, from the GSR signal, several features were exctracted in order to recognize the activation of the sympathetic system in response to events which perturbate the normal state of a person.
The arterial blood pressure (BP) is another critical vital sign which assumes an important role in predicting cardiovascular risks. Several efforts have been carried out on developing methods to estimate non-invasively BP for wearable systems. One of the most widespread approach, also adopted in this project, is based on the calculation of the Pulse transit time (PTT). This method involes the use of two signals: ECG and photoplethysmogram (PPG). PPG waveform is obtained by using a pulse oximeter which illuminates the skin and measures changes in light absorption. The PTT measurement is based on the calculation of the time delay for the pressure wave to propagate between two arterial sites within a cardiac cycle. This delay is represented by the distance between ECG peak and a characteristic point of the PPG signal.
The main use of the pulse oximeter is the determination of the percentage of hemoglobin satured with oxygen, known as oxigen saturation (SpO_2). This parameter provides early warning signs of malfunctions of vital organs (such as respiratoy system). In order to have information about SpO_2 levels, an algorithm was implemented. Furthermore, taking as reference a medical pulse oximeter a calibration process was carried out. From the PPG signal also HR parameter was extracted in order to compare it to the HR measured from the ECG signal.
Finally, an accelerometer-based fall detection system was carried out to distinguish the different person's movements and detect fall event which can be associated to injuries in hazardous environments.
Combining all the information extracted from each sensor, a full picture of the health status is obtained. Thus allowing a quick response in case of emergency, increasing the workplace safety.

Chapter 2

Medical background

This chapter provides a summary of the anatomy and physiology of the organs involved in the physiological processes of interest for the thesis development.

2.1 Heart

The heart is the central organ of the circulatory system and it is located in the middle compartment of the chest. It pumps blood through the blood vessels providing oxygen and nutrients to all parts of the body.

2.1.1 Heart anatomy

From a structural point of view, the heart is divided into two sections called 'right heart' and 'left heart' separated from the Septum, a wall of different types of muscle. Each part is composed of an atrium and a ventricle. The two parts are independent and they play a different role in the operation of the cardiac pump. Fig.2.1 shows the anatomy of the heart with indicated the two parts of the organ.

- *Right heart:* the blood poor in oxygen reaches the right atrium. The blood coming from the coronary system drains through the superior vena cava, instead the blood from the middle and lower body drains through the inferior vena cava. The coronary circulation, through the coronary sinus, also contributes to the blood accumulation in the right atrium. After the atrium contraction, the blood is sent to right ventricle positioned in the lower part of the heart. The right atrium and ventricle are separated by a valve called "tricuspid". Once the right ventricle is full, it contracts and pumps the blood through to the lungs via the pulmonary artery. The pulmonary valve lies between the right heart and the pulmonary artery.

- *Left heart:* the left heart consists of two chambers, atrium and ventricle, separated by the mitral valve. The oxygenated blood returns to the left atrium via the pulmonary vein and it is pumped into the left ventricle through the mitral valve. The left ventricle pumps blood to the body through the aortic valve into the aorta.

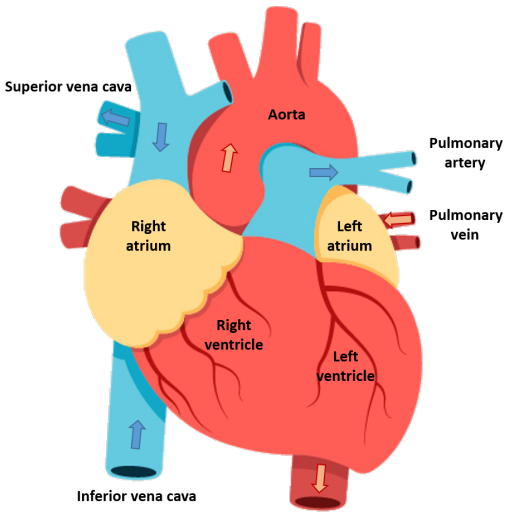

Figure 2.1. Anatomy of the heart. Adapted from [1].

2.1.2 Heart physiology

The heart function is to provide a continuous blood flow in the circulatory system which is divided into: pulmonary circulation and systemic circulation. To accomplish this role, the heart acts as a pump. The cardiac cycle is referred to the contraction and relaxation of the heart in every heartbeat. Thanks to the perfect heart coordination, the blood is efficiently pumped throughout organs. The cardiac cycle presents two main phases: systole and diastole. Systole refers to the time in which ventricles are contracted and the blood is pumped into the aorta and pulmonary artery. Diastole is the period in which ventricles are relaxed and are filled with blood coming from the atria.
The cardiac cycle starts when the ventricles are relaxing. The blood passes through the mitral and tricuspid valve and the ventricles are passively filled. Then, atria contract pumping further blood into the ventricles. When ventricles are almost completely filled start to contract. The ventricles contraction entails an increase of pressure within them. As a result, the mitral and tricuspid valves are forced shut. When the pressure within the ventricles exceeds that exerted by the aorta and pulmonary arteries, the aortic and

pulmonary valves open and the blood is pumped from the heart. Consequently, the pressure inside the ventricles drops drastically. At the same time, the blood flows through the superior and inferior vena cavae (right atrium) and through the pulmonary veins (left atrium). As the pressure within the ventricles come down below the pressure within the aorta and pulmonary arteries, the aortic and pulmonary valves close.
Finally, the ventricles relaxing and the mitral and tricuspid valves open. After that, the cardiac cycle begins again.

2.1.3 Electrical system of the heart

Electrical impulses coordinate the activity of the heart. These electrical signals are propagated by the cardiac conduction system. The sino-atrial (SA) node is the origin point of heart contraction in fact it is called the heart's pacemaker. The SA node is located at the top of the right atrium. In response to these signals, atria contract and the blood is injected into the ventricles. Sympathetic and parasympathetic nerves could influence the speed stimulation of the SA node. When the electric impulse propagates, the cells of the heart depolarize. As a result, the internal potential of cells, measured with respect to the exterior, becomes positive. This phase is known as "cell depolarization". The successive phase, known as "repolarization", brings the internal potential back to its negative value [2]. The electrical impulse propagates to the atrioventricular (AV) node, located at the bottom of the right atrium. AV node slows the signal so that is responsible of the time delay between the contraction of the atrium and ventricle (between 120 ms and 200 ms for healthy hearts). Another role of the AV node is to intervene in case of failure of the SA node.
The electrical signal is carried along Purkinje fibers to the ventricular walls. The impulse causes the ventricles contraction. The electrical signal generated from the heart can be recorded using skin electrodes, obtaining the Electrocardiogram described in detail in section 3.4.1.

2.2 The circulatory system

The pressure generated by the heart contraction constitutes the propulsive force that pushes the blood through the vessels of the cardiovascular system.
Blood is a fluid tissue composed of specialized cells and a liquid extracellular matrix, called plasma, which gives it the characteristics of a non-Newtonian fluid. The blood performs numerous functions that vary according to the cells considered. The main function is to deliver necessary substances such as nutrients and oxygen to the cells. In addition, blood transports the metabolic products (waste) away from the cells. Thanks to the circulatory system, the blood reaches all parts of the body.
The circulatory system can be compared to a closed hydraulic circuit and it is composed

of the blood vessels and two pumps placed in series, combined in a single structure (the heart). The vessels that carry blood to the heart are called veins, those that carry it away from the organ are called arteries. Moving away from the heart, the blood vessels gradually reduce in diameter. The circulatory system is a two-part system connected in series: the systemic circulation and the pulmonary circulation.
The systemic circulation starts from the left ventricle which contracting pushes the oxygen-rich blood into the aorta and from there into all the arteries of the body, which carry the oxygenated blood to the different tissues and cells. The blood drops off oxygen and collecting carbon dioxide and waste products.
The blood, low in oxygen, is collected in veins and travels through venae cava to the right atrium where starts the pulmonary circulation. From the right ventricle the low-oxygen blood is pumped, through the pulmonary artery, into the lungs. A rich network of capillaries surrounds the alveoli and there, the blood releases carbon dioxide and picks up new oxygen. Through the pulmonary veins the blood reaches the left atrium where the previous cycle starts again. The two cycles happen at the same time and approximately it takes about 30 second for a given portion of the blood to complete the entire cycle. The amount of blood expelled by a ventricle at each pulse multiplied by the number of beats per minute (heart rate) is indicated as "cardiac output" and for an adult at rest is around 5 l. A key feature of the circulation system is the elasticity of the vessel walls. In fact, the elastic force of the vascular wall transforms the intermittent flow generated by the cardiac pump into a continuous flow. When blood leaves the left ventricle, the aorta and large arteries expand to pick it up. On the contrary, when the ventricle is released and the semi-lunar valves close, an elastic return of the arterial walls occurs.
The blood flow follows the thermodynamic laws: it is directly proportional to the pressure gradient between any two points of the vascular network, and inversely proportional to the vessel resistance. This relation is expressed by the Eq.2.1 [2].

$$F = \frac{\Delta P}{R} \tag{2.1}$$

The blood flow varies according to the geometry of the vessels: the larger is the diameter, the greater is the flow. Blood pressure is high in the arteries and it decreases along the circulatory system. The decrease in pressure is also due to the loss of energy caused by the vessel resistance to the flow and the friction caused by the moving blood cells.
The Poiseuille's law (Eq.2.2), applied to hemodynamics demonstrates that: vessel resistance (R) is directly proportional to the length (L) of the vessel and the viscosity(η) of the blood, and inversely proportional to the radius to the fourth power (r^4).

$$R = \frac{8\eta L}{\pi r^4} \tag{2.2}$$

The above expression combined with Eq.2.1, results in the following formula:

$$F = \frac{\pi r^4 \Delta P}{8\eta L} \tag{2.3}$$

The Poiseuille's law describes the behavior of a homogeneous fluid that flows in a cylindrical duct with continuous flow and laminar mode. The blood is a non-Newtonian fluid so it does not conform exactly to this relationship. Nevertheless, the relationship clearly shows the dominant influence of vessel radius on resistance and flow. The radious is the key parameter for the blood pressure regulation. The blood pressure is controlled by the variation of the arterial peripheral resistance and it depends on both physiological and pathological factors. Fig.2.2 shows the two parts of the circulatory system.

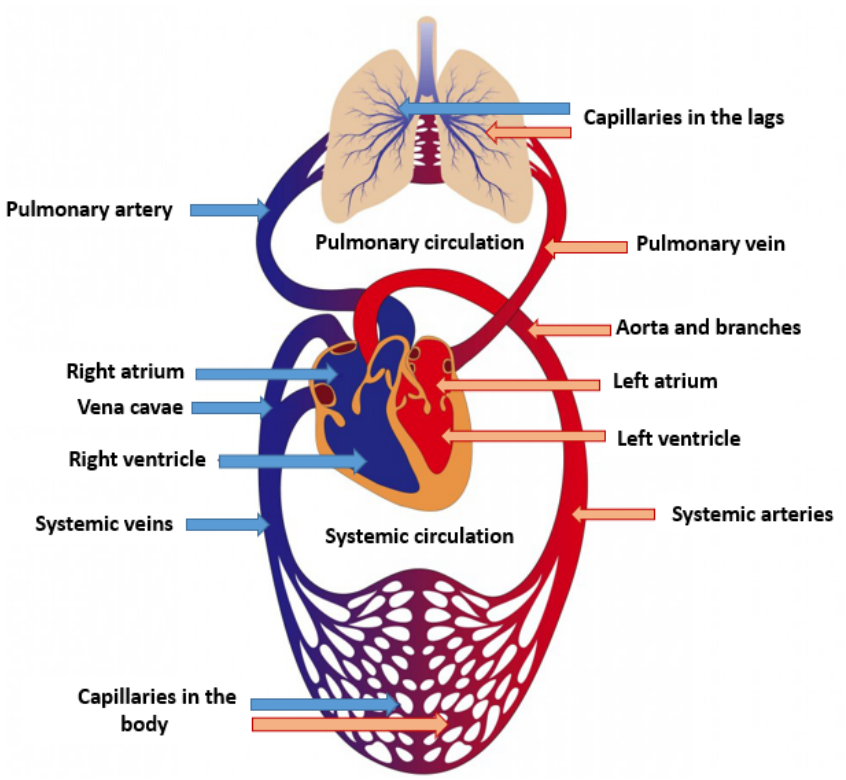

Figure 2.2. The circulatory system. Adapted from [4].

2.3 Arterial blood regulation

The Blood pressure (BP) is the force of circulating blood on the walls and it is produced primarily by the contraction of the heart [3]. In the circulation, the highest pressure is present at the aortic level and it reflects the pressure generated by the left ventricle. The large arteries have resistant and elastic walls. Therefore, they are suitable to withstand the high pressure generated by the ventricular pump during systole.
Blood pressure is measured in millimeters of mercury (mmmHg), above the surrounding atmospheric pressure. The mean arterial pressure is of 100 mmHg in the aorta, and slowly

decreases towards the capillary network. At each systole the heart generates energy. A portion of this energy is used to accelerate blood during the ejection phase (kinetic energy), the remainder instead is converted into a pressure. At this stage, blood pressure is usually expressed in terms of the systolic pressure and it reaches its maximum value.
During the diastole (relaxation phase), the pressure doesn't drop to zero because large arteries accumulate blood and elastic energy in the previous contraction phase. So, the potential energy stored in the walls is converted in kinetic energy i.e. in flow. This characteristic guarantees a continuous flow in the arteries, although the cardiac pump is intermittent, and allows to minimize the work of the heart. The blood pressure, called diastolic pressure, reaches the minimum value. According to the American Heart Association (AHA), physiological values are around 120/180 mmHg for adults.
The arterial pressure waveform, illustrated in Fig 2.3, shows that the pressure fluctuates cyclically, reflecting the pump action of the ventricle. The ventricular pressure rapidly increases at the beginning of the systole, causing the semilunar valve opening and the blood flow. A further increase in pressure occurs resulting in a peak in the pressure waveform called "systolic peak". At about half of the systole, the pressure decreases, and the blood flow decelerates, causing the closure of the valve. This last event is marked by the" Dicrotic notch". The interval between the dicrotic notch and the subsequent upward trend is the diastole, characterized by a valley that reflects the end of this period.

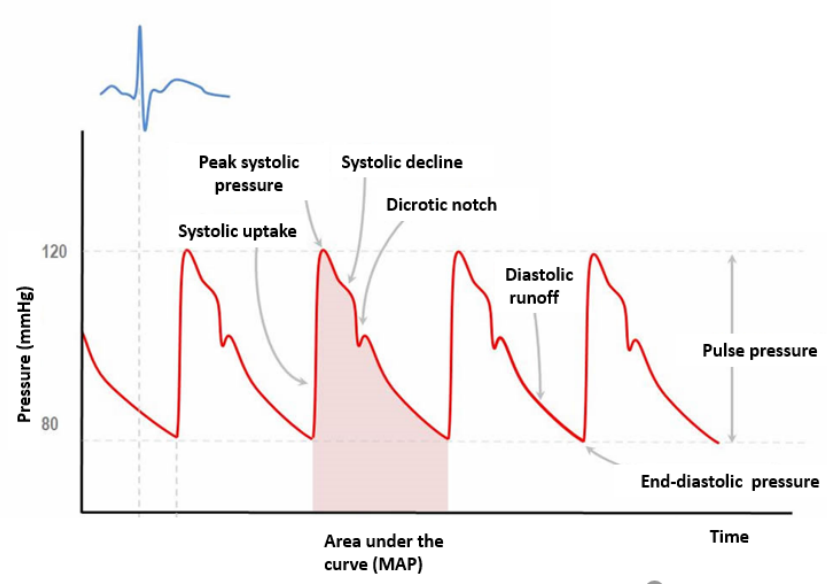

Figure 2.3. Pressure waveform. Adapted from [5]

Blood pressure is determined by the balance between the amount of blood that enters the arteries and the amount that comes out of it. If the incoming flow exceeds the outflow,

the blood accumulates in the arteries and the arterial pressure increases. If the opposite occurs, the mean arterial pressure decreases. The flow of blood entering the aorta corresponds to the cardiac output of the left ventricle. On the other hand, the outflow of the arteries is mainly influenced by the peripheral resistance, defined as the flow resistance offered by the arterioles. Many organs, such as the brain, implement regulation mechanisms to keep the flow constant.
The mean pressure value is also affected by the total volume of blood and the blood distribution in the systematic circulation. In fact, the cardiovascular system responds to pressure changes increasing or decreasing the blood volume.

2.4 Gas exchange

The process called "gas exchange" simply refers to the movement of oxygen and carbon between the bloodstream and the lungs [6]. The movement occurs throw the respiratory membrane which includes the alveolus and pulmonary capillary. This is an essential process since it ensures a constant supply of oxygen to tissues. When gases are diffusing through tissues exert a pressure on the cell walls because the molecules move, and a kinetic energy is generated. Gas are exchanged between the alveolar air and the blood by the diffusion process. As the Fick's law states, the rate of diffusion is influenced by a variety of factors:

- *Pressure difference across the diffusion barrier*
- *Gas solubility*
- *Cross-sectional area of the fluid*
- *Molecular weight*
- *Fluid temperature*

The net diffusion of the gas is mainly established by the partial pressures difference: from a region with higher pressure, to one with lower pressure. If the partial gas pressure is greater in the alveoli than the capillaries, as normally happens with oxygen, a greater number of molecules will pass into the blood. On the contrary, if the gas pressure is higher in the blood, as normally occurs for carbon dioxide, the net diffusion will take place towards the gaseous phase in the alveoli. Thus, carbon dioxide enters the alveoli to leave the body.

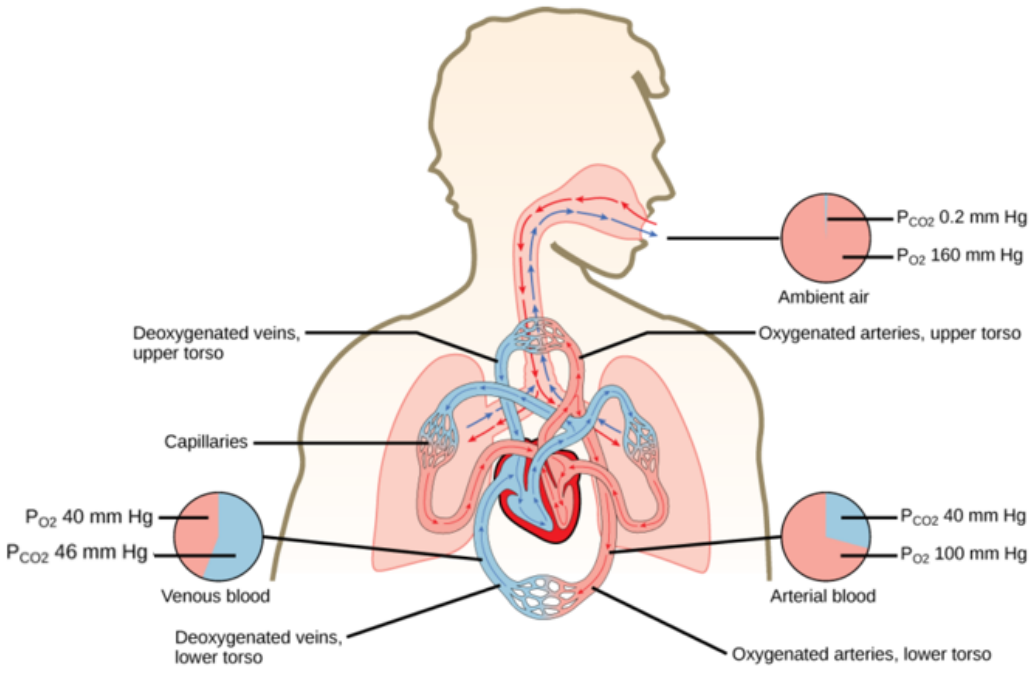

Figure 2.4. Representation of partial pressure along the circulatory system [7].

At sea level the air is composed of about 21% of oxygen, so the partial pressure of oxygen available for inspiration is:

$$P_{O_2} = 760mmHg * 0{,}21 = 160mmHg \tag{2.4}$$

Within the first section of the respiratory tree, O_2 is humidified by the addition of water vapor (partial pressure of 47 mmHg), so a decrease in P_{O_2} occurs:

$$P_{O_2} = (760 - 47)mmHg * 0{,}21 = 149mmHg \tag{2.5}$$

After the alveolar ventilation, C_{O_2} production and O_2 consumption causes a further drop in P_{O_2} at the alveolar level which passes from 149 mmHg to 104 mmHg.
The P_{O_2} of venous blood instead has a value of 40 mmHg because the blood has transferred oxygen to the capillaries of the peripheral tissues. Consequently, the pressure difference within the pulmonary capillaries is over 60 mmHg and according to Fick's law, oxygen diffusion occurs from the alveoli towards the capillaries, enriching the blood in oxygen. The pressure gradient generates an increase in P_{O_2} in the capillary. When the pressure in the capillaries is equal to that in the alveoli, the gas flow is interrupted.
When the arterial blood reaches peripheral tissues, the partial pressure difference between oxygenated blood and cells is around 60 mmHg and it provokes the diffusion of oxygen

from the blood to the tissues. Consequently, the P_{O_2} in the capillaries decreases until reaching the partial pressure of the cells (40 mmHg). The cells consume oxygen which leads to the production of carbon dioxide and a consequent increase in P_{CO_2}. Therefore, carbon dioxide diffuses from cells (P_{CO_2} = 46 mmHg) to tissue capillaries (P_{CO_2}= 40 mmHg). After, it reaches the lungs through the bloodstream, it spreads to the alveoli and leaves the body. At each point of the gas transport chain, carbon dioxide always diffuses in the opposite direction to that of oxygen diffusion, allowing an efficient gas exchange necessary for maintaining the vital functions of the tissues.

2.4.1 The role of hemoglobin in oxygen transport

The oxygen transport through the body is facilitated by the presence of hemoglobin (Hb), an iron-containing protein found in the red blood cells (erythrocytes). This molecule is responsible for carrying 98.5 % of the oxygen in the blood [8]. Hemoglobin has a quaternary structure: it is composed of four subunits, each with a heme group plus a globin chain. There are four different types of chains: alpha, beta, gamma and delta. Each heme group can reversibly bind oxygen through the iron atom, that is normally in the ferrous Fe_{2+} oxidation state. So that a hemoglobin molecule can carry a maximum of four oxygen molecules. Hb molecule has competitive binding for other compounds than O_2 such as nitrogen dioxide, cyanide, carbon monoxide etc. Fig.2.5 presents the hemoglobin molecule structure.

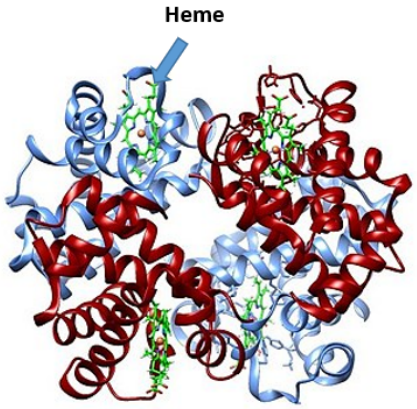

Figure 2.5. Molecule of hemoglobin.

The subunits can have two different conformations, one of these predominates when the iron atoms are saturated with oxygen and the other predominates when these binding sites are vacant. In the first arrangement the molecule is called oxyhemoglobin, in the second one it is called deoxyhemoglobin. In normal condition, about 97% of oxygen is

chemically linked to the hemoglobin and only 3% is dissolved into the plasma.
Oxygen saturation is the fraction of oxygen-saturated hemoglobin relative to the total hemoglobin (unsaturated + saturated) in the blood. It is a dimensionless quantity whose value is between 0 and 100 (often expressed in percentage terms).
Indicating with $C(HbO_2)$ and C(Hb) respectively the concentration of oxyhemoglobin and deoxyhemoglobin, the oxygen saturation is calculated as:

$$\text{Oxygen saturation} = \frac{C(HbO_2)}{C(HbO_2)+C(Hb)} * 100 \tag{2.6}$$

The oxygen–hemoglobin dissociation curve relates oxygen saturation and the partial pressure of oxygen in the blood (Fig.2.6). It describes the change in the hemoglobin affinity for oxygen as the partial pressure changes. At high P_{O_2}, most hemoglobin is oxygenated (pulmonary capillaries level). Instead, when the P_{O_2} is low, oxygen is released (peripheral tissues level).
Since the arterial blood has the P_{O_2} in the range of 96-100 mmHg it can be deduced that the normal value of oxygen saturation is about 97-99%. On the contrary, the P_{O_2} in the venous blood is 40 mmHg and the saturation is about 75%.
Many factors, such as PH, temperature, hydrogen ions, 2,3-bisphosphoglycerate (2,3-DPG) concentration, influence the hemoglobin affinity for oxygen, moving the dissociation curve to the left (higher affinity) or right (lower affinity). For example, increasing acidity moves the curve to the right because the hemoglobin structure is altered by the increase of hydrogen ions. The increase of hemoglobin oxygen-carrying capacity occurs also when the temperature and 2, 3-DPG concentration increase.

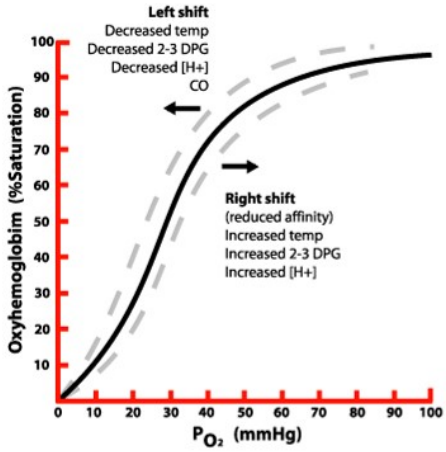

Figure 2.6. The oxygen dissociation curve [8].

Chapter 3

Wearable devices

3.1 Health risk in Oil & Gas industries

The oil and gas industry is a really global business presents in different environmental conditions including arctic or tropical. By its nature, the Oil&gas industry is plenty with hazards to the health and safety of workers. When working with heavy equipment, power tools, scaffolding, ladders, electricity, toxic materials, even small mistakes can quickly turn into grave emergencies.
In the United States, the agency *"Occupational Safety and Health Administration (OSHA)"* is in charge to assure safe and healthy working conditions for operators. The agency has stipulated regulations in order to decrease the health risks in workspace. Despite every standard and precaution, workers suffer injuries on the job every day.
Preventing occupational accidents and diseases requires, first, the identification of hazards [12]. In this regard, the *"Health Risk Assessment (HRA)"* has as a primary objective to identify health hazards and evaluate risks to health [11]. Figure 3.1 shows a typical process of health risk assessment. This process is represented through a block diagram which has different color in order to distinguish the different steps.
A general classification of hazards that pose a potential threat to the health of workers could be the following:

- *Hazardous chemical exposure*
- *Hazardous environment:* fire, intoxication and electric shock danger
- *Temperature extremes*
- *Collision with moving parts*
- *Fatigue*

The risks associated to the chemical exposure, that could be dangerous for the health, are different and particularly common in Oil&gas industries. Contact, ingestion or inhalation of hazardous chemicals could result in the onset of illness such as skin irritants or worse respiratory distress. In this type of workplace, the most relevant chemical substances are: hydrogen sulphide H_2S, silica, heavy metals. In the same way, gases and vapors pose serious risks to workers especially when they are accidentally released from tanks or trucks. The loss of these gases, as well as compromising the health of the operators (such as breathing), could cause the onset of a fire or explosion after the contact with electrical sources, open flames, cutting tools.
Of course the incidents concerning electric shock are not rare. An electric shock occurs when a person comes into contact with a power source, causing energy to flow throughout its body. Depending on the type and level of electrical current, electrical shock injuries can compromise in more or less serious ways the health, and more in specific, the electrical activity of the heart.
Temperature extremes due to the climate or a particular condition in workplace, cause illnesses including heat stroke, heat exhaustion, heat syncope, heat cramps.
Oil and gas workers often have to perform their job duties in locations high off the ground, which makes them more vulnerable to injuries associated with falls. These workers often climb on elevated equipment such as drilling and service rigs, so falls can cause serious injuries. Accidents very frequent occur as a result of hazards associated to collision with moving parts or with worker being struck by equipment.
Fatigue is the enemy for the oil and gas workers because of their exhausting shift patterns and long work durations. The performance, safety and productivity in the workplace are so impaired.
The determination of measures to address these potential risks regards first of all the identification of problems that could be potentially avoided (distractions due to the fatigue, working in dangerous weather condition etc). For each hazard present, an assessment is undertaken to show whether control measures in use are effective in reducing the risk to an acceptable level [10].
It is essential to review all operating procedures including routine tasks and emergency activities [12]. Personal protective equipment requires special consideration, especially in the case of is used incorrectly or it has been poorly designed. An aspect that should not be overlooked is the education and training of the employees in oil and gas industry. This can be achieved through visual displays, training, toolbox talks, health events and discussion at safety meeting [13]. The plan for health risk assessment should be reviewed periodically since activities, equipment or personnel change frequently.
The risks identification and the consequent measures adopted to reduce them, often are not sufficient to preserve the health of operators.

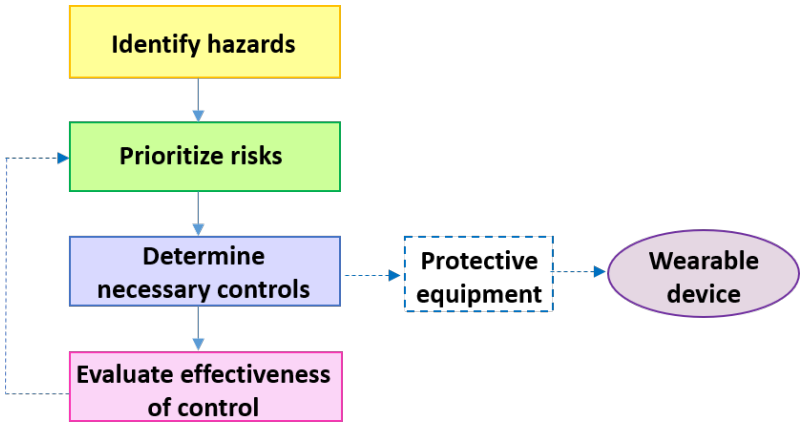

Figure 3.1. Health risk assessment process.

In this respect, **wearable devices** can certainly make a valid contribution, because they can monitor continuously vital parameters of oilfield workers. An alarm system should be included in order to alert in case of emergency so first responders quickly act. Wearable technologies are in continuous evolution and lead to the discovery of new avenues for innovation especially in this type of application. Therefore, these systems can be implemented easily in the harsh environments enhancing the workplace safety.
The same technology implemented for fitness tool could be extended to workers in oil and gas industries. Thus, workplace safety and workers efficiency are enhanced with minimal cost. It is necessary to give more attention to the development of wearable devices intended for this type of application. Since the environment is dangerous and the conditions in which operators work can be extreme, the gadgets must be resistant both high temperatures and harsh environment. Furthermore, despite the hard operating conditions, these devices must measure accurately vital signs and also transmit data to a central unit.

3.2 Wearable device definition

In recent years the design and development of wearable devices for vital signs monitoring has attracted considerable attention at both scientific community and industry [14]. The objective of this systems is providing real-time feedback information regarding the health status during daily life (sport activities, at home, at work, etc.)[13]. Wireless monitoring systems increase the mobility of patients who would otherwise be forced to stay home. In addition, these non-invasive devices provide sufficient information for determining diagnosis early.
Wearable Health Devices (WHDs) include multiple science domains (biomedical, electronic, material, communication technologies) that intersect with each other. They refer

to devices in the form of watches, glasses, rings, belts that are appropriately attached to the body of a worker, athlete, elderly person, etc. [15].

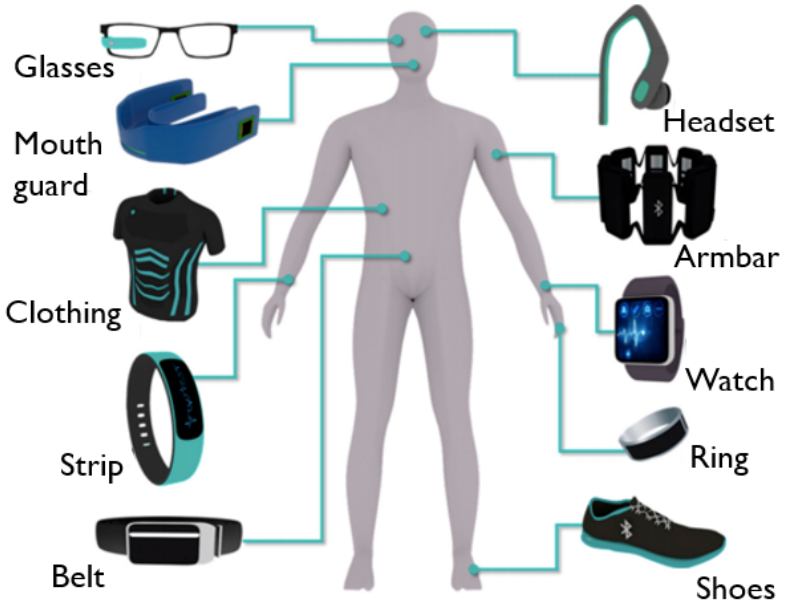

Figure 3.2. Wearable sensors [15].

A wearable device for health monitoring need to satisfy rigorous criteria. The goal of researches is the development of wearable systems that can continuously and unobtrusively monitor health status without any restriction by the person's movement [15]. In this regard, wearable sensors have gradually been developed in the form of small accessories with the advantage of minimizing discomfort. Considering that these devices are continually in contact with the skin, the components must be chemically inert and hypo-allergenic to the human body. In addition to that, radiation concerns and aesthetic issues are to be considered [14]. Obviously the robustness and the reliability are two requirements that cannot miss in a biomedical device.
In Fig.3.2 several portable devices that belong to different classes (watches, glasses, helmets, coats, shoes) are represented [15].
The most widespread devices are the wrist ones because of their comfort. Supporting this, "Statista", a German portable for statistics, reported that the most common wearable devices currently are smart watches and fitness trackers. Moreover, the development of the smartwatch is expected to grow at high rate. Among its competitors, Apple dominates the smartwatch market by far.

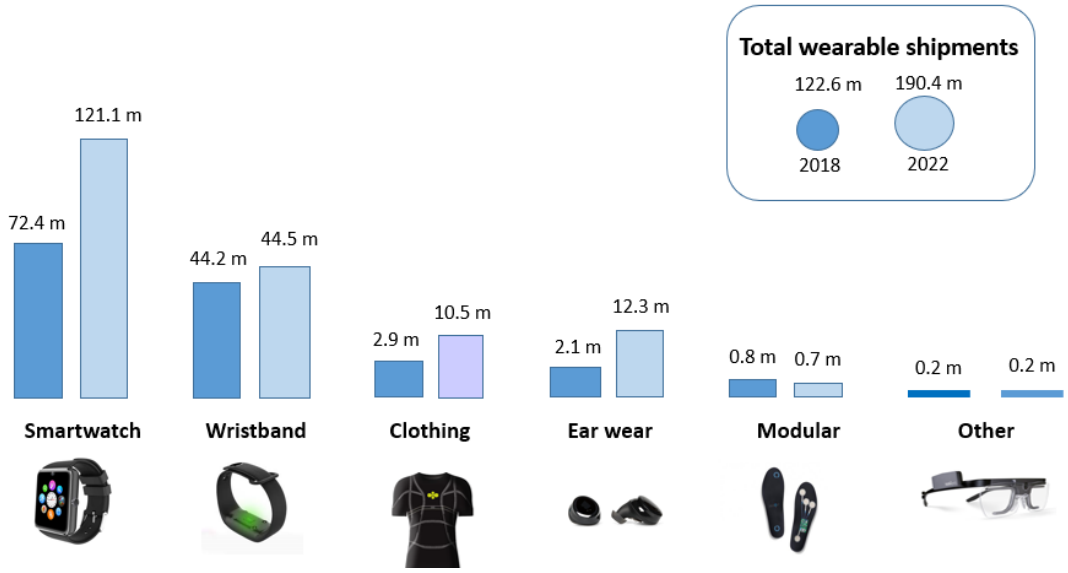

Figure 3.3. Estimated worldwide wearable device shipments (in million units) [16].

All wearable devices sharing a common architecture that consists of: sensors, central unit, power supply, trasmission module and monitoring system. Generally there are different types of sensors capable of measuring physiological parameters such as heart rate, blood pressure, body temperature, oxygen saturation, sweat rate, respiration rate, etc. Signals are collected by a central system, generally called "processing unit". Signal processing can be made in the processing unit or after the data transmission. After having extracted features necessary to evaluate the subject health, information are stored in a memory and communicated via wireless to a user interface or medical center. The wireless protocols most popular in wearable devices are Bluetooth, Wi-Fi, ZigBee and more recently LoRa (Long Range radio)[14].
Certainly, the system includes a power supply which allows a continuous all-day and any-place health monitoring. So, WHDs are the combination of a variety of components (sensors, communication modules, interface for the user etc.) that require technological advances in the most disparate industry sectors.
In Fig.3.4 a general wearable health monitor system architecture is depicted and it includes the typical features present in commercial products or prototypes. The most important blocks are: data capture represented by the sensors, data processing unit which performs parameters extraction and data communication and power supply. This structure should not be considered as the standard since many systems could present changes in the communication module or in the pre-processing unit.

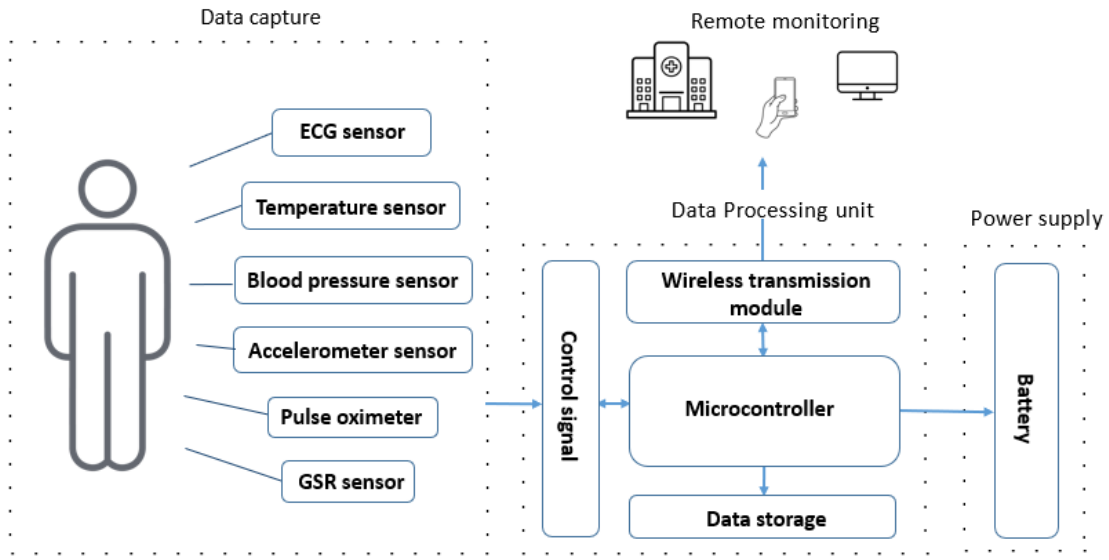

Figure 3.4. Architecture of wearable devices.

3.3 Wearable devices application

Wearable technologies are differentiated based on scenario of use and the type of monitoring [17]. Non-invasive devices are used in a variety of domains allowing individuals to optimize training, prevent hazards and to change their lifestyle [18]. The main domains in which wearable devices can be used are:

- *Medicine*: patient's health monitoring for the purpose to prevent illnesses so that doctors may act early. Widely used by elderly people, helping them to check disorders age-related;
- *Work*: employee's vital signs monitoring, especially in risky professions (heavy industries, firefighting, military). The aim is to prevent accidents/injuries and to intervene promptly;
- *Sports*: person's health monitoring during training activities to prevent potential injuries and to improve athletic performance;
- *Lifestyle*: person's health monitoring in order to change lifestyle and to asses sleep quality.

Since wearable devices can be of different size, shape and technology, they are used for a broad spectrum of purposes. As explained previously, these devices can be used in harsh environments, such as in Oil and Gas industries, in order to ensure the safety of operators. The use of these electronic devices in hazardous locations is more complicated in terms of certifications and norms. The regulation is the *ATEX Directive 2014/34/EU* and its aim is to protect health and safety of workers. This directive must be correctly applied during the design process of equipment and protective systems. Considering all the associated risks in potentially explosive environments, the devices have to respect several roles. The most important aspect is that they shall not cause explosions. For this regard, an electronic device must be considered "intrinsically safe". This implies that the electrical and thermal energy must be limited in order to prevent the formation of explosive atmospheres.

3.4 Monitoring of physiological signs

Wearable sensors can measure multiple physiological signs, from electrical signs to biochemical. The parameters generally considered essential to evaluate human health are: heart rate (HR), blood pressure (BP), body temperature, oxygen saturation (SpO_2) and respiration rate. In addition, micro-electro-mechanical systems(MES) are widely used for systems that measure sweat rate. This parameter is useful to monitor a person's physiology (such as hydration) through the analysis of electrolytes and biomolecules.
Generally, the most widespread sensors used to extract physiological signs are: electrocardiogram, pulse oximetry, galvanic skin response sensor and also motion sensors such as acccelerometrs for measuring activity. The main technologies used in wearable devices are described in the following paragraphs.

3.4.1 Electrocardiogram

Electrocardiogram is the most popular technology for heart monitoring because of its high accuracy.
Willem Einthoven invented the first practical ECG in 1895. An electrocardiogram is a recording of the electrical activity of the heart [19]. During the heart chambers contraction, the extracellular fluid, that surrounds the myocardial tissue, becomes never more negatively. On the contrary, the heart regions of depolarization and repolarization remain more positive. As a result, the cardiac dipole, generated by the positive and negative regions, creates a potential difference. Electrodes placed on the skin detect these small electrical changes.
The cardiac dipole behaves like a vector, in fact it has a direction (from the most negative to most positive regions of the heart) and an amplitude in voltage. The movements of the cardiac dipole are recorded from different points (angles) of view by a 12-lead ECG.
In a standard 12-lead ECG, there are 12 leads calculated using 10 electrodes. Each lead

is defined as an electric potential difference, so there are 12 different voltage signals, obtained by a linear combination of 10 electrodes. Four of these electrodes are positioned on the patient's limbs and six on the chest surface. The electrodes placement is shown in figures 3.5 and 3.6:

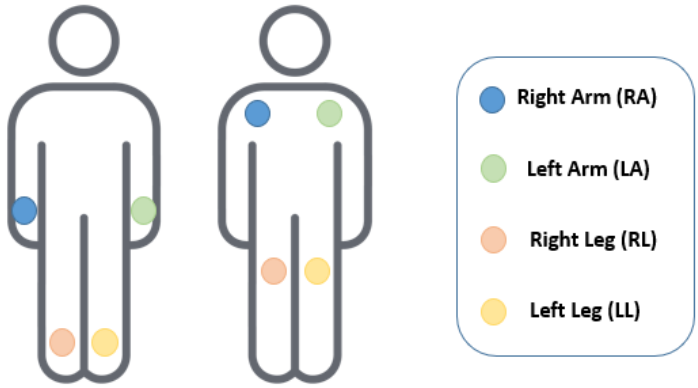

Figure 3.5. Electrodes positioning on the legs and arms for ECG recording.

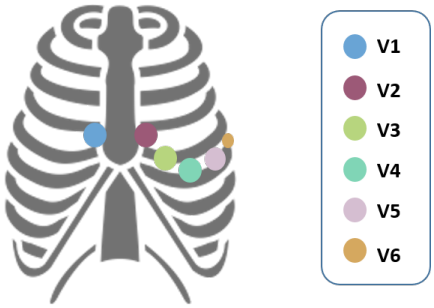

Figure 3.6. Electrodes positioning on the chest for ECG recording.

Leads are divided in three classes:

1. Limb leads: three leads (I, II ,III) that form the points of what is known as Einthoven's triangle. The imaginary triangle is an inverted equilater which the heart is located at the center. Each lead has a specific quantity and direction (vector) produced by adding or subtracting voltages from the recording electrodes. Summing the voltages the potential is zero. The leads are:

    - *Lead I* is the voltage difference between the left arm (LA) and right arm (RA) electrodes: I = LA-RA

- *Lead II*: is the voltage difference between the left leg (LL) versus right arm (RA) electrodes: II = LL-RA
- *Lead III* is the voltage difference between the left leg (LL) versus left arm (LA) electrodes: III = LL-LA

Figure 3.7 shows the Einthoven's triangle and the polarity of each lead measurement. The electrodes can be also positioned on the shoulders and lower torso. From a pair of electrodes is measured an electrical potential difference (i.e. "lead"). One of the two electrodes can also be a virtual electrode. This electrode is known as the Wilson's central terminal whose potential is the average of the vertices of the triangle and it can be taken as a reference for the unipolar leads.

$$V_w = \frac{1}{3(RA + LA + LL)} \tag{3.1}$$

2. Augmented limb leads: aVR, aVL, aVF. These leads use the same three leads that form the limb leads but they use the Goldberger's central terminal as their negative pole.

3. Precordial leads (also called unipolar chest leads)

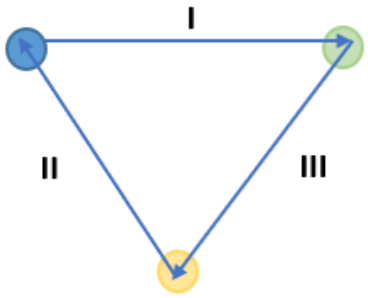

Figure 3.7. Einthoven's triangle.

Despite a standard 12-lead ECG permits to have a complete picture of the heart activity, this configuration is not applicable to the wearable ECG devices. An ideal long-term and continuous ECG monitoring system should measure vital signs with no impact on quality of life in terms of comfort.
For this purpose, the reduction of the number of electrodes is required. Of course, reducing the number of ECG leads the information extracted from the signal will be limited.

A lead is a differential signal, so a minimum of two electrodes are necessary to obtain the signal. The choice of which electrodes use depends to the device position on the person's body. For example, chest leads V1 and V2 are usually exploited by chest belt systems.

ECG signal

An ECG trace has a characteristic appearance that varies only in the presence of cardiac problems (such as arrhythmias). The waveform is characterized by different waves, positive and negative, which are repeated at each cycle heart (Fig.3.8).

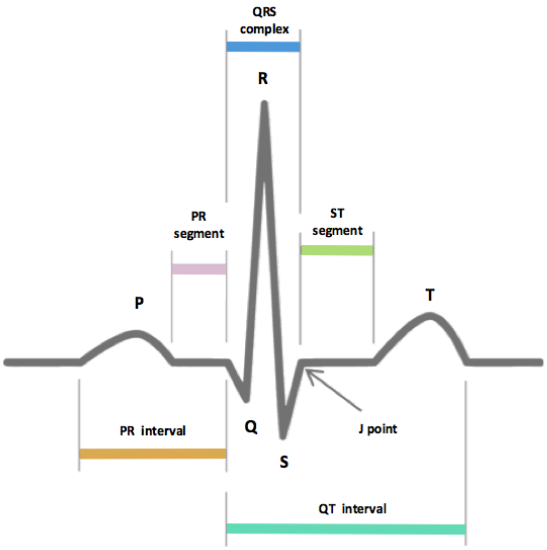

Figure 3.8. ECG signal.

The typical ECG signals from different leads include:

- *P wave*: is the first wave that is generated in the cycle. It corresponds to the depolarization of the atria which causes atrial systole. Since the contraction of the atria is not so powerful, the amplitude of P wave is small. Its duration varies between 60 and 120 ms.
- *PR interval*: is the time necessary for the depolarization wave to propagate from the atrial sinus node through the electrical conduction system (AV node and Purkinje fibers). This interval usually last between 120 and 200 ms.
- *QRS complex*: is a set of three waves that follow one another, and corresponds to the depolarization of the ventricles. Q wave is a negative and small peak, and corresponds to the depolarization of the interventricular septum; R wave is a very high

positive peak, and corresponds to the depolarization of the apex of the ventricle; S wave is a negative peak with low amplitude and corresponds to the depolarization of the basal and posterior regions of the ventricle. The duration of the entire complex is between 60 and 100 ms. At the same time as the ventricular depolarization, the atrial repolarization occurs. This event is not visible on the ECG graph because it is masked by the ventricular depolarization due to the larger magnitude of the QRS complex.

- *ST segment and T wave*: represent the ventricles repolarization. ST segment is the period in which the ventricular cells are all depolarized therefore no electrical movements are detectable. For this reason the ST segment is usually isoelectric.

- *QT interval*: represents the activity of the ventricles (depolarization and repolarization). Its duration varies with the heart rate (between 350 and 440 ms).

From the eleletrocardiogram the HR parameter is extracted. HR measures the number of times per minute that the heart contracts or beats (bpm). HR is a standard vital sign considered a routine measurement in several applications. Different factors influence the speed of heartbeat, such as physical activity and emotional responses, but a normal HR of an adult should be between 60 and 100 beats per minute. So, by indicating changes in the heart activity, the HR provides information about the physiologic status.
Considering a regular cardiac rhythm, the heart rate can be easily determined by the distance in time between two R peaks (R-R interval). For this purpose, several algorithms are proposed in literature. To obtain the HR parameter in beats per minute it is necessary divide 60 seconds by the R-R interval (equation 3.2).

$$\text{Heart rate} = \frac{60}{\text{RR interval}} \tag{3.2}$$

3.4.2 Photoplethysmography

Pulse oximetry is a state-of-the-art noninvasive method for determining the percentage of hemoglobin saturated with oxygen, known as oxygen saturation [20]. Blood oxygen level has long been recognized as a parameter that provides early warning signs of malfunctions of vital organs [21]. If the amount of oxygen exchanged and delivered throughout the tissues and organs becomes insufficient, the body cannot provide the necessary nutrients to the cells. Since SpO_2 is an important indicator to monitor the key organ's wellbeing, it is extensively used for both in-home and clinical environments.
Pulse oximeters have been developed and widely used since 1930s[20]. Because of their simplicity of use and the ability to provide continuous SpO_2 measurements, these devices are widely used in wearable systems. Furthermore, pulse oximeters are cheap, small and well suited to a universal application.

Physical principles of oximetry

The amount of light absorbed or reflected by the blood is the principle underlying the pulse oximetry. Pulse oximetry estimates peripheral SpO_2 using a variation of the Beer-Lambert law. It is an empirical relationship that relates the amount of light absorbed to the properties of the material through which the light is travelling. A common definition of the Beer-Lambert law relates the optical attenuation of a material to the optical path length through the sample and absorptivity of the material. The expression is:

$$\mathrm{I} = I_0 e^{-\varepsilon_\lambda cl} \tag{3.3}$$

Where:
I is the intensity of the transmitted light
I_0 is the intensity of the incident light
l is the optical path length
ε_λ is the extinction coefficient or absorptivity of the absorbent
c is the concentration of the absorbent

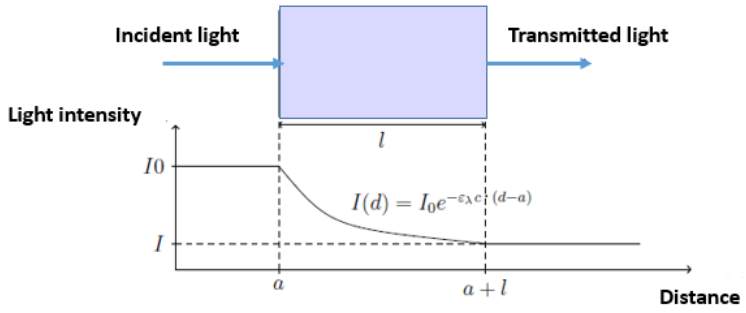

Figure 3.9. Beer-Lambert law.

An important parameter is the Transmittance (T) of the material sample and it is expressed as the ratio between the transmitted light and the incident light:

$$\mathrm{T} = \frac{I}{I_0} \tag{3.4}$$

The Absorbance is expressed as:

$$\mathrm{A} = ln\frac{I_0}{I} = ln\frac{1}{T} \tag{3.5}$$

The expression of the Beer-Lambert law can be applied also in case where the sample is composed of different layers of absorbents, such as the blood. The blood contains different substances that can absorb light at different wavelenght and absorptivity. In this case, the total intensity of transmitted light is expressed by a linear superposition of intensities of each material (Eq. 3.6).

$$\mathrm{I} = I_0 e^{\sum -\varepsilon_{\lambda,a} c_a l_a} \tag{3.6}$$

The total absorbance results:

$$A_{tot} = ln\frac{I_0}{I} = ln\frac{1}{T} = \sum -\varepsilon_{\lambda,a} c_a l_a \tag{3.7}$$

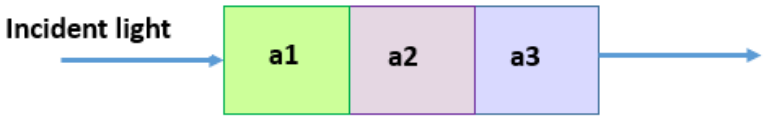

Figure 3.10. Beer-Lambert law for more absorbent layers.

In conclusion, given a sample containing several substances that absorb light at different wavelengths, it is possible to know the transmitted light of each substance.
The extension of the Beer Lambert law is the fundamental principle on which pulse oximeters are based. Optical oximetry devices measure oxygen saturation by evaluating the difference in the absorption spectra of the oxygenated and deoxygenated hemoglobin. For this reason, these devices normally contain two or more LEDs with different wavelengths. The most commonly used are 660 nm (red) and 940 nm (infrared). Their selection is due to the different behavior of the two types of hemoglobin: deoxyhemoglobin absorbs light with wavelengths closer to the red, whereas oxyhemoglobin absorbs heavily the infrared light. Figure 3.11 shows the trend of absorbance for HbO and Hb as a function of wavelength. The different absorbances could be explained by the fact that the arterial blood (rich in oxygen) appears to the human eye red because it reflects mostly red-light respect to the venous blood (poor in oxygen) that instead absorbs more light [22].
It should be specified that even if deoxyhemoglobin and oxyhemoglobin are the substances that absorb more light in the blood, hemoglobin can also bind to other substances such as monoxide of carbon (CO). In the absorbance calculation only the hemoglobin that reversibly binds to the oxygen is considered.

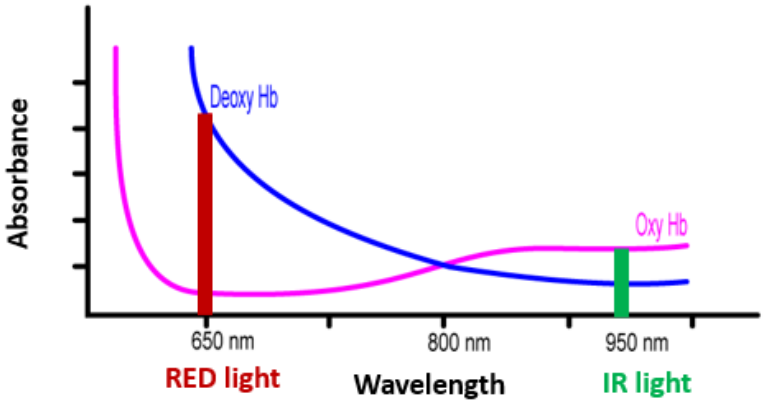

Figure 3.11. Trend of absorbance for HbO and Hb as a function of wavelength.

It is now possible to write the Beer Lambert law considering the blood as a simplified model composed of two different media inside it, consisting of deoxygenated hemoglobin (Hb) and oxyhemoglobin (HbO_2). The absorbance is only a function of Hb and HbO_2.

$$A_{tot} = \varepsilon_{\lambda,HbO_2} C_{HbO_2} l_{HbO2} + \varepsilon_{\lambda,Hb} C_{Hb} l_{Hb} \tag{3.8}$$

Considering the equation 2.6, it is rewrite as:

$$C_{HbO_2} = SpO_2 (C_{HbO_2} + C_{Hb}) \tag{3.9}$$

Assuming that the path length is the same for both lights, the total absorbance is:

$$A_{tot} = [\varepsilon_{\lambda,HbO_2} SpO_2 + \varepsilon_{\lambda,Hb}(1 - SpO_2)](C_{HbO_2} + C_{Hb}) l \tag{3.10}$$

Pulse oximetry

A typical noninvasive pulse oximetry sensor uses small light-emitting diodes (LEDs), an electronic processor, and a photodiode to detect the backscattered or transmitted light. Hertzman was the first to find a relationship between the intensity of backscattered light and blood volume in 1938 [23].
The pulse oximetry analyzes the light absorption of the two wavelengths from the volume of the arterial blood. Only a small part of the emitted light reaches the photodiode, while the remaining is absorbed by the various tissues of the skin. The light detected by the photodiode can be the transmitted light or the reflected one, depending on the sensor configuration. Transmission and reflectance are the two main modes of pulse oximetry and their difference is the probe position on the human body [24].

- *Transmittance Pulse Oximeter (TPO)*: the two LEDs (RED and IR) and the light detector are situated in two opposite areas of the human tissue, reason why this mode can not be used in all areas of the body. Typically, finger and ear are the areas where transmittance pulse oximeter is placed. The upside is the ease to attach and remove it and the simplicity of signal analysis. However, it is not comfortable especially for long period. Indeed, this type of pulse oximeter is commonly used for clinical application.
  Basically, the functioning is the following: LEDs emit light that passes through tissues and blood vessels. Then, the not-absorbed light, i.e. the transmitted light, is received by the photodiode. The resulting signal is the intensity of the transmitted light.

- *Reflectance Pulse Oximeter (RPO)*: the LEDs and the light detector are situated on the same side. A reflectance probe structure has light emitters and sensing diodes on a single surface. Unlike the other mode, the reflectance oximeter can be placed in various anatomical locations. This is because the single surface doesn't require two parts of the body close to each other. Thus, reflectance probes can be used in various application, such as wearable devices (wristbands, belts, rings) due to their comfortable wear for long-term HR and SpO2 monitoring.
  In the reflectance setup, the LEDS emit light that passes through tissue. After passing through the blood vessels, it reflects off the bone and passes through the tissues again. A significant amount of light is reflected and detected by the photodiode. This type of setup requires a greater amount of light and more photodiodes could be useful in order not to lose the reflected light.
  Compared to the transmittance oximeter, the signal resulting from this sensor, has a lower signal-noise ratio.

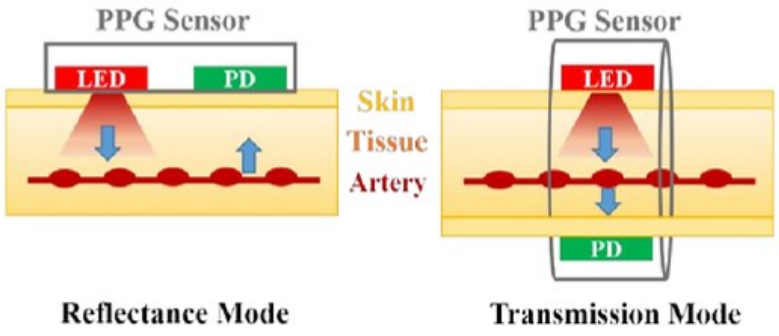

Figure 3.12. Reflectance and transmission mode [25]

The signal obtained, known as "photoplethysmography' (PPG), is the measurement of

light absorption changes. The PPG signal reflects light absorption changes due to the arterial blood flow variation [26]. The waveform is shown in Fig. 3.13.

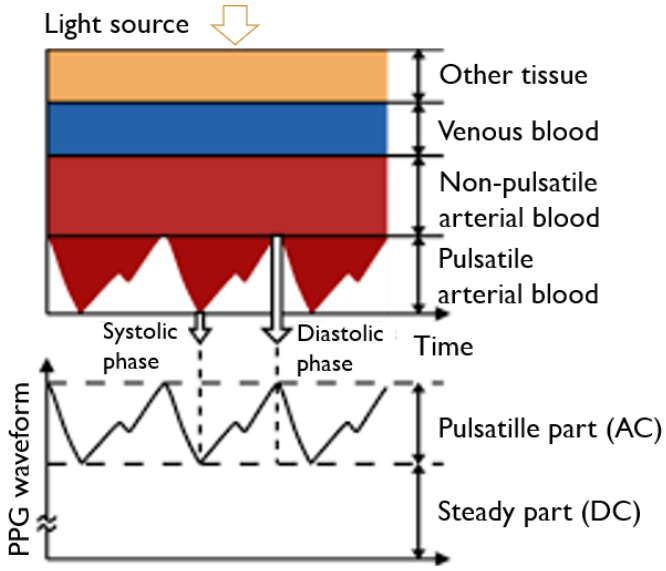

Figure 3.13. Features of a PPG waveform [27]

Generally, the PPG signal is composed of two components: "alternating current" (AC) and "static current" (DC). The AC component is provided by the cardiac variations in blood volume so represents the pulsatile arterial blood. The DC component varies only slowly due to thermoregulation, respiration, sympathetic nervous system activity and it represents the light absorption of the tissue, venous blood and non-pulsatile arterial blood. Since the changes in blood volume are caused by the cardiac activity, the AC component depicts the information about the systolic and diastolic phase of the cardiac cycle. So, the AC component can be used as a source of heart rate information [28].
Analyzing more specifically the PPG signal, valleys and peaks are clearly visible in all the pulse waves. During systole, the arterial blood volume increases because of the major ejection volume by the ventricles. Therefore, the light transmission through blood vessels decreases and the amount of the light detected by the photodiode is lower. Hence, the PPG signal generated from the intensity of the transmitted light presents a minimum, or valley, representing the systole phase. On the contrary, the blood volume during the diastole phase decreases, so the light that reaches the photodetector is greater. The pulse wave shows the diastolic phase that starts with a minimum and ends with a peak. Furthermore, the signal presents another small peak, called aortic or dicrotic notch. It is situated between systolic and diastolic phase and it is a small downward deflection in the pulse

wave due to the closing of the aortic valve [29]. The shape of the signal varies according to the location in which the sensor is attached. Different subjects have different PPG waveforms but the distinctive points of the PPG signal, such as the valleys and peaks, are in common for all subjects.

Heart rate measurement

Significant portion of wearable technologies for long-term applications use the pulse oximetry to extract HR parameters in addition to the oxygen saturation values. PPG sensor technology facilitates the development of HR monitoring because the hardware is simple and low cost. In the HR monitoring devices based on PPG technology, one LED is sufficient to extract the required parameter. The methods to obtain HR values from the PPG signal are essentially two.
The first method exploits the PPG signal shape to identify the cardiac cycle. To make clearer the similarity with the ECG signal, the PPG signal generated from the light absorption by the pulsating arterial blood is taken into account. The peaks highlighted in Fig.3.14 are due to the systolic events after the ventricle contraction during which the arterial blood volume increases as also the light absorption. It should be noted the different physiological meaning of the maxima (systolic peack in this case) present in the absorption signal rather than the transmitted signal.

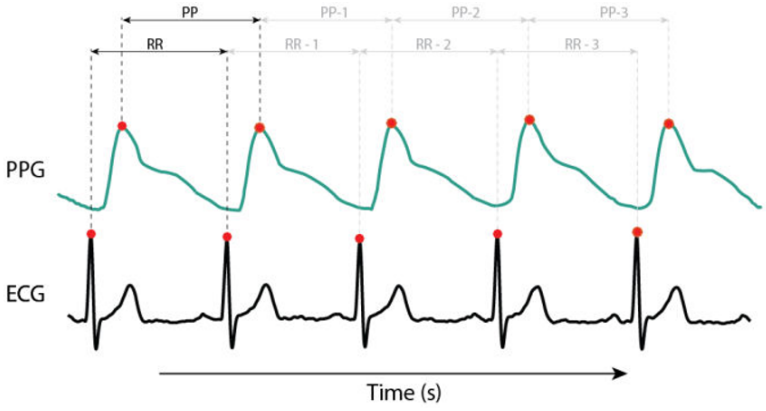

Figure 3.14. ECG and PPG signals [30]

The peak to peak time interval is determined by the calculation of the distance between two successive peaks (PP). This interval corresponds to the time to complete one cardiac cycle and from this, HR parameter can be calculated.
The formula is expressed as:

$$\text{Heart rate} = \frac{Fs * 60}{\text{PP interval}} \tag{3.11}$$

From both PPG and ECG signals is extracted the same information regarding the heartbeat frequency. In fact, HR can be measured accurately from ECG data as R peaks interval, where R peak is also originated by the systole phase of the cardiac cycle.
The second method is based on the identification of the frequency of cardiac pulsations. Usually, a Fourier transform is performed to estimate the energy difference in the frequency range of the PPG signal. HR has shown to be correlated to the frequency where the cardiac spike is observed in the spectrum[31].

Oxygen saturation measurement

As regards the procedure to obtain the information about the level of oxygen saturation in percentage, current conventional pulse oximeters use two light-emitting diodes (red and infrared) and a photodetector. Since the red and the infrared light are absorbed in different quantities from the hemoglobin, in order to easily compare the absorption at λ= 660 nm and λ= 940 nm it is necessary to normalize the result.
The ratio of the two absorptions with different λ is called "Ratio-of-ratios" and it is defined as:

$$\mathrm{R} = \frac{A_{tot,R}}{A_{tot,IR}} \tag{3.12}$$

Thus, the result is only dependent on the absorption of pulsatile arterial blood components. Based on the Lambert-Beer law, R can be calculated by the equation:

$$\mathrm{R} = \frac{\varepsilon_{\lambda_R,Hb} + (\varepsilon_{\lambda_R,HbO_2} - \varepsilon_{\lambda_R,Hb})SpO_2}{\varepsilon_{\lambda_{IR},Hb} + (\varepsilon_{\lambda_{IR},HbO_2} - \varepsilon_{\lambda_{IR},Hb})SpO_2} \tag{3.13}$$

which can be solved for SpO_2 as expressed in equation:

$$SpO_2 = \frac{\varepsilon_{\lambda_R,Hb} - (\varepsilon_{\lambda_{IR},Hb})R}{\varepsilon_{\lambda_R,Hb} - \varepsilon_{\lambda_R,HbO_2} + (\varepsilon_{\lambda_{IR},HbO_2} - \varepsilon_{\lambda_{IR},Hb})R} * 100 \tag{3.14}$$

The previous formulas are based on the simplified Lambert-Beer assumptions. In addition to the hemoglobin carrying oxygen, the blood contains other substances. The light emitted from the LEDs can be scattered, reflected and transmitted. The light detected by the receiver consists of photons that travel several paths. Some of them keep the right route without migrating, other photons instead scatter farther.
Because of the path variation due to the scattering phenomenon, the relationship between the SpO_2 parameter and the R parameter could be estimated with low accuracy.
Consequently, commercial pulse oximeters are empirically calibrated to give better estimation of SpO_2.

Calibration test

The calibration phase includes measurements of R in several healthy volunteers. The tests follow specific procedures and the main steps are presented in Fig.3.15.

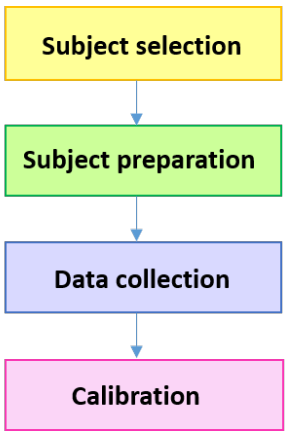

Figure 3.15. Calibration procedure of pulse oximetry.

First, a careful selection of the volunteers is required. Subjects having different range in age, skin tone and gender are selected. After the subject selection, the test preparation occurs. During the calibration test partecipants use a gas mask to control their SpO_2 level. According to the FDA (Food and Drug Administration) regulations, during data collection the oxygen level is reduced incrementally from 100% to 70% SpO_2. After collected R values and corresponding SpO_2 values, outliers are removed from the dataset. Finally, a best curve is fitted to the data.
An example (provided by Maxim Integrated) of a calibration plot is shown in Figure 3.16 [32]. The graph represents the relationship between R and SpO_2 values.
Using the acquired set of R and SpO_2 it is easy to find the "calibration coefficients". After that an empirical calibration formula is created. In literature several calibration formulas have been proposed but the choice depends on different factors. For this reason, tests should be performed in order to identify the formula most suitable. The following equation is an example of calibration formula:

$$SpO_2 = K_1R^2 + K_2R + K_3 \tag{3.15}$$

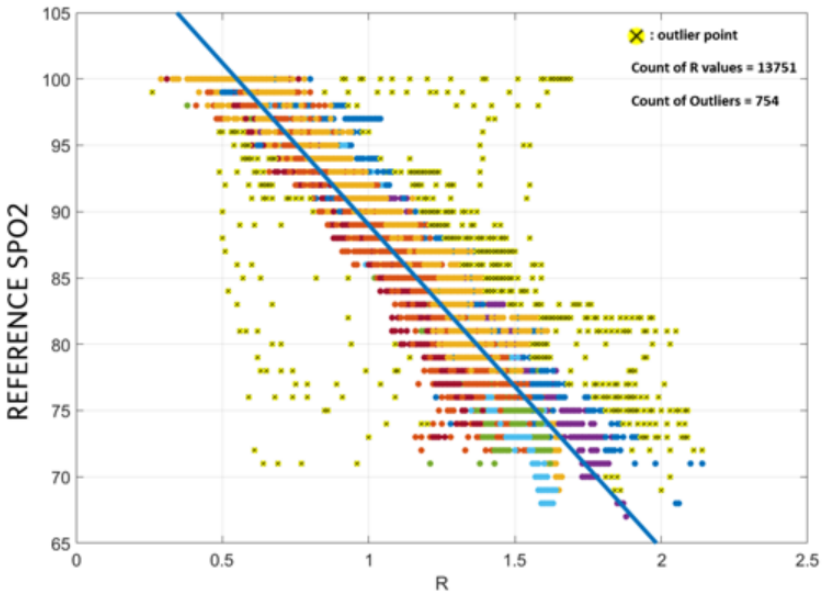

Figure 3.16. Reference SpO_2 values and R values measured from the sensor test [32].

3.4.3 Blood pressure

The arterial blood pressure is a critical vital sign which assumes an important role in predicting cardiovascular risk such as stroke, myocardial infarction and chronic diseases [33]. Monitoring of BP, especially for subjects with hypertension problems, can help to improve the lifestyle. It is estimated that the impact of the hypertension is over 35% of people worldwide and causes 12.8% of the total of all deaths [34].
The gold standard of the noninvasive BP monitoring is a cuff-based method known as sphygmomanometer which is made up of cuff, inflating bulb and a manometer. This method is commonly used because of its high accuracy. This device is not only obtrusive but also requires uncomfortable arterial compression for every measurement.
Another traditional method is the invasive catherization (a catheter is inserted into the arteries) but also this method is time consuming, measurement requires cumbersome tools and it is painful. Hence, cuff-less BP estimation has attracted attention by many researches. Because the BP fluctuations over time, long term continuous blood pressure monitor is the goal. Several studies have been carried out on developing a method to estimate non-invasively the BP, in order to easily monitor it in wearable applications. Currently, reliable wearable devices do not yet exist or at least they are not easily found on the market such as pulse oximetry [36].
Nowadays, wearable cuff-less BP monitors are created using different existing technologies. These BP monitoring systems allow high wearability and user-friendly features.

One of the most widespread methods is based on the use of both ECG and PPG signals taken simultaneously [37]. Thus, the development of this BP estimation method requires two different types of sensors. This non-invasive measurement can be used for long time monitoring and it does not require a skilled operator. It should be emphasized that this method, as well as other techniques, estimates the blood pressure value but doesn't measure it in a realistic way (like the sphygmomanometer and the catherization method).
This method is principally based on the measure of the velocity propagation of pulse waves (PWV) along the arterial tree. The PWV is generated when the left ventricle ejects blood, after the aortic valve opening. The pressure wave travels along the elastic arteries and it is felt as a pulse beat.
The approach is founded on the calculation of a parameter known as Pulse Transit Time (PTT). The PTT is defined as the time delay for the pressure wave to propagate between two arterial sites (where the measurement is undertaken) within a cardiac cycle. PTT can be used as a reliable marker for BP estimation [34].
The PTT values is calculated as the distance between the ECG peaks and a certain point of the PPG signal. Regarding the ECG wave, the reference point is the R peak. It represents the beginning of the systole. The R peak is a good reference for the origin of the pressure pulse wave. Furthermore, simple algorithms to detect R peaks are required. For the PPG wave there are several possible points to use as time stamp: maximum, foot or the midpoint between these two points.

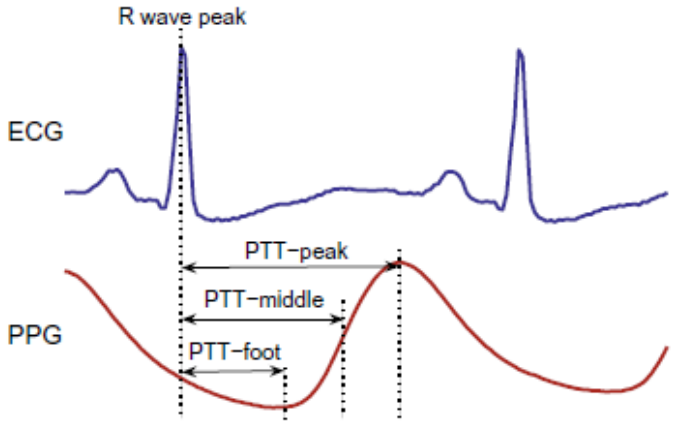

Figure 3.17. Pulse transit time definition [35].

More specifically, the measurement explained is called pulse arrival time (PAT). The main difference between the two nomenclatures is that PAT parameter includes also the pre-ejection period (PEP). The PEP is the time needed for the propagation of electrical

signals and the conversion into mechanical force. It represents the period of left ventricle contraction with the cardiac valves closed before the beginning of the ventricular ejection. PEP in a non-constant electromechanical delay because it changes in response to different factors such as stress, emotional stimuli and physical effort. In this case, pulse arrival time is made up of two parts:

$$\text{PAT} = PTT + PEP \tag{3.16}$$

To measure PEP additional signals are needed. Usually, an impedance cardiography (ICG) or a phonocardiogram (PCG) are introduced. The addition of another signal requires extra hardware, losing in terms of wearability. Since the PEP value is difficult to measure often is neglected in BP measurements. Therefore, the PTT measurement is generally referred to the method based on the ECG and PPG signals taken simultaneously, neglecting the mechanical delay.
The PTT value is affected by different factors: elasticity coefficient, thickness of the arterial wall, blood density and the diameter of the vessel lumen.
In 1878 Moens and Korteweg introduced a mathematical model which correlates the pulse wave velocity (PWV) and the above described factors. The mathematical expression is:

$$\text{PWV} = \frac{D}{PTT} = \sqrt{\frac{tE}{\rho d}} \tag{3.17}$$

Where:
PWV is the pulse wave velocity
D is the vessel length
PTT is the pulse transit time
t is the thickness of the vessel wall
E is the Young's modulus of the elasticity of the arterial wall
ρ is the blood density
d is the vessel diameter

Geddes [39], in 1991, demonstrated that the Young's modulus of the elasticity of the arterial wall is variable and more precisely there is an exponential relation between the Young's modulus (E) and the pressure of the fluid (P).

$$\text{E} = E_0 e^{\alpha P} \tag{3.18}$$

Where:
E_0 is the zero pressure modulus
α is dependent of the vessels

Replacing the equation 3.18 in the Moens and Korteweg equation:

$$\text{PWV} = \frac{D}{PTT} = \sqrt{\frac{tE_0 e^{\alpha P}}{\rho d}} \tag{3.19}$$

In the last years, in literature several efforts have been made to find an accurate method for blood pressure estimation using PTT values. The relationship between BP and PTT has been subjects to years of reformulations. In 2004 a PTT-BP model was estimated, and the PTT was calculated as the delay between the R peak and the maximum peak of the PPG signal. The formula is:

$$\mathrm{BP} = \frac{A}{(PTT)^2} + B \tag{3.20}$$

A and B are constants which varies from subject to subject.
A linearized version of the Moens-Korteweg equation was proposed by Zhang [40]:

$$\mathrm{BP} = aPTT + b \tag{3.21}$$

Proneça et al [41] described a non-linear version of the BP-PTT relation:

$$\mathrm{BP} = a \ln PTT + b \tag{3.22}$$

Several other studies have integrated the linear BP algorithm with other influencing factors, such as heart rate[38]. An example is the study conducted by Whong and Poon [42] which have found the correlation between the BP, PTT and HR. The formula is:

$$\mathrm{BP} = aPTT + bHR + c \tag{3.23}$$

The constants a,b,c in each of these models are subject dependent and they can be found from a calibration step. Several calibration procedures are proposed in literature and each of them was tested in laboratory.
Each of these approaches and others have been successful in providing a reliable blood pressure measurement. But so far, these approaches are not widely used in the development of devices, but they are applied to some prototype devices or patents.
The method based on the PTT measurement for the estimation of the blood pressure explained above, requires the simultaneous acquisition of both ECG and PPG signals. To obtain the electrocardiogram it is necessary applying electrodes on the patient skin. In order to accomplish a simpler measurement without the use of the ECG signal, several studies were carried out. Furthermore, since PEP is variable and it cannot be calculated precisely, the result could be compromised.
Another approach based on the PTT calculation is the estimation of the BP from two different PPG signals. This method follows the real definition of PTT, i.e. the time delay for the pressure wave to travel between two arterial sites [42]. This technique, as the previous one, requires two sensors but the need of electrodes is eliminated. PTT is calculated as the time difference between two pulse waves generated from the pulse oximeters placed in different body locations. An example is given by [43] in which one sensor is positioned on the wrist and the other one on the fingertip.
However, in this case too, an algorithm of peaks detection is necessary to calculate the

time delay between to points of the PPG waves (Fig.3.18). The results obtained by many researchers are good in terms of accuracy of the BP estimation, but a great deal of progress is still required[44].

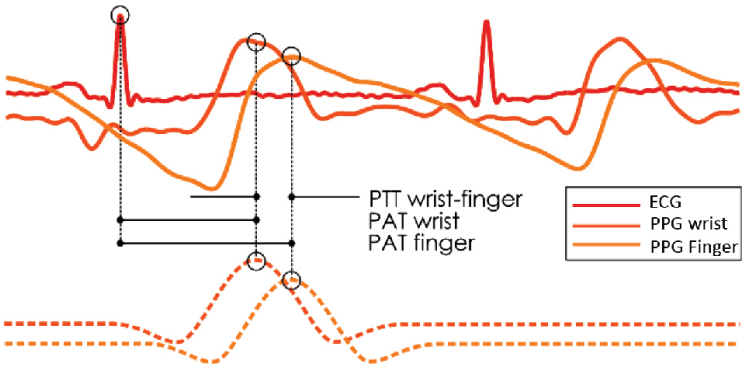

Figure 3.18. The figure shows the PTT calculation from two PPG signals (wrist and finger), and PAT calculation from ECG and PPG signals.[45]

3.4.4 Body temperature

Body temperature is an important indicator of human health and it is considered one of the oldest diagnostic parameters. The physiologic temperature usually varies between 36.6 and 37 °C. The body temperature is maintained constant by a mechanism of thermoregulation. In case of malfunctioning of the body system a temperature variation occurs.
An increase over 41 °C or a decrease below 33.5 °C can be due to injuries and in the most serious cases death. Several causes can induce changes in the normal range of the temperature, the most frequent causes are infection and shocks caused from bleeding, heart deficiency, cranial trauma etc. Thus, the temperature measuring assumes a fundamental importance in everyday life and in both contexts of medical care and wearable technology[46]. The most used temperature sensors in the market including thermistors, resistance temperature detectors (RTDs), thermocouples, semiconductor sensors and infrared sensor. Each of them measures temperature by sensing a variation in the physical property. In many wearable devices one of these types of temperature sensors is included. Together with other vital signs, such as HR, blood pressure, SpO_2, helps in providing real-time feedback information regarding the health status.

3.4.5 Galvanic skin response

As one of the most readily accessible human biofluids, sweat can be used to provide information about the health status of a person [47]. Sweat is of interest owing to its relative ease of noninvasive measurements. A variety of information can be extracted from sweat

because of its rich content of important biomarkers (electrolytes, small molecules, proteins) and its correlation with emotionally changes.
Nowadays, the analysis of biological information from sweat can be performed by wearable electrochemical sensing system [48]. To determine the sweat rate, biosensor based on the Micro-Electro-Mechanical Systems (MEMS) technology are used. Biosensor is a device composed of a bioreceptor and a transducer element. The role of the biosensor is to detect the concentration of a specific analyte. The bioreceptors are responsible for the recognition of the analyte of interest. When a biological molecule interacts with the bioreceptor, a chemical-physical changing occurs. These interactions produce variations of a different nature such as heat, light, electron flow, and they are converted by the transducer. The produced signal is proportional to the concentration of the chemical species that is analyzed. The nature of the signal produced by the biosensor depends on the transducer element used. Most of these systems base their quantitative measurement on amperometric and potentiometric methods. The analysis of biomarkers such as Sodium, Potassium, Lactate can help in the recognition of malfunctioning. For example, abnormal levels of sodium and potassium could result in hyponatremia, hypokalemia or dehydration. The development of biosensors is a not easy process because it requires a convergence of advances in materials, mechanics design, and specialized device architectures. This developing field involves innovative ideas that are not yet widely applied to wearable devices on the market, but in literature enormous progress has been made.
Sweating is controlled by the sympathetic nervous system which drives cognitive and emotional states on a subconscious level. The sympathetic nervous system (SNS) is one part of the autonomic nervous system, instead the other part is referred to the parasympathetic nervous system. The SNS stimulates the response known as "fight-flight-or-freeze" which is a physiological reaction in consequence of an event perceived as harmful. A stressful situation activates the sympathetic nervous system which prepares the body to respond to alarm. The changes in autonomic arousal trigger body responses: heart beats faster, the flow of saliva is inhibited, sweat secretion increases. When the sweat glands are activated, they secrete moisture. The unbalance caused by the positive and negative ions present in the secreted fluid generates an electrical current flow. The result is a measurable change in the skin electrical properties i.e. an increase in skin conductance (corresponding to a decrease in skin resistance). This phenomenon is called "galvanic skin response (GSR)".
The galvanic response of the skin, also called Electrodermal Activity (EDA) is the measure of the variations in the electrical characteristics of the skin following the sweating event. Further studies have highlighted the relationship between the GSR signal and mental states, such as stress, fatigue and involvement. The hardware required to record GSR signal is: two electrodes (usually applied to the fingers), an amplifier and a convertor which transform the analog signal to a binary data stream. The logic behind GSR is simple: a low voltage is applied and an electrical current is generated since the skin is a

good conductor. The current between the two electrodes is measured. Changes in conductivity are reflected by the variation of the resistance or its reciprocal, skin conductance expressed in microSiemens (μS).
According to the Ohm's law, the skin resistance is equal to the voltage applied, divided by the current that flows through it. Since the voltage is known and the current flow can be measured, the resistance is determined by:

$$\mathrm{R} = \frac{V}{I} \tag{3.24}$$

The raw GSR signal is composed of two main parts: skin conductance level (SCL) and skin conductance response (SCR). Figure 3.19 shows the main features of the GSR signal.

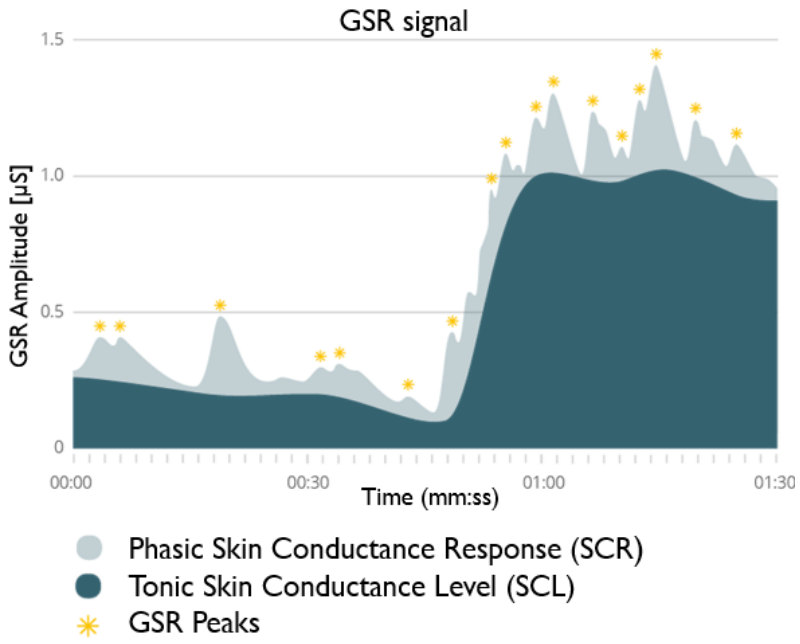

Figure 3.19. Phasic and tonic level of the GSR signal [51].

The SCL level, also known as tonic level, slowly varies [49]. The SCL trend depends on the subject, on its nervous system regulation and its skin hydration. The tonic level content is not informative, and it is used as baseline. To record the baseline, the subject must be in a relaxed position without emotional stimuli.
The SCR signal, also known as phasic response, has faster changes. These alterations are manifested as peaks and they occur after emotionally arousing events. Considering the phasic skin conductance response, the waveform is characterized by four metrics [51]:

1. Latency: it is the time needed to the onset of the SCR peak after a stimulus (usually 1-5 s).

2. Amplitude of the peak: it is the difference in amplitude between the stimulus onset and peak. The higher amplitude the more intense is the stimulus [50].

3. Rise time: it is the duration from onset of the phasic burst to peak. This parameter may vary from 1-5 s.

4. Recovery time: it is the duration from peak to the total recovery. Typically, the recovery time is long. In some cases the total recovery may not occur. Thus, it is measured as the time between the peak and a point of 50% recovery. The half-recovery vary from 1-10 s.

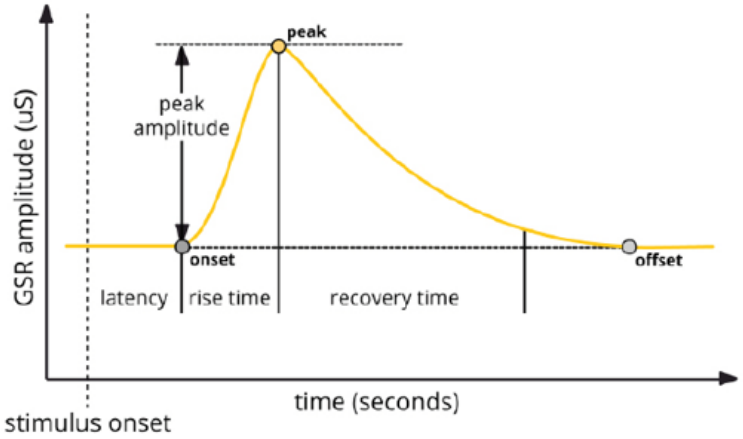

Figure 3.20. Characteristics of the galvanic skin response signal [52].

Figure 3.20 is a semplification of the real GSR signal because it is not completely flat before and after a peak. On the contrary, several GSR peaks can occur due to the changes in conductance levels or movement artifacts. This implies a more complex features extraction. All the explained features are used to model arousal event. The GSR amplitude is the feature more useful to recognize the onset of emotional event, as it was reported in [59]. Furthermore, rising time and the number of responses are parameters widely used to classify a SCR event. To better recognize changes on the GSR signal after the activation of the sympathetic system in response to events which perturbate the normal state of a person, post-processing is performed. Filtering to isolate the phasic tone and threshold to recognize the onset of an emotional event are usually applied on the raw signal.

3.4.6 Accelerometer

Fall accidents are a major safety issue and a perennial problem in many workplaces, especially in the construction and oil and gas industries. Several causes can be attributed to falls. Accidents very frequent are associated to elevated equipment (such as drilling, service rigs) or collision with moving parts. Furthermore falls can happen after an injury or illness due to other causes. Depending on where and when the worker falls, it may happen that the injury is noted too late to alert emergy responders. To avoid that the physical condition becomes even worse, in case of falls alert systems have been developed.
Few studies in literature have focused on detecting fall in several fields [54]. Most of these studies use inertial sensors (accelerometers and gyroscope) to monitor different types of motions. Thanks to the development of MEMS, these sensors are small and lightweight thus can be inserted easily in wearable devices. Another advantage is the ease of operation for monitoring activities. In fact, the monitoring of human body movements can be performed by extracting measures such as acceleration, velocity, orientation and gravitational forces [55]. The accelerometer-based fall detection system uses a three-axis accelerometer, a microcontroller and a communication device.

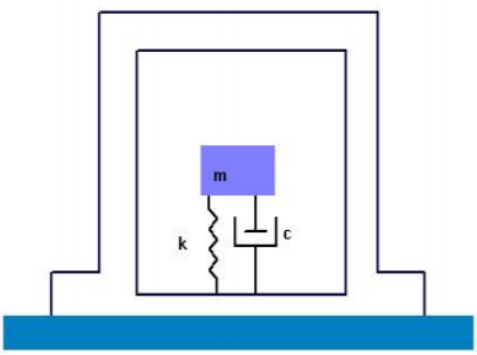

Figure 3.21. Accelerometer sensor approximated as a damped mass-spring system.

The accelerometer is an eletromechanical device which measures the acceleration of the body respect to its instantaneous coordinate frame. This sensor can be placed in different parts of the body, such as waist, wring, chest etc.
Most of the MEMS accelerometers base their measurement on the principle of inertia: the force against a known mass is measured in order to derive the acceleration. An accelerometer behaves as a damped mass on a spring. When an acceleration occurs, the mass is displaced and through a sensor this displacement is transformed into electrical signals. A small mass (called proof-mass) is etched into the silicon surface of the integrated circuit and it is suspended by small beams. The support beams act as a spring, the air trapped inside the integrated circuit acts as a damper providing a damping effect (Fig.3.21).

The principle of operation employs the Newton's second law of motion:

$$F = ma \tag{3.25}$$

Where F contains all real forces ($F_{applied}$, F_{spring}, $F_{damping}$) acting on the proof-mass. F is equal to the inertia force on the mass.
Accelerometers can be classified according to the functional principle used to convert the mechanical motion into an electrical signal. A summary is provided by the following table:

Technology	**Measurement**
Capacitive	Change in electrical capacity due to the distance variation of the capacitor armatures
Piezoresistive	The electrical resistance varies with the displacement
Strain gauge	The resistance variation of the strain gauge is caused by its length change
Piezoelectric	The mass compresses the crystal generating an electrical signal

The output from these devices can be used to calculate several parameters important to distinguish the motion of the body. In figure 3.22 the acceleration in x,y and z axis during a fall event are rapresented.

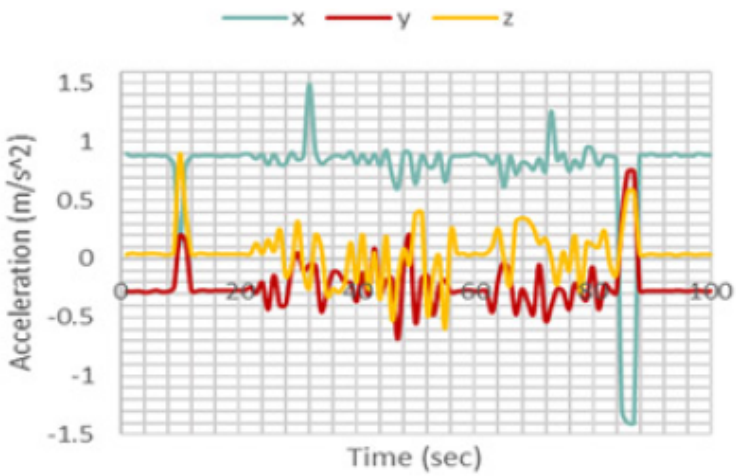

Figure 3.22. Accelerometer readings for a fall motion [56].

Since the acceleration is a vector, it is possible to measure both direction and magnitude. The magnitude can be used to extract information about the motion. To detect falling down, two main approaches can be used: machine learning and thresholds. Machine learning methods reguire big physical size and high computing cost. Consequently, this method has an high energy consuption. The advantage is the good accuracy in fall detection. Instead, threshold method has a lower accuracy but has low energy consuption and it does not require big memory for the computation. In fact threshold-based methods are more suitable for wearable applications.

The information extracted from the accelerometer sensor can be used, together with the other parameters explained previously, to monitor health status and stress levels of a person during working days in potentially dangerous environments. Considering all the information extracted from sensors, a complete picture of the health of a person can be obtained. The system implemented in this thesis includes all the technologies explained in this chapter.
In the table below are summarized the main parameters monitored by wearable devices and the sensors mostly used to extract them. Furthermore, typical applications of each type of device are mentioned.

Parameter	**Sensor**	**Application**
HR	ECG Pulse oximeter	Operators, elderly people, patients, sport
BP	Arm-cuff cuffless system	Operators, elderly people, patients, sport
SpO_2	Pulse oximeter	Operators, elderly people, patients, sport
EDA	GSR sensor	Operators, patients
T	Thermoresistor Thermocouple Integrated circuit Optical sensor	Operators, elderly people, patients, sport
Acc	Capacitive Piezoresistive Strain gauge Piezoeletric	Operators, elderly people, patients, sport

Chapter 4

State of the art

Monitoring of physiological signal using wearable devices is a widespread domain because of they provide great convenience in terms of prevention of health diseases. For this reason, the attention of many companies is focused on the development of systems which perform monitoring of vital signs such as those described in the previous section. In this section, several examples of wearable health-monitoring devices are discussed. In the last ten years there have been numerous efforts to develop devices to include on the big family of the wearable devices. A brief summary of the available systems present on the marked is given.

Equivital

Equivital has developed a chest belt for monitoring the health status of people operating in extreme environments [57].

Figure 4.1. Equivital [57].

The belt is placed close to the heart in order to acquire a single lead ECG. It is a non-standard lead, in fact V1 and V2 are not referred to a central reference but they form a bipolar lead. Equivital offers the first device with ATEX, IECEx, and FDA certifications so it can be worn in explosive environments. The body can perform continuous ECG signal measurements and extract information about heart rate. Other physiological parameters are also monitored such as body temperature, breathing rate and body position. The belt is made of a lightweight material in fact its weight is only 60g. In addition to the belt, a LifeMonitor is provided in order to store, process and send physiological data. The transmission unit is equipped with a Li polymer battery (18 hours of data transmission) and 8GB SD memory that allows data download and analysis. The device communicates via Class 1 Bluetooth version 2.1 to a phone or computer. From the hardware point of view, Equivital performs 10 bit of acquisition at a sample rate of 256 Hz for ECG acquisition and 25.6 Hz for respiratory signal.

QardioCore

QardioCore is the first electrocardiogram monitoring device in the world [58]. It was designed to provide continuous medical data monitoring and it is suitable for daily use. Qardiocore monitors the heart performing a single lead ECG. In addition to heart rate measurements, respiratory rate, skin temperature and activity are also provided. The device also performs heart rate variability measurements. The system includes a Lithium-Ion Polymer battery (1 day of autonomy) and a Bluetooth module version 4.0 to enable communication with iOS devices. The information about the physiological parameters are transmitted to an app which also displays the ECG waveform. QardioCore acquires 600 samples per second with 16 bit of resolution. The device is water resistant (IP65) and the materials are lightweight (130g).

Figure 4.2. QardioCore [58].

The advantage of chest straps is the accuracy in heart rate measurements. The reason why chest belts are more accurate is because the sensor is placed closer to the heart than other devices such as wrist-watches. Consequently, a better heart-beat signal is recorded, and better performance are guaranteed. A downside is the wearability, especially in case of extended use. A further disadvantage is the inability to provide an accurate information about the percentage of oxygen saturation. In literature, several attempts are being made to include pulse oximeters in chest straps.
An example is a chest strap covered by patent [59] that measures heart rate, blood pressure and pulse oximetry. The invention includes electrodes for ECG recording, a pulse oximetry and a processing unit that post-elaborate data. The system also includes a wireless transmitter which send data to an external device.

Biobeat

The Biobeat is a wristwatch whose core functionality is to measure physiological parameters with the added value of being comfortable and easily wearable [60]. The wrist-watches are devices especially used in daily activities (walking, running, sleeping). Furthermore, they can analyze data and give indications about the performance during sport activity.
Biobeat includes a pulse oximeter which provides SpO_2 measurements and HR monitoring. It also includes a galvanic skin response sensor to recognize emotional alterations, a body temperature sensor and an accelerometer. The device is equipped with Bluetooth communication and a user-friendly application for both IOS and android systems. The sensor device weights 100 g and it is suitable for patients of all ages and workers. It has a good battery life, up three days with continuous use. The range permitted for HR measurement is 35 to 250 BPM and for HR variability 0.15-0.4 Hz.

Figure 4.3. Biobeat watch [60].

The description of these WHDs brought out the need of a WHD which can monitor more vital parameters simultaneously and that can be used in hazardous environment. For this reason, the objective of this work is the experimentation of a more complete wearable device providing more attention to the application in Oil&Gas industries.

Chapter 5

Trade-off and baseline definition

After a brief review of the state of the art, this section provides the baseline definition of the solution implemented in this thesis. The general requirements of a wearable device have been described in section 3.2 and are summerized as follows:

- *Comfortable*
- *Robustness*
- *Accurate*
- *Continuous operation*
- *Low power*
- *Cost-effectiveness*

These requirements have been considered to guide the project development. The goal of the proposed prototype was the monitoring of the health status of workers in heavy industries. Considering all the associated risks involved in dangerous enviroments, wearable technologies can certainly make a valid contribution by monitoring continuously vital parameters. To reach this aim the design goals taken as benchmark were:

1. Lead I ECG
2. Heart rate
3. Oxygen saturation
4. Skin temperature
5. Pulse transit time

6. Galvanic skin response
7. Body motion
8. Wireless communication

Considering the technologies taken into account, all the requirements are impossible to be satisfied at the same time. At this point, considerations about the device configuration must be introduced in order to have a complete picture. Considering that this device was intended for a particular application, like oilfield workers, the configurations considered were only two: wrist bracelet and chest belt. It was assumed that other types of configuration cannot be suitable for this type of application. Since the body position is different, not all the parameters can be measured. Requirements 2, 4, 6, 7, 8 can be satisfied from both the configurations. Since HR parameter can be extracted from ECG signal and also from PGG signal this parameter does not involve any restrictions. To measure skin temperature only a small integrated circuit sensor is required and it can be positioned on both the locations. Of course, the sensibility of the temperature measurement changes depending on the positioning.
The GSR measurement is generally carried out using two electrodes attached to the skin. Thus, the two solutions can include a GSR sensor. Regarding the body motion, an accelerometer acts as fall detector measuring the accelerations along three axes. Since the arms perform highly complex movements, the chest is the best location to place an accelerometer-based fall detection system. To perform the ECG acquisition, a differential measurement must be done. Thus, the chest belt is more suitable to record ECG signal compared to the wrist. The parameters 3 and 5 require more attention. To get information about the oxygen saturation of a person, pulse oximeter must be used. The common application is the finger-tip, but other solutions, including chest belt and wrist bracelet, have been implemented in the state of the art. Regarding the estimation of the blood pressure, as said in section 3.4.3, it can be performed by using synchronized PPG and ECG waveforms. To implement this solution, both ECG and pulse oximeter are necessary. Consequently, chest belt is more suitable for this requirement. In this thesis PTT is measured in order to preparing the ground for future BP estimations.
The configuration taken as benchmark is the chest belt, because allows to satisfy more requirements.
Since the study conducted in this thesis is an initial stage of the design process, all the sensors have been positioned on body locations that are usual for that specific technique. For example, the GSR electrodes have been positioned on two fingers, oxygen saturation has been measured from the finger.
Regarding the wireless connection, all wearable devices communicate with a central unit (smartphone, PC). Thus, a summary of the main wireless technologies that could be suitable for this project is performed.

Chapter 6

Prototype development

The aim of this thesis is the development of a prototype which is able to record biological signals and process them in order to extract useful information. Basically, the project consists of five tasks: sensor interfacing, data reading, signal processing, parameter extraction and wireless communication (Fig.6.1).

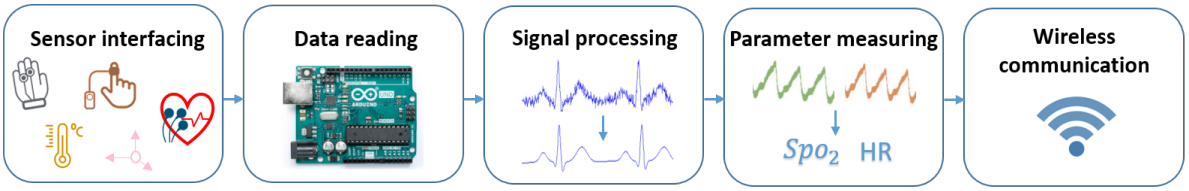

Figure 6.1. Main steps of the prototype development.

The prototype includes the following sensors:

1. *Maxim Integrated 86150*: electrocardiogram and pulse oximeter sensors are included in the package. It allows both ECG and PPG signals to be recorded simulataneoulsy in order to monitor heart functioning and oxygen saturation. Furthermore, from these two signals is possible to obtain an estimation of BP by measuring the PTT value.

2. *Maxim Integrated 30205*: integrated circuit which provides body temperature measurement.

3. *Seeed Studio Grove GSR*: measures the skin electrical conductance by attaching two electrodes on the human skin.

4. *MPU 9265*: MEMS-based accelerometer which measures the acceleration along x,y,z axes.

6.1 Hardware design

All sensors are interfaced with Arduino UNO, which is a microcontroller board based on the ATmega328. Data are processed and converted into digital form by an Analog-to-Digital Converter (ADC) included into the board. The specifications are:

- Operating voltage : 5 V
- Digital I/O Pins : 14
- Analog Input Pins : 6
- DC Current per I/O Pin : 40 mA
- Clock Speed : 16 Mhz

Sensors are connected to the power, ground, clock(SCL) and serial data(SDA) of Arduino. Digital sensors, i.e. MAX86150, MAX30205 and MPU-9265 communicate to Arduino with I^2C protocol. It requires comunication between a master (microcontroller) and multiple slave devices (sensors). Since multiple sensors are connected to the same SDA and SCL lines, in order to distinguish them each sensor has a specific 7 bits adddress. The GSR sensor is connected to one of the analog PINs of Arduino.

6.1.1 MAX86150

The MAX86150 is an integrated sensor module which includes an electrocardiogram and a photoplethysmogram, allowing a trio of functions for human vitals monitoring [61]. It is the only sensor module available to record both PPG and ECG signals allowing to determine the SpO_2, HR and PTT values. Furthermore, it has been selected because it allows a good tradeoff between performance and simple hardware to be reached. The breakout board contains both the ECG touchpad and the external Qwiic connector. MAX86150 on itself is 3.3mm x 5.6mm x 1.3mm and ships with an Organic Land Grid Array (OLGA) package. The sensor operates on a 1.8V supply voltage and it includes a separate power supply for the LEDs of the pulse oximetry (typically V_{LED} = 3.3 V).
One of the two components of the bio-sensor module is the reflective pulse oximetry. Its hardware includes two LEDs (RED and IR) and one photodetector, both on the same side of the sensor surface. The pulse oximeter subsystem has low-noise electronics with ambient light rejection (ALC) which corrects and eliminated the ambient light, thus increasing the effective dynamic range. Furthermore, a discrete time filter to reject the line interference (50 Hz) is also included.
The subsystem is composed of a continuous-time sigma-delta ADC with 19-bit resolution. Modern sigma-delta ADC offers high resolution and integration, and low power

consumption. The data rate of the convertor can be selected from 10 to 32000 samples per second. The MAX86150 integrates LED drivers to modulate LED pulses (from 50 to 400 μs). The current can be programmed from 0mA to 100mA. The two LEDs have different wavelengths, RED λ= 660, IR λ= 880. The sensor provides a proximity function which role is to reduce red light emission in order to save power when the sensor is not in use (the finger is not placed on the sensor). This function can be enabled by setting a dedicated register. Depending on which measurement is wanted to be carried out, it can be selected only one LED for HR or two LEDs for SpO_2.
The single-lead ECG subsystem comprises several stages (Fig.6.2). The system is optimized for using of dry electrodes, usually in Ag/AgCl, which convert ionic current into electronic potential.

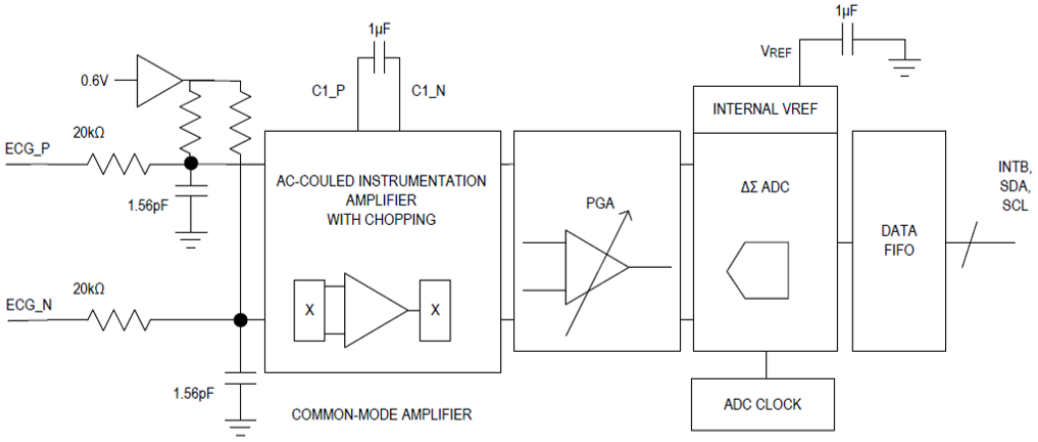

Figure 6.2. ECG block diagram [61].

The voltage is in the range of 1-5 mV and it is also accompanied by interference caused mainly by the capacitance between power lines in the equipment and around the patient. The input signal has a small AC voltage and it is superimposed by a large AC common-mode component (about 1.5 V) and a large variable DC component. The amplitude of the DC offset depends on the electrodes. This offset is due to the presence of bias currents generated by non-ideal op-amp. In order to overcome these problems, an Instrumentation Amplifier (INA) is interfaced with the electrodes. It is a differential amplifier which has the following characteristics: high common−mode rejection ratio (CMRR), high input impedance, low output impedance, low offset drift and low level of self-generated noise. The second stage is a Programmable Gain Amplifier (PGA), which facilitates high SNR. A high-pass filter is included on the chip in order to eliminate low frequency components such as baseline wander and motion artifacts. The gain value can be selected by setting dedicated registers. After the filtering process, analog signals are

converted into digital signals by an 18 bit ADC. The data rate can be programmed from 200 to 3200 sps. The most important aspect of the MAX86150 sensor is the possibility to synchronize the collection of PPG and ECG signals, thus ensuring the correct measuring of the PTT for the BP estimation. The sample rates of the two subsystems are selected from two different registers, but the PPG sample rate by default is programmed same as that ECG (if supportable).
The MAX86150 incorporates an internal memory of the type "first in first out (FIFO)". Samples are stored in the 32-deep FIFO memory and their location depends on which elements are activated (red LED, infrared LED, ECG). Each element takes three bytes in the memory. The ECG data are in bipolar two's-complement format. To read one complete sample, the data register must be read a number of times given by the number of active elements multiplied by the number of bytes (three). MAX86150 sensor features an I^2C protocol which permits the communication to and from the module. I^2C is a serial communication protocol that transfers data along a single wire, called serial data (SDA) line. A clock signal is carried by a line called serial clock (SCL). The I^2C bus consists of one master and one slave. The microcontroller is the master which drivers the clock signal and transfers data on the bus. The MAX86150 sensor is the slave and responds to the master.

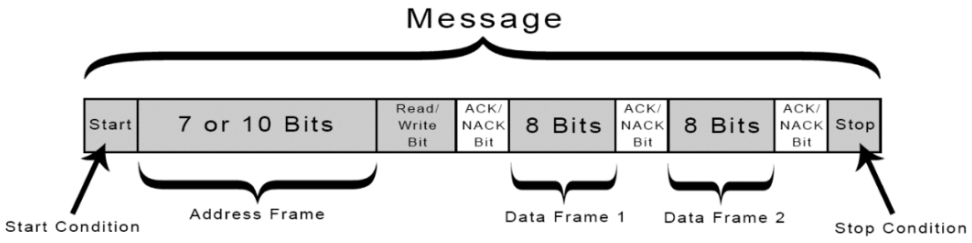

Figure 6.3. Typical message structure with start and stop condition, ACK and NACK bits and data frame [62].

The communication between master and slave initiates when the master sends the start condition (Fig. 6.3). This condition is represented by the switch of the SDA line from a high voltage to a low voltage level while the SCL is high. After that, the master transmits the proper slave address flowed by 8 bits long data. When all the data have been sent, the master sends a stop condition to the slave. The stop condition is the switch from a low to high level of the SDA. Each sequence is followed by a bit called acknowledge (ACK) or no-acknowledge (NACK). It is received an ACK bit if the address or data frame was successfully sent. On the contrary a NACK bit is returned. SCL and SDA operate in two different ways: SCL only as an input, SDA as an input and an open-drain output. A pullup resistor is required on SDA.

6.1.2 Grove GSR

The prototype developed in this thesis includes a sensor to measure the galvanic skin response. The sensor used is the Grove GSR (Seeed Studio) [63]. The basic functioning of the sensor is the detection of arousal by simply attaching two electrodes in Nickel in two fingers. As explained in Section.3.4.5, the GSR method allows to detect emotional activity due to the activation of the sympathetic nervous system. Grove GSR sensor measures the skin resistance (Ohm) and it will be converted into conductance (Siemens) during the post-processing stage. It is an analog sensor, so data are read by the analog input of Arduino. Arduino UNO contains a multichannel 10-bit analog to digital converter. Thus, the GSR signal is measured by voltage and it is represented in the Serial Port as an integer value between 0 and 1023. The Arduino resolution between readings is 5 Volts/1024 units. In this work, it was provided a voltage of 5V. With the aid of a screwdriver, the resistor was adjusted in order to have a serial output of 512 (half value of the ADC output full range).
Regarding the sensor hardware, it includes two Voltage Follower and an Op-amp subtractor. A Voltage Follower is an Op-amp circuit which does not provide any amplification to the signal, so it has a voltage gain of 1. The output voltage follows the input voltage. Thus, the input and the output have the same value. This Op-amp provides only buffering and it has a very input impedance. Instead, an Op-amp subtractor provides an amplification of the two input signals. Referring to the schematic in Fig.6.4, the two Voltage Follower are on the left and the Op-amp subtractor is on the right.

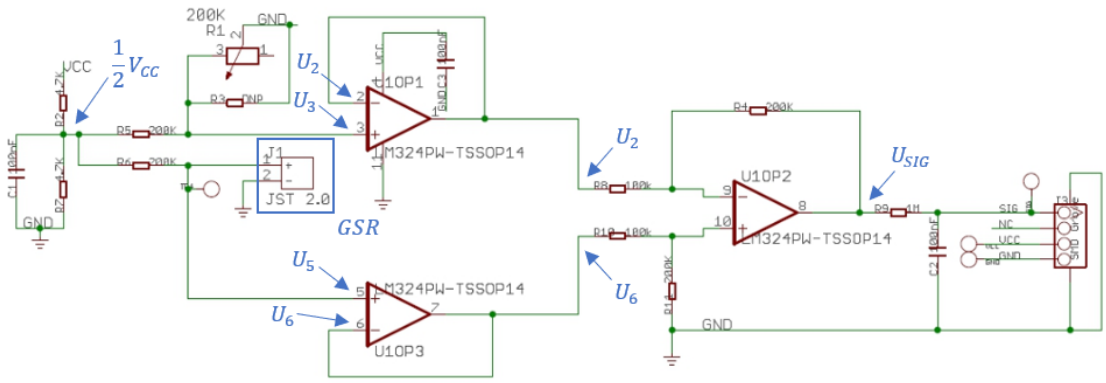

Figure 6.4. Electric schematic of GSR grove sensor [63].

The main steps to determine the skin resistance, are explained in the following mathematical expressions.

Since the resistances R_2 and R_7 have the same value, the voltage is expressed as:

$$R_{27} = \frac{V_{cc}}{2} \tag{6.1}$$

The presence of the voltage follower permits to assume: U_2=U_3 and U_5=U_6. Considering R_1 and R_5 equal, the voltage is:

$$U_3 = \frac{V_{cc}}{2}\frac{R_1}{R_1 + R_5} = \frac{V_{cc}}{4} = U_2 \tag{6.2}$$

The voltage at the point U_5 is:

$$U_5 = \frac{V_{cc}}{2}\frac{R_{GSR}}{R_{GSR} + R_6} = U_6 \tag{6.3}$$

Where R_{GSR} indicates the skin resistance. According to the characteristics of Op-amp subtractor: $\frac{R_4}{R_8} = \frac{R_{11}}{R_{12}}$ and the signal voltage is measured as follows:

$$\mathrm{U_{sig}} = 2(U_5 - U_3) = 2(\frac{V_{cc}}{2}\frac{R_{GSR}}{R_{GSR} + R_6} - \frac{V_{cc}}{4}) \tag{6.4}$$

The output full range of the 10-bit ADC is 1024.

$$\frac{U_{\mathrm{sig}}}{V_{\mathrm{cc}}} = \frac{SerialPort}{1024} \tag{6.5}$$

The final result is the skin resistance expressed by:

$$\mathrm{R_{GSR}} = R_6\frac{2 * SerialPort + 1024}{1024 - 2 * SerialPort} \tag{6.6}$$

This formula is used to convert in Ohm the value read from the serial port (ADC counts).

6.1.3 MAX30205

MAX30205 is the sensor used to measure body temperature. This sensor uses a sigma-delta ADC to convert temperature to digital values. The sensor specifications are:

- Operating voltage: 2.7-3.3 V
- Accuracy: 0.1°C (37°-39°)

- Resolution: 16-Bit (0.00390625°C)
- Operating supply current: 600 μA

Also in this case, I^2C is the protocol used to communicate with the master device. An over-temperature alarm can be setted if the temperature is over the accettable range. During the reading process if a change in temperature occurs it is ignored until the reading process is finished.

6.1.4 MPU-9265

MPU-6295 is a multi-chip module (MCM) including a 3-axis accelerometer used to monitor the motion of a person. This sensor has a dimension of 3x3x1 mm providing a very small package. In addition to the accelerometer, also gyroscope and magnetometer are included but they will not be used in this project. The sensor uses separate proof masses for each axis. When the acceleration along a specific axis occurs, it causes displacement on the corresponding proof mass. The displacement is detected by capacitive sensors. The accelerometer is developed using the CMOS-MEMS fabrication process. Thermal drift are limited by the MPU-9265 architecture.
The sensor measures 0g on the x-y axes and +1g on the z axis, if it is positioned on a flat surface. Three 16-bit ADCs for providing digital outputs. The full scale range is adjustable ($\pm$2g, $\pm$4g, $\pm$8g or $\pm$16g) and it is setted at $\pm$4g. The communication is performed by the I^2C protocol. The MPU-9265 always acts as a slave when communicating to the system processor. The accelerometer features are:

- Operating voltage: 2.4-3.6 V
- Operating current : 450 μA
- Sleep mode current : 8 μA
- User programmable interrupts
- Programmable digital filters

6.2 Firmware

In this section the main steps of the firmware are analyzed. The explanation is referred to the MAX86150 sensor in order to provide an example, but the algorithm architecture is similar also for the others digital sensors used in this thesis.

The ATmega328 firmware has been designed to perfom the following operations: data acquisition, data processing and data transmission. Data is exchanged with the PC over microcontroller UART(Universal Synchronous Asynchronous Receiver-Transmitter) peripheral. A dedicated RS232-USB adapter makes it possible to interface with a modern laptop. The Arduino RX (receiving) pin receives samples at a precise rate. The TX (transmitting) pin is responsible for send data packets.
The algorithm is based on the use of interrupt signals which are generated from events by hardware or software. The processor responds to the interrupts by executing a specific code sequence. In the proposed firmware, an interrupt has the priority over a task. Basically, two different interrupts are used in the algorithm:

- *UART RX INT*: interrupt generated when a command is inserted by the user.
- *DATA READY INT*: interrupt generated when the sensor INT pin goes to low level.

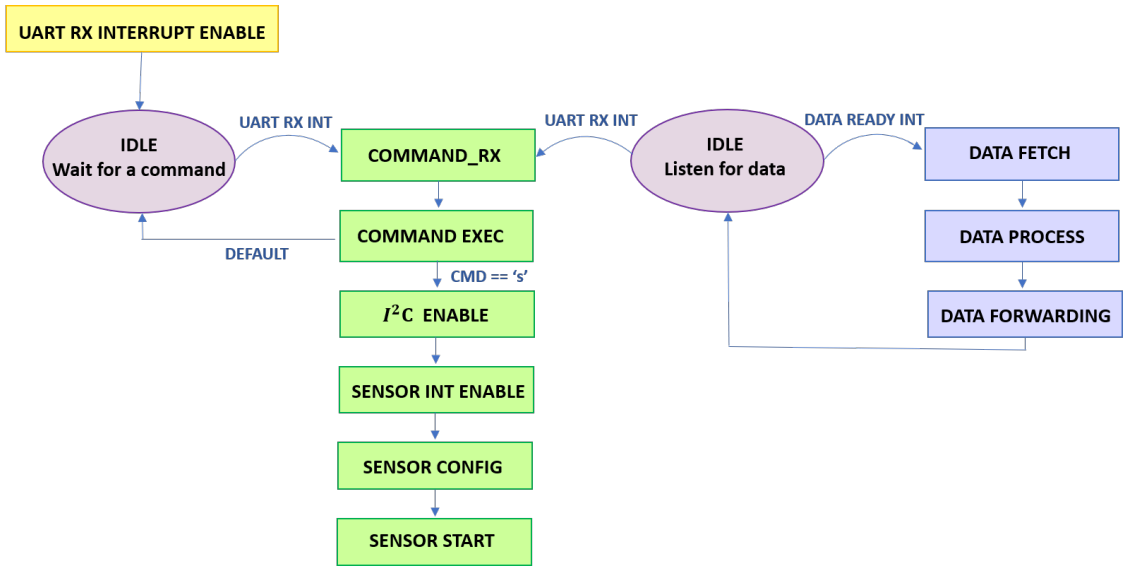

Figure 6.5. Flow chart of the workflow executed by the firmware during a sensor reading.

The general structure of the firmware is shown in Fig.6.5. The first step is to enable the UART RX INT. The processor remains in a state of ”sleep” if no interrupts occurs. The processor is sensible to an interrupt generation only in the idle state. In particular, two sleep modes (IDLE) are used in the algorithm: ”wait for a command” and ”listen for data”. In the first case, the processor is triggered only when an UART RX interrupt is generated, thus after the insertion of a command by the user. Depending on which command is sent, different tasks can be performed. If the letter 's' is received the operations

perfomed are: I^2C and sensor interrupt are enabled, sensor configuration and sensor start. The sensor configuration includes the settings of several registers. Some of these registers control the FIFO configuration which defines parameters such as sample length, FIFO depth in number of samples, free space before an interrupt generation, FIFO buffer overflows etc. Other registers define the sensor configuration: sample rate of ECG and PPG sensors, LED pulse width control, current pulse amplitude, ECG amplifier gain. Furthermore, by setting a dedicated register, if data flow need to be reduced, adjacent samples can be averaged on the chip.
The MAX86150 includes also a "proximity function" that can be enabled during the sensor setup. This function allows to save power by reducing visible light emission when no object is close to the sensor. If this function is enabled, the sensor generates an interrupt when the light detected from the photodetector exceeds a pre-setted threshold.
The MAX86150 is configured to generate interrupts whenever the FIFO is almoust full. This condition has been configured to be triggered when the remaining positions are 15. The maximum number of samples contained in the FIFO memory is 32. After the sensor activation, the processor waits for an interrupt arrival.
In this second case both interrupts (UART RX and DATA READY) can trigger the processor. In case of UART RX INT generation, the processor receives a command and executes it. If DATA READY INT triggers, the following operations are executed:

- *Data fetch:* data packet with a predefined size is read from the sensor data register. The packet size is given by the formula:

$$\text{Packet-Size} = 3 * ActiveDevices * FIFOdepth \tag{6.7}$$

  Where:
  3 is the number of bytes for each element
  Active devices is the number of elements active, for example if IR led, RED led and ECG are active, the number of elements is 3.
  FIFO depth is the maximum number of samples that FIFO can hold up

- *Data processing:* once a packet is read, data are processed in order to convert them into the right format. After the conversion, PPG data are expressed as 32-bit integers, instead ECG samples as signed 32-bit integers.

- *Data forwarding:* the last step is the data packet transmission.

At the end of these steps, data are ready to be processed. Since the sensor reading process is the same for all digital sensors which communicates through I_2C protocol, the general architecture of the proposed firmware is applied to the other digital sensors.

6.3 Software

This section illustrates the algorithm development which aim is to process signals in order to extract the physiological signs of interest. All the algorithms have been implemented in Python environment. Regarding the ECG, PPG and temperature signals data are collected for 1 minute and saved in dedicated vectors. Because of the different nature of GSR and acceleration signals the recording is longer.
Afterwards, the signals are processed and the required parameters are calculated offline. Signals taken from the body are susceptible to several types of artifacts. All signals are firstly filtered because a good signal quality is an important requirement for the next steps of the analysis.
Regarding the PPG signal, the first step is the filtering. After that, in case of very noisy signals that can compromise the final result, outliers are removed in order to have a better parameters estimation. Finally, R and subsequently SpO_2 values are derived. From the PPG signal, also the HR parameter is measured.
Similar steps are applied to the ECG signal. First, filtering and outliers removing are performed in raw signals. After, HR is measured. Furthermore, from the two synchronized ECG and PPG signals, an algorithm to determine PTT is developed.
The temperature values are simply averaged since the body temperature is quite constant during the brief time of observation (1 minute).
The output of the galvanic skin response is converted from ADC counts to resitance values by applying the formula reported on the datasheet. After filtering, signal is processed to recognize the onset of a stimulus.
Accelerations values are processed in order to extract the features useful to distinguish the motions of a person and in particular detect falls.

6.3.1 PPG signal processing

The algorithm is applied to the signal generated from the reflective pulse oximeter included in the MAX86150 sensor. PPG signal is processed in order to extract R and subsequently the SpO_2 parameter. Furthermore, HR is also extrapolated from PPG signal in order to compare it to the HR calculated from the ECG signal. The main steps of the algorithm are presented in Fig.6.6.
The typical condition of the MAX86150 acquisition is 1 minute at a frequency of 200 Hz. Data are taken placing the pulse oximeter on the finger in order to have the best signal quality.
Both signals are composed of an AC component superimposed to a large DC component. More details about the physiological aspects of the PPG signal are given in section 3.4.2. It should be specified that DC component is not constant, but it has a slowly varying baseline. Generally, the first samples of each record are excluded because they are subject to errors. At this point, a detailed explanation of the post-processing is given.

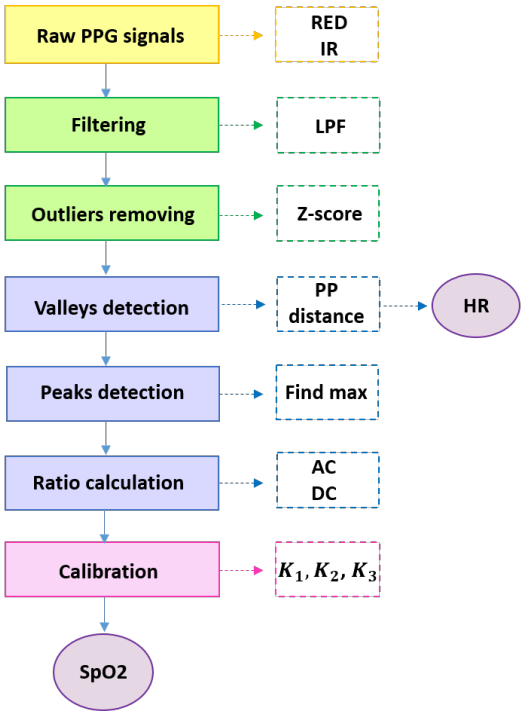

Figure 6.6. Main stages of algorithm developed to measure HR and SpO_2 from the PPG signal. The different colours represent: yellow=acquisition, green=processing, blue=features extraction, pink=calibration process, purple=parameters calculation.

Firstly, a low-pass filter (LPF) is performed because both RED and IR signals are affected by high frequency noise. The LPF is an infinite impulse response Butterworth filter. It has been chosen a Butterworth filter because it allows to obtain good performance with a low complexity of implementation. The implemented tenth-order filter has a cut-off frequency of 10 Hz. The filter is applied in both the forward and reverse directions in order to have a zero-phase distortion on the filtered signal. Results are shown in Fig.6.7 and 6.8.

During the data acquisition process, measurement errors can happen. These errors are mainly due to motion artifacts and are commonly called “outliers”. Outliers are values that deviate from an overall pattern. Since the quality of data is an important factor for the success of the algorithm, outliers detection is a necessary step. This process denotes the identification and removal of those data that differ significantly from the normal profile of a certain measure. Several solutions can be applied in order to identify unusual values in a database. Graphical methods such as scatterplots, boxplots, histograms can highlight outliers. These types of methods are less automatable, and they require the analysis of the graphs to recognize abnormal values.

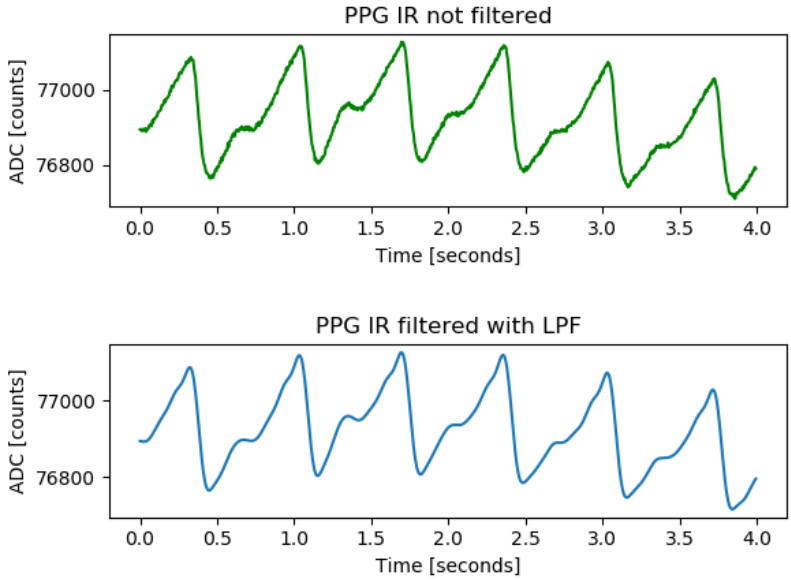

Figure 6.7. Signal generated from IR LED before and after LPF. The signal amplitude is expressed as ADC counts and its value is around 76900 counts. This value changes depending on the subject.

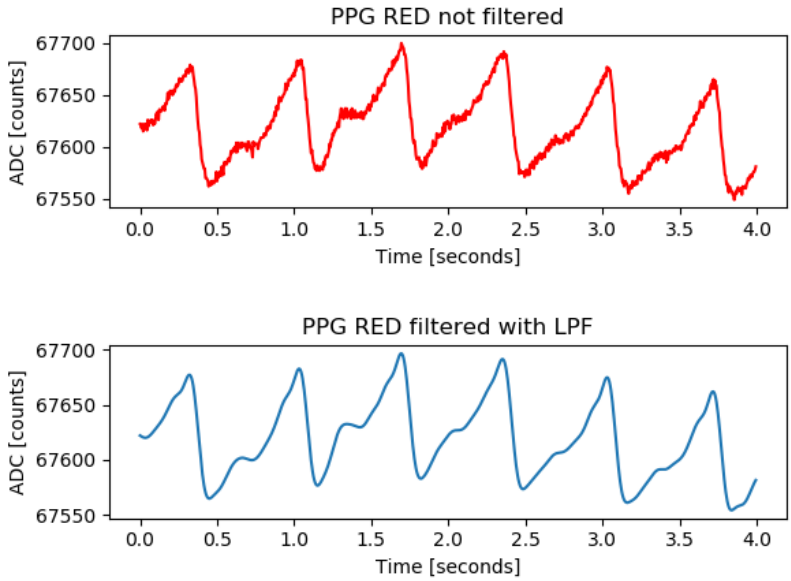

Figure 6.8. Signal generated from RED LED before and after LPF. The RED amplitude is around 67630 counts and it is smaller than the IR amplitude.

The approach used to detect outliers is the Z-score calculation. This method quantifies the unusualness of a dataset when data follow the normal distribution. It is based on the relationship between the mean and standard deviation. Specifically, Z-score is defined as the number of standard deviations that are above the mean value of the data observed. Values with Z-score away from zero are classified as outliers. As far away from zero, the more unusual they are. The Z-score method is computed using a specific function in Python. Once Z-scores have been calculated, a cut-off value was chosen in order to find outliers. The threshold is not constant, but it depends on the data quality. If the dataset is composed of values which differ significantly from the normal profile, the threshold will be small. Otherwise, if all values are similar the threshold will be higher.
In order to calculate the parameters of interest without sources of errors, the next step is to remove the outliers identified. Starting from the whole dataset, the subset which has the highest number of consecutive samples with a Z-score below the threshold is identified. The portion of signal selected by this procedure will have no values different from the normal distribution (Fig.6.9). Since measurements error happen at the same time on both IR and RED channels, this procedure is performed only on the IR signal. At the end of the process, the same subset (with identical samples lenght) is selected from the RED signal.

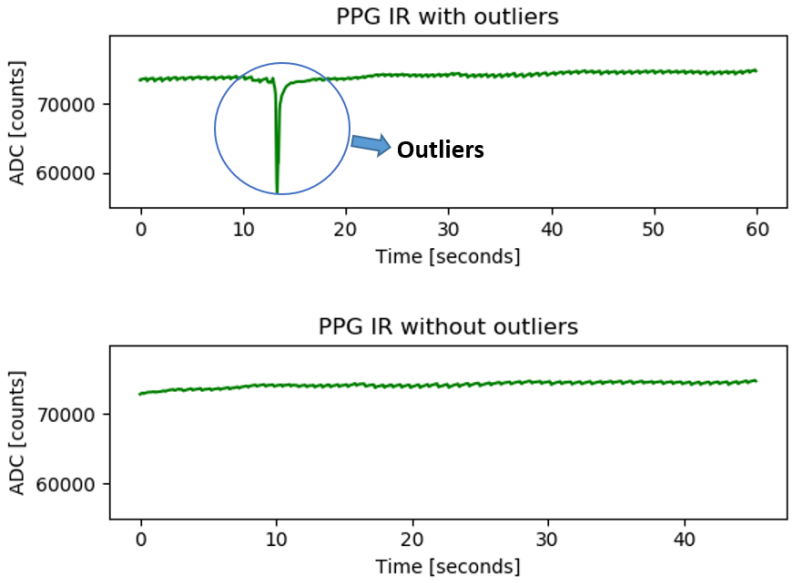

Figure 6.9. PPG IR signal before and after outliers removing based on the Z-score method. The process has identified a portion of signal which starts approximately at t=15s of the original IR signal. This subset has the highest number of consecutive Z values that are below the threshold.

The rest of the algorithm represents the core of post-processing phase. After removing outliers, peak and valley recognition is applied to the signals.

Valleys are detected using a simple algorithm that exploits a Python function, called "findpeaks", which finds all local peaks by comparison of neighbouring values. Since this function is implemented to recognize maximum values, the first step is the inversion of the signals. Consequently, all the minima are considered as maxima. The function requires some peaks specification. The arguments specified into the function are:

- *Height of peaks:* minimal height acceptable to recognize a peak.
- *Minimal distance between neighbouring peaks:* it was chosen a number of samples which changes depending on the sample rate and considering a distance physiologically possible (normally in the range of 60-90 bpm).

At this point, before proceeding with the SpO_2 measurement, heart rate can be easily estimated by using just one signal, IR for instance. Starting from the valleys location, the distance (PP) between two successive minima is measured. Including the sample rate, HR expressed in beats per minute(bpm), is calculated by the equation 3.11. In Fig.6.10 the PP distance is indicated.
The HR calculation is performed in order to compare it to the one extrapolated from ECG. For the heart rate calculation, and subsequently for the SpO_2 measurement, the distances out of the physiologic range are excluded because considered as errors of the procedure. For the sample rate used, distances of about 80 samples or 300 samples are not considered. With a view to ensuring greater accuracy for the SpO_2 measurements, it is necessary to make certain that minima of the two signals belong to the same cardiac cycle. To verify the alignment of the channels, the two lists of valleys are analyzed. The procedure discards minima which differ by more than 20 samples. This difference in time corresponds to 20/Fs, if the sample rate is setted at 200 Hz the lag corresponds to 0.1 ms.
The algorithm for the estimation of SpO_2 starts with the calculation of the R parameter. Basing on the theory (section 3.4.2), the DC component is due to the light absorption of non-pulsatile blood, instead the AC component is attributed to the pulsatile blood. The DC and AC components of the two LEDs have different amplitudes. In order to normalize them the ratio is determined by the formula:

$$R = \frac{\frac{AC_{red}}{DC_{red}}}{\frac{AC_{ir}}{DC_{ir}}} \tag{6.8}$$

The individuation of the AC and DC components is performed by several steps applied to each period (duration of one cardiac cycle) of the two signals. The first step is the detection of peaks. Maximum of a period is searched between two successive minima (previously identified). Having the reference points is possible to proceed to the AC component measurement. To explain the procedure, an example is given.
With reference to Fig.6.10, the maximum is indicated with the number 2, instead the two minima are indicated with the numbers 1 and 3. The AC component is the distance

between the point 2 and a point (4) identified by the intersection of a line parallel to the y axis and a line between 1 and 3 points. Finally, the DC component is represented by the amplitude of the point 4 (from origin of the axes). Once the AC and DC components for a specific period have been calculated, the Ratio is estimated using the formula 6.8.

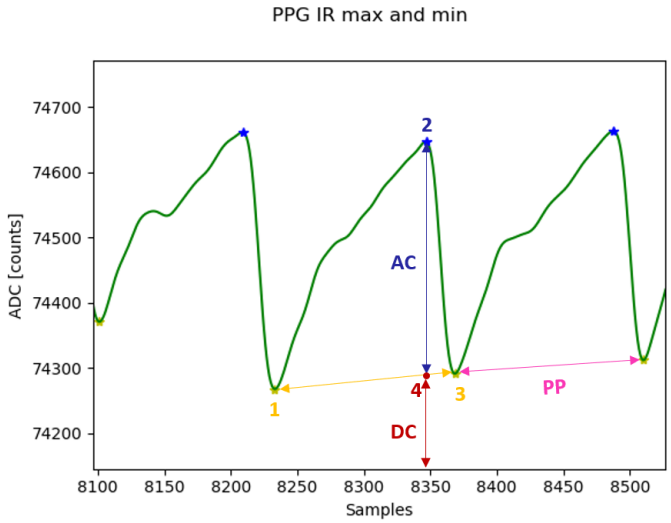

Figure 6.10. Rapresentation of: PP distance between two minima, AC and DC components of the PPG IR waveforms.

During this process, if a waveform is particularly affected by noise, a further check is made: the difference between vertical positions of two successive minima is compared to a pre-set threshold. This threshold is chosen considering the average trend of the signal. If the quality of a specific waveform is not sufficient (for example due to a pressure variation on the pulse oximetry), it is discarded and the Ratio calculation is not performed.
At the end of the R calculation process, the R values of each period are averaged in order to have a single value representing the whole acquisition interval.
Finally, R is linked to the SpO_2 by a relationship that differs from sensor to sensor. Maxim Integrated provides the formula 3.15 in which K_1, K_2, K_3 coefficients have to be determined through the calibration process. This formula is applied to determine the SpO_2 and the calibration phase is explained in the following subsection.

Pulse oximeter calibration

The aim of this procedure is to find a relationship between R values calculated by the algorithm developed in this thesis, and SpO_2 values read from a reference pulse oximeter.

The sensor chosen for this procedure is the "*Beurer PO 30 pulse oximeter*. It performs oxygen saturation and HR measurements. This sensor is a medical device particularly suitable for persons with pulmonary diseases and heart failure.

Figure 6.11. Beurer PO 30 pulse oximeter.

Specifications	**Values**
Measurement	SpO_2 0 - 100 % HR 30 - 250 bpm
Accuracy	SpO_2 70 - 100 % $\pm$2 % HR 30 - 250 bpm $\pm$2 bpm
LED	Red and infra-red

To correlate the sensor output (SpO_2) with the input (R values) it is mandatory the synchronization of the two measurements. In order to obtain a high accuracy result, the test must be repeated several times and on different subjects. In this thesis, two subjects have been selected. The test is the same for everyone and it is structured as follows:

1. *Subject preparation:* the subject wears the reference sensor on a finger of the right hand and the MAX86150 pulse oximeter on the other hand.

2. *Data collection:* at the beginning of the test, the subject breathes air with a normal oxygen content. The SpO_2 values indicated by the reference pulse oximeter are within the normal range (98-99%). After one minute, the subject breathes into a bag through a mouthpiece. The content of oxygen inside the bag is reduced incrementally, with the increase of CO_2 production (waste product of metabolic process). The consequent de-saturation effect is subject dependent because it varies according to the respiration rate. The SpO_2 values reported by the reference sensor start to decrease gradually.

3. *Calibartion curve:* samples are collected for four minutes. The scatter plot of the R values with respect to the reference SpO_2 is obtained. A best curve is fitted to the collected samples using regression method. The required calibration coefficients are the output of the system.

Despite a careful attention has been paid to avoid motion artifacts during test performance, some outliers were created. Before obtaining the calibration curve, R values out of normal profile have been excluded from the final dataset. At the end of tests an overall calibration curve is obtained for a SpO_2 interval ranging from 99% to 82%. The curve is fitted considering all the measurements taken from the two subjects. Fig.6.12 shows the calibration curve and the formula with the coefficients obtained by this procedure. This formula will be applied to determine SpO_2 parameters.

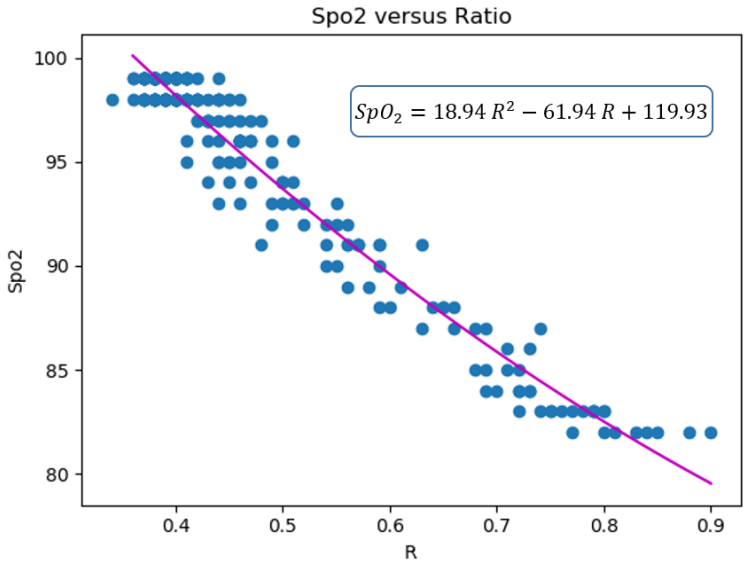

Figure 6.12. SpO_2 calibration curve.

6.3.2 ECG signal processing

The MAX86150 sensor provides a single lead ECG. The final morphology of the ECG trace depends on the application of several steps that start with a good signal recording and proceed with the post-processing. The first step of the ECG signal processing is the denoising, which is performed paying attention to preserve the features of the ECG signal. During the ECG recording several conditions can cause disturbances or artifacts. These causes can be external to the patient, such as interference due to the alternating current, or

internal to the patient as in the case of muscle tremor. Among the factors of disturbances, line interference is one of the most frequent. It is a signal distortion caused by the alternating interference that produces a stable frequency vibration (50-60 Hz). This interference is due to the presence of electromagnetic field generated from cables and instrumentation close to the patient. This type of problem can be reduced applying a specific filter, called notch filter, which attenuates the components at 50/60 Hz.
Another common problem in ECG recording is the presence of contaminations due to artifacts from skeletal muscle tremors. These interferences appear like rapid, wavy deflections which cause a difficult reading of the ECG waveform. Since the energy of the artifact signal is higher than the main ECG frequency, a typical solution is applying a LPF. The LPF reduces muscle artifacts but also the amplitude of the QRS complex. This is a disadvantage because the filter attenuates the components in high frequency of the QRS complex. Consequently, the recognizing of R peaks for the HR estimation can be more difficult.
In addition to these problems, at the electrode-skin interface, potentials are generated and are superimposed on the cardiac electrical signal of interest. This baseline wander also arises from breathing or subject movements. In order to remove these low frequency artifacts, a HPF with an appropriate frequency is applied. An incorrect cut-off frequency may cause deflections especially on the ST segment and the T wave. Typically, the cut-off frequency is in the range of 0.05 Hz and 0.5 Hz. Another way to attenuate these slow fluctuations is to perform a detrending method.

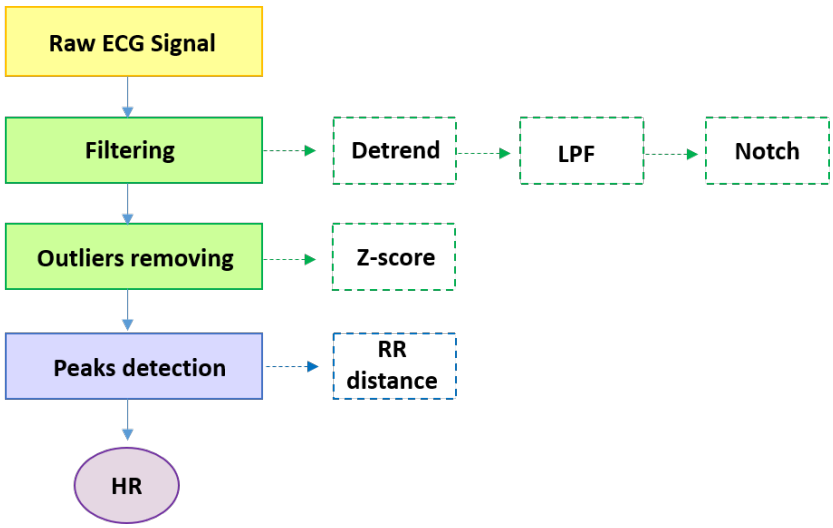

Figure 6.13. Flow chart of the main stages of the ECG algorithm.

In the light of what explained, the algorithm of post-processing includes different

types of filters to attenuate interferences and artifacts. Figure 6.13 shows the main steps of the ECG post-processing. The specifications of the filters implemented to improve the quality of the ECG signal are explained as follows:

- *Detrending:* the presence of trend in raw signal is addressed performing a ”detrending” step which aim is to remove the baseline wander. The trend observed was non-linear. The method chosen to eliminate it, was fit a low-order polynomial to the signal and subtract it from the initial dataset.
- *Low pass filter:* fourth order Butterworth LPF with a cut-off frequency of 45 Hz. The filter is applied in both the forward and reverse directions in order to have zero phase distortion.
- *Notch filter:* line interference is removed applying a finite impulse response (FIR) type. The filter requirements are respected: interference with constant amplitude and frequency and sample rate must be multiple of the line interference frequency (50 Hz).

The result of filtering process is shown in Figure 6.14.

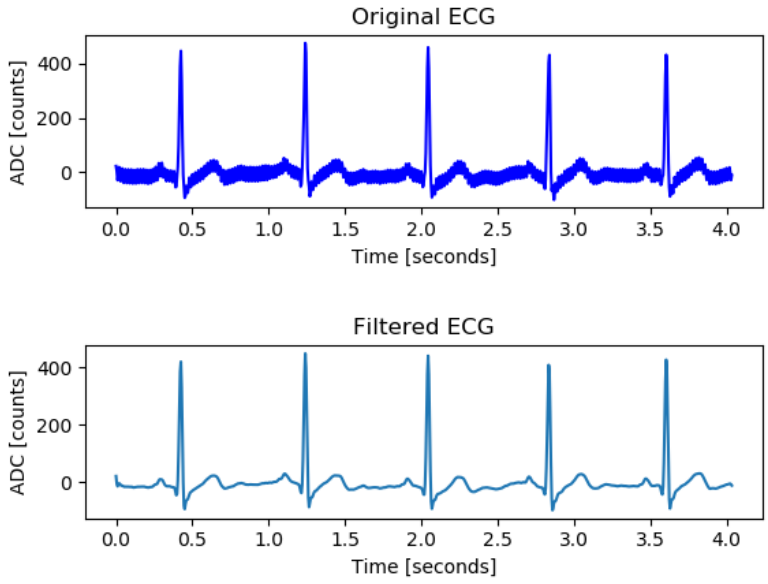

Figure 6.14. ECG signal before and after filtering process.

The filtering process helps to improve the signal quality, allowing a better performance of parameter estimation. However, this stage is not sufficient in case of measurement

errors. Therefore, the algorithm to detect outliers, already explained in section 6.3.1, is performed to ECG signal.
The most important stage of the algorithm regards the HR measurement. The procedure to recognize R peaks from the denoised ECG is similar to that implemented for PPG signal. The Python function, "find peaks", is used to find R peaks. The specifications introduced are: threshold beyond which a peak can be found, minimal distance between peaks and the height of peaks (prominence). The setting of the minimal distance between peaks depends on the beat frequency of each person. Usually, the HR interval is 60-90 bpm. Thus, this parameter requires an initial calibration to identify the beat frequency and select a proper minimal peaks distance.
Once identified all peaks of the ECG signal, the HR calculation is carried out. Distances (in samples) between adjacent peaks is calculated. Before proceeding with the application of the formula 3.2, distances considered not-physiological are excluded. Finally, the HR parameter in beats per minute is measured. At the end of the algorithm, the HR values are averaged in order to have only one parameter representative of that period.

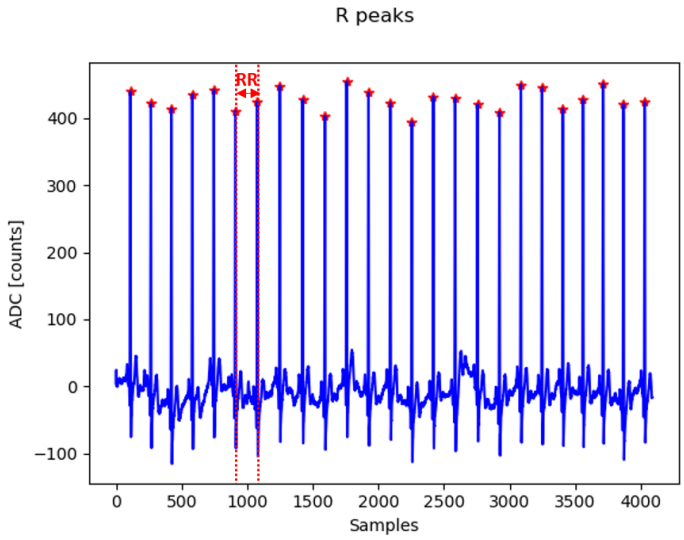

Figure 6.15. Result of the R peaks detection algorithm.

6.3.3 PTT estimation

As explained in section 3.4.3, a widespread method to estimate non-invasively blood pressure, is based on the use of both ECG and PPG signals. Several studies have been carried out to identify the best location of PPG (peak, middle, foot). In this thesis, PPG foot has been selected as reference point to measure PTT. In this work, only the first stage of

the BP estimation is carried out, i.e. the algorithm to extract PTT from ECG and PPG. Future work should include the estimation of the relationship between PTT and BP. In the following paragraphs are detailed the main steps for the PTT measurement.
To perform the PTT extraction only the IR signal is used because of its higher stability compared to RED signal. The algorithm starts processing PPG signal. In addition to LPF (see section 6.3.1 for filter specifications), also HPF is implemented. The HPF is a 5th order Butterworth with a cut-off frequency of 0.5 Hz. Consequently, the DC component of the IR signal is removed. Furthermore, a detrending step is also performed because PPG signal is affected by a non-linear trend. Regarding the ECG signal it is filtered with the same procedure explained in section 6.3.2.
As explained previously, outliers must be removed to avoid wrong parameter estimation. Since the synchronization of PPG and ECG signals is an essential requirement to obtain an accurate PTT measurement, it is very important to preserve this feature during outliers removing. Thus, the removal of abnormal values must be performed identically for the two signals. As a result, the same cardiac cycles are considered. Since PPG and ECG are extracted from two different sensors, different errors can happen. For this reason, the following complications have be taken into account during the algorithm development:

- Outliers may be present only in one of the two signals
- Outliers may be present in both signals but in a common interval
- Outliers may be present in both signals but in two not-coinciding intervals

The strategy adopted in this work was to select a common period in which the two signals have sufficient quality. The algorithm implemented is based on the Z score method (section 6.3.1). Firstly, a portion of signal without outliers is selected. The subset identified has the highest number of consecutive samples with Z-score below the threshold. Once obtained the two subsets, the next step is to verify their overlapping. The algorithm is based on the research of a common interval. At the end of this routine, two subsets with identical length are selected. An error message is sent if no overlap is identified. In this case the other steps will not performed. The algorithm proceeds with the identification of peaks and valleys if the result is positive.
As previously said, the PTT definition used in this work is the time difference between R peak and PPG foot of a specific cardiac cycle. First, the research of ECG peaks is carried out (see section 6.3.3 for more details). After that, the PPG valleys identification is implemented considering the fact that PTT interval begins with a R peak. Thus, all PPG valleys are positioned between two consecutive R peaks. The algorithm implemented is based on the research of the minimum value of PPG waveform between two ECG peaks. The two identified points belong to the same cardiac cycle. To improve the accuracy, a check about the distance between R peaks is carried out. If this distance indicates a non-physiological condition due to an incorrect location estimation, the research of PPG valley is avoided.

From this routine, two vectors containing the location of R peaks and valleys are obtained. At this point, PTT is calculated as the difference between each position of the two vectors. In figure 6.16 is represented the PTT at each heartbeat. The PTT values obtained in one minute of recording are averaged in order to avoid redundant information.

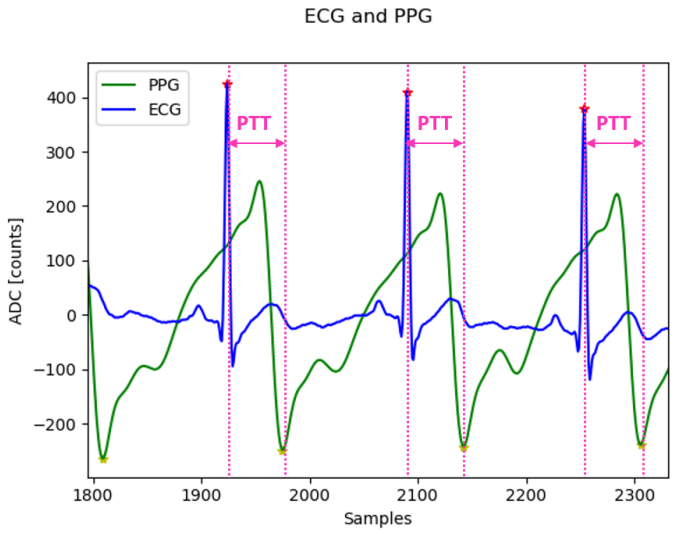

Figure 6.16. Portion of PPG and ECG signals: are highlighted the PPG valleys (yellow asterisks), the ECG R-peaks (red asterisks) and the PTT interval.

Once estimated PTT values, the second stage is to correlate PTT and blood pressure. One promising method used in literature is the BP estimation through the equation 3.22. This equation has unknown coefficients which are subjects dependent. To identify them, a calibration phase must be performed. In this work, the calibration step has not been carried out but a summary of the procedure is given in the following paragraph.

BP calibration

The linear model expressed by the formula 3.22 is adopted because it is affected by less artifacts, allowing a better performance for BP estimation [35]. The most common approach to know the coefficients a and b is a statistical method: least square algorithm. This method is based on the minimization of the error squares. Usually, an arm-cuff device is chosen as reference sensor because of its high accuracy.
The method is stated as follows. Coefficients a and b, for systolic blood pressure (SBP) and diastolic blood pressure (DBP), are gathered into the matrix:

$$\beta = \begin{bmatrix} a \\ b \end{bmatrix}$$

It is necessary to have many PTT and BP measures, which are expressed as:

$$Y_{\mathrm{n}} = \begin{bmatrix} BP_1 \\ . \\ . \\ BP_n \end{bmatrix}$$

$$X_{\mathrm{n}} = \begin{bmatrix} PTT_1 \\ . \\ . \\ PTT_n \end{bmatrix}$$

The matrix β is obtained from the minimization of $\|Y_{\mathrm{n}} - X_{\mathrm{n}}\beta\|^2$:

$$\beta_{\mathrm{n}} = \left[X_{\mathrm{n}}^T X_{\mathrm{n}}\right]^{-1} X_{\mathrm{n}}^T Y_{\mathrm{n}}$$

The estimation of BP can be easily performed measuring BP values from the reference sensor, and calculating PTT values with the algorithm developed. The PTT-based BP method requires periodic re-calibration since the accuracy is an important requirement. The mean of error estimation (in absolute value) must be lower than 5 mmHg for systolic and diastolic pressure.

6.3.4 GSR signal processing

As already explained the GSR is the measurement of the electrical characteristic of the skin. Before performing features extraction, the GSR signal is converted from the units of the ADC levels to the resistance in Ohm. The conversion is made possible by the formula 6.6. Since GSR signals are expressed as the variation in conductance, the resistance values are transformed into conductance values by simply inverting R values. The acquired GSR signal contains several artifacts:

- *Power line interface:* the frequency is around 50 Hz. It is generated by current flowing in cables and instrumentation.
- *Electrode-skin contact:* the interface between Ag/AgCl electrodes and the skin can varies during a recording. This artifact is due to several causes such as the detachment of electrodes, the polaritations effects and bias potentials. This noise can effect both SCL and SCR components of the signal [64].
- *Motion artifacts:* rapid changes due to movement which provokates variation in impedance. This artifact is in the high frequency spectrum.

According to [65], the frequency interval of interest of the GSR signal is 0.01-3 Hz. Firstly, the raw signal is filtered with a fourth-order LPF Butterworth with a cut-off frequency of 3 Hz. The LPF is applied to remove high-frequency signal noise leaving unaltered the GSR responses.
Afterwords, a second-order HPF is implemented with a cut-off frequency of 0.05 Hz to separate the SCL and SCR components of the GSR signal according to [66]. Only the phasic skin conductance response of the GSR signal is analyzed in the next step.
In figure 6.17 is shown the result of the filtering process on a GSR recording. The sample rate is 55 Hz. From the figure, it is evident that the GSR signal within the interval of 170-230s has more oscillations. This variation is due to the sympathetic nervous system activation. After an emotional arousal event, the return to the signal baseline is not immediate because the skin moisture causes a change in conductance.

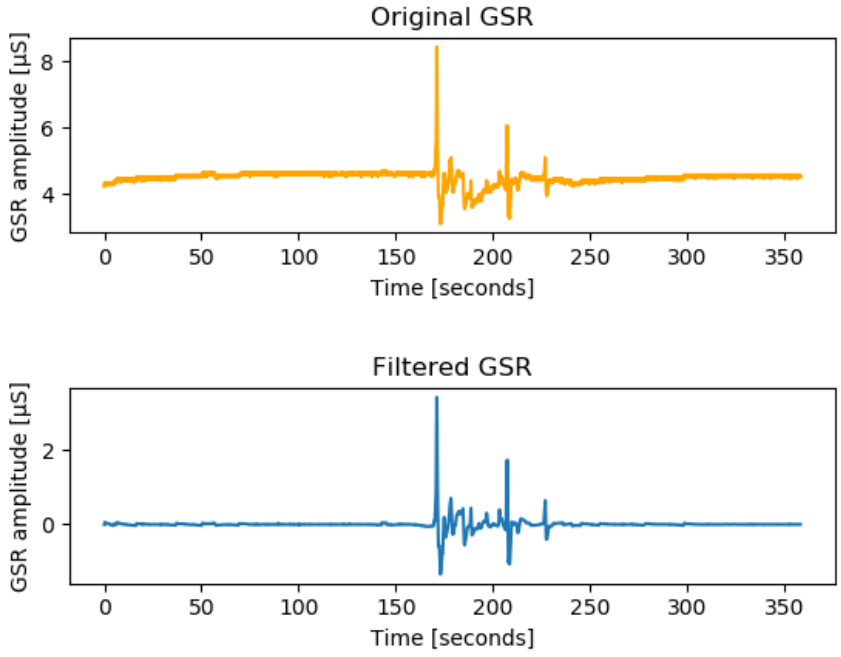

Figure 6.17. GSR signal before and after the application of LPF and HPF.

The aim of the second stage of the algorithm is the extraction of the most significant GSR features necessary to detect a ”stress event”. Firstly, all the maxima of the filtered GSR signal are searched using the Python function ”find-peaks”. This function requires as input the threshold of the peak height to be considered as a SCR event. As already said, the amplitude of a SCR peak can be approximately from 0.01 to 5 μS depending on the sensor specifications and how a subject perceives an emotional stimulus. The choice of the threshold value was made on the basis of observations of the Grove GSR sensor

performance. The threshold to detect a peak is setted to 0.3 μS. Once all peaks have been identified, the algorithm proceeds with the peaks analysis to confirm or not the presence of a stress event. This procedure is based on the derivative method. To better understand the algorithm implemented in this thesis, an example is given.
Starting from the position of a local maximum, the research of the onset point is performed. It is known that the onset of a SCR event can happen within 1-5 seconds from the stimulus. Thus, to find the start of the peak, the sign of the first derivative of the GSR signal is analyzed. The first derivative should be positive in the interval 1-5 s that precedes the maximum. Starting from the position of the maximum considered, when the first derivative becomes negative, that point is the onset of the probable SCR peak. In this step a possible complication could be the presence of a not so smooth peak. This may cause an errata identification of the onset or offset point.
The peak amplitude is estimated by calculating the vertical distance between the peak and its onset. Instead, the rise time is the horizontal distance between these two points. The offset point is searched as follows: since after a peak the slope is negative, the point in which the GSR derivative becomes positive is considered as the offset. The recovery time is calculated as the horizontal distance between the offset and the maximum point. To confirm that a peak corresponds to a stress event, the features extracted are analyzed and compared to thresholds. The thresholds have been chosen considering that: a stress event has a maximum duration of 10 s; the rise time may vary from 1 to 5 s; the recovery time is longer (typically from 1 to 10 s). If a peak satisfies all the criteria selected, it is considered as a SCR event. In that case, the assumption that only one SCR event can happen in a time window of 10 s is made.

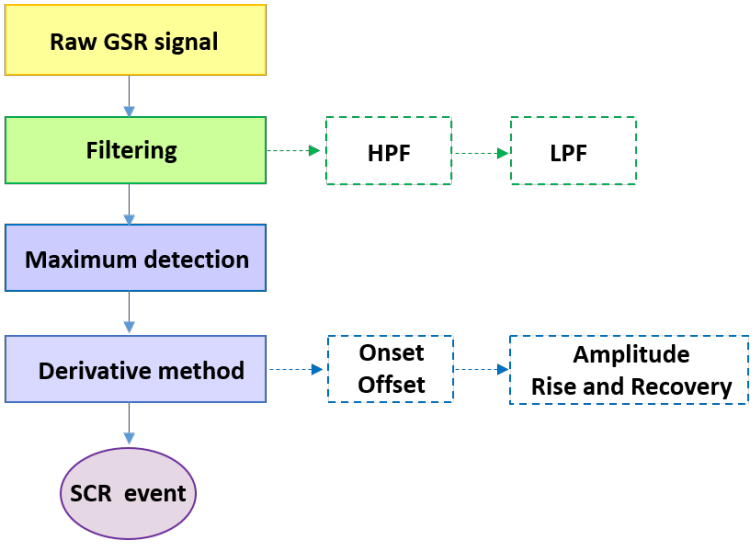

Figure 6.18. Flowchart of the proposed stress detection algorithm.

The features (amplitude, onset, offset, rise-time, recovery-time) of each SCR peak and the number of emotional events detected are indicated at the end of the implemented algorithm (Fig.6.18). In figure 6.19 is represented a SCR peak with the features extracted. This GSR signal is measured from two fingers of the right hand. It has been chosen a signal with a very high amplitude in order to better display its features. In general the amplitudes are smaller (between 0.8 and 2 μS).

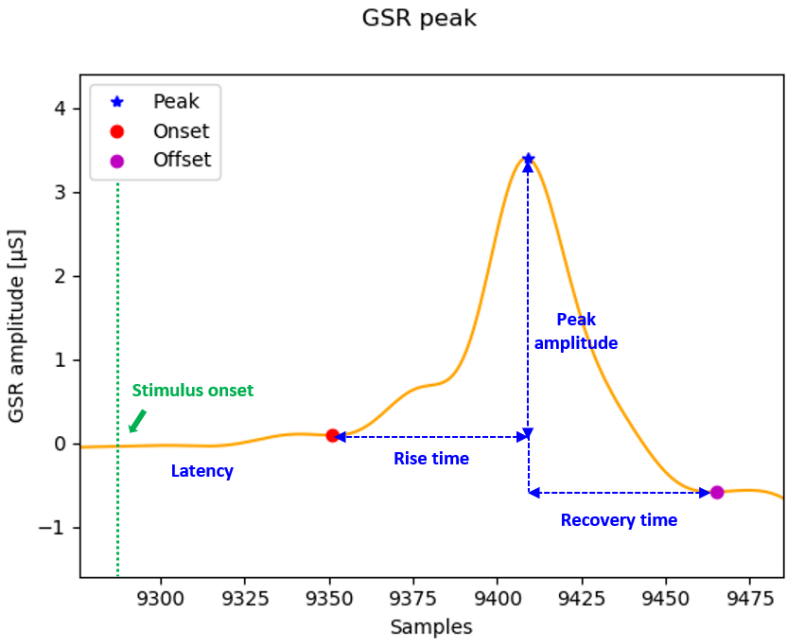

Figure 6.19. Peak amplitude, rise time, recovery time and latency are the features extracted from a SCR peak of the GSR signal.

6.3.5 Accelerometer signal processing

The proposed fall detection algorithm uses acceleration signals acquired by a triaxial accelerometer mounted to the chest. The aim of the proposed algorithm is to identify fall events from simple activities such as walking, sitting, bend-over. Other activities such as fast running, fast walking, climbing were not taken into account during the algorithm development process. This choice is due to the final goal of this project: the motion monitoring of an operator working in heavy industry to recognize an illness state.
Data acquired (sample rate of 200 Hz) are processed offline, such as for the previous signals. With the data from the MPU-9265 sensor, different parameters, such as Euler angle (pitch and roll) are measured (Fig.6.20). The cartesian coordinate system is oxyz and the origin in located at the center of the upper trunk.

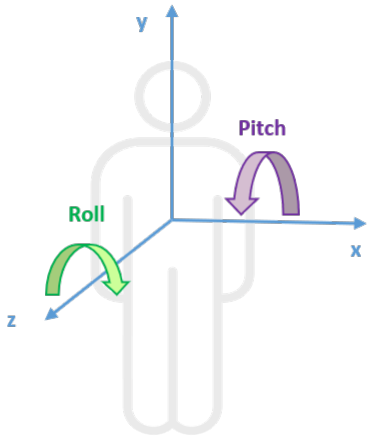

Figure 6.20. Rapresentation of pitch and roll rotations.

A fall down to the ground can be: forward, backward, off side. The difference between forward and backward is the final position after a fall, i.e.prone and supine position respectively. Depending on how a person falls, different parameters and thresholds are considered into the proposed algorithm. Figure 6.26 provides a general indication of the main steps of the algorithm. Basing on the use of flags, the algorithm recognizes a fall event when all the thresholds are excedeed: SVM, A_z, Pitch for fall forward and backward, and SVM, A_x, Roll for fall on left and right side. Thus, the algorithm indicates the type of fall according to which flags have been setted and which thresholds have been exceeded. The first feature extracted from data is the total acceleration, vector or commonly called the signal vector magnitude (SVM). It is calculated as the sum of squares linear acceleration in the x,y and z axes (Eq. 6.9).

$$\text{SVM} = \sqrt{A_x^2 + A_y^2 + A_z^2} \tag{6.9}$$

The SVM parameter is measured because it carries information about the acceleration variation during movements. In contrast to normal activity, fall has an acceleration in the three axes that rises suddenly, resulting in a higher SVM value. Figure 6.21(a) shows an example of SVM values during a fall event. Before the fall, the subject was in a standing position. As it can be observed from the graphic, the instant of fall is characterized by an increase of SVM values. Initially SVM values were about 1 m/s^2, during the fall simulation instead were above 2 m/s^2. After a fall event, the subject was in the prone position in fact SVM values are decreased. The SVM measurement is different when a subject executes activities such as walking, bend-over and other movements. In this case the SVM parameter has many oscillations which can reach values around 2 m/s^2. Figure 6.21 (b) represents SVM parameter measured when a subject makes movements like jumping and light running. During these activities higher SVM values are obtained.

Instead, the fall event has a similar SVM amplitude of the previous case. Basing on this evidence, the threshold on SVM values is setted to 2.2 m/s^2.

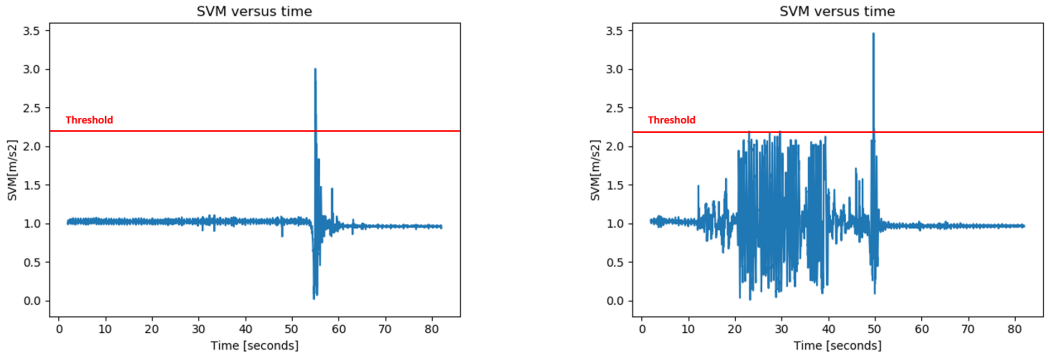

(a) Standing still

(b) Running

Figure 6.21. SVM values during a fall event. (a) The subject is initially in standing position. At t=55s it falls and SVM exceedes the threshold setted. After that, the subject remains in prone position without making movements for the remaining 17s. (b) The subject is initially in standing position. In the time interval between 12s and 48s the subject makes movements (light running). At t=49s the fall takes place and then the subject remains in prone position.

As explained, the acceleration magnitude can increase also when a fall does not occur. During normal activities the SVM threshold can be overcome. Thus, a single threshold on SVM values is not sufficient to recognize a fall event. In order to avoid false allarm, when SVM values exceed the threshold for a window time of 0.5s, other parameters are analyzed. In the next paragraphs is explained how the algorithm recognizes a fall and which parameters it calculates to distinguish the different types of fall.
Regarding the fall backward and forward the parameters observed are:

- Acceleration along the z axis: the A_z output of the MPU-9265 sensor changes sign and amplitude when a fall event occurs.
  Basing on the example provided in Fig.6.22, a first difference is the opposite trend of A_z values in forward and backward fall. During normal activities, in both cases A_z values are in the range of -0.8 and +0.8 m/s^2. Actually, also biggest peaks are present and they are due to the sudden change of motion, such as skips. A fall forward event (Fig.6.22(a)) is characterized by an increase of A_z module and a successive stabilization around -1 m/s^2. The threshold selected is -0.7 m/s^2. Instead, a fall backward event (Fig.6.22(b)) is characterized by an increase of A_z module and a successive stabilization around +1 m/s^2. The threshold selected is +0.7 m/s^2. In both cases (forward and backward), a flag is setted if the A_z values exceed the threshold for a window time of at least 2.5s.

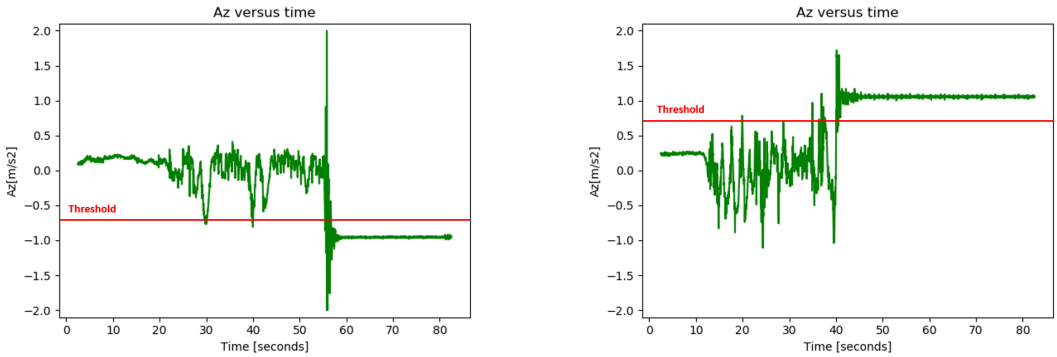

(a) Fall forward (b) Fall backward

Figure 6.22. A_z values during a fall event. (a) The subject is initially in standing position. In the time interval between 20s and 54s the subject makes movements (walking and bend-down). At t=55s it falls and A_z exceedes the threshold setted. After that, the subject remains in prone position without making movements for the remaining time. (b) The subject is initially in standing position. In the time interval between 12s and 42s the subject makes movements (light running and skips). At t=44s the fall takes place and then the subject remains in supine position.

- Pitch angle: it represents the inclination angle with respect to the z axis of the user's body. In figure 6.20 is represented the pitch rotation.

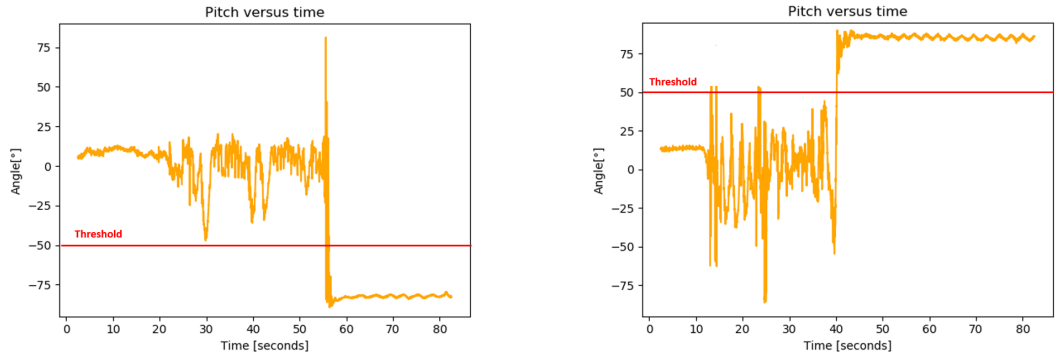

(a) Fall forward (b) Fall backward

Figure 6.23. Pitch values during a fall event. (a) During the first phase, the subject makes movements such as jumps which are related to the peaks present on the signal. The subject at t=55s falls and A_z exceedes the threshold setted. After that it remains in prone position. (b) At t=44s the fall takes place and then the subject remains in supine position. In both cases, slow oscillations after a fall event are evident. These are due to the normal breathing process of a person.

The algorithm calculates the pitch angle through the formula expressed as:

$$\text{Pitch} = tan^{-1}\frac{A_z}{\sqrt{A_x^2 + A_y^2}} \tag{6.10}$$

During normal activities pitch angle values are mostly between -50 and +50 degrees. In a fall forward the pitch values becomes more negative so the threshold is setted to -50 degrees. In a fall backward pitch values becomes more positive so the threshold is setted to +50 degrees. In both cases, a flag is setted if the pitch values exceed the threshold for a window time of at least 2.5s.

Regarding the fall on the right and left side, the parameters observed are:

- Acceleration along the x axis: A_x values change sign and amplitude when a fall event occurs. A similar behaviour than the previous case is observed. Thus, the thresholds selected are -0.7 m/s^2 and +0.7 m/s^2 respectively for fall on the left and right side (Fig.6.24). Also in this case, a flag is setted if the A_x values exceed the threshold for a window time of at least 2.5s.

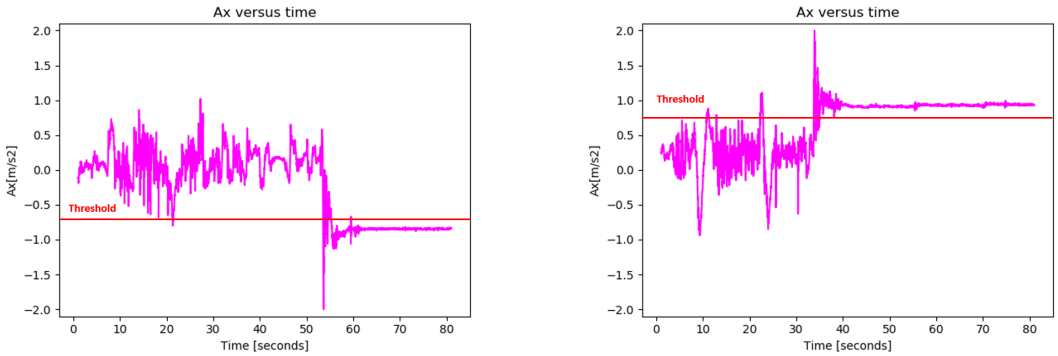

(a) Fall on the left side

(b) Fall on the right side

Figure 6.24. A_x values during a fall event. (a) In the time interval between 0s and 53s the subject makes movements (walking and bending). At t=54s it falls and A_x exceedes the threshold setted. After that, the subject remains on the left side. (b) In the time interval between 0s and 38s the subject makes movements (light running and skips). At t=39s the fall takes place and then the subject remains on the right side.

- Roll angle: it represents the inclination angle with respect to the x axis of the user's body. The algorithm calculates this angle through the formula expressed as:

$$\text{Roll} = tan^{-1}\frac{A_x}{\sqrt{A_z^2 + A_y^2}} \tag{6.11}$$

The thresholds selected are -50 degrees for left side and +50 degrees for right side (Fig.6.25). Also in this case, a flag is setted if the Rolls values exceed the threshold for a window time of at least 2.5s.

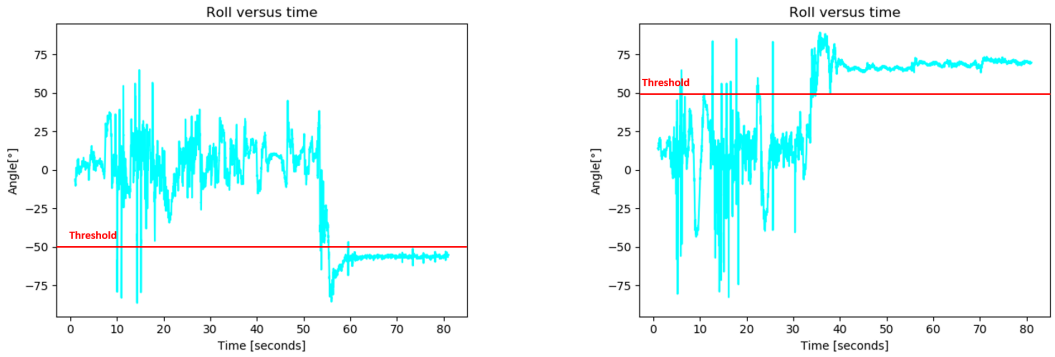

(a) Fall on the left side

(b) Fall on the right side

Figure 6.25. Roll values during a fall event. (a) The subject at t=55s falls and roll exceedes the threshold setted. Then it remains on the left side. (b) At t=44s the fall takes place and then the subject remains on the right side.

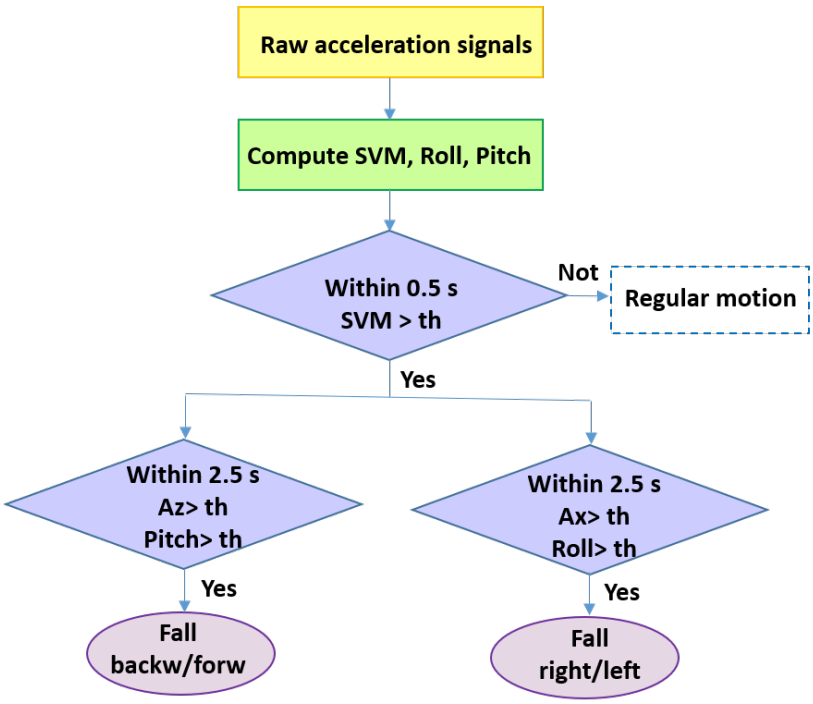

Figure 6.26. Fall detection algorithm.

6.4 Wireless communication

This section provides a review of the wireless protocols most popular in wearable health monitoring systems.
A general architecture of a wearable system includes a portable unit (PU) which is responsible for the data acquisition and post-processing. Feature extraction can be made directly in the CPU or in other systems after the data transmission [13]. However, data are wireless transmitted to a main device, such as smart-phone, PC or a custom designed microcontroller-based system.
Several communication protocols are available to reach this goal. The most widespread standards in WHD are Bluetooth Low Energy (BLE), Wi-Fi, ZigMee and LoRa (Long Range Radio).

- *Wireless Fidelity (WiFi) :* it is a successful wireless networks architecture which operates in the 2.4 GHz band. It is based on a serial standard of IEEE 802.11: 802.11b, 802.11g, 802.11n. These standards differ mainly for the maximum data rate and the number of access points.
  The first standard operates at a data rate of about 11 Mbps and it has a limited number of access points.
  The 802.11g standard operates at about 19 Mbps (maximum 54 Mpbs). It has multiple channels which allows a faster throughput. The main disadvantage is the single access point.
  The IEEE 802.11n is a better version of the previous standard because allows up to 300 Mbps and it has multiple-input multiple-output (MIMO).
  The range of communication of IEEE 802.11 standard is within a radius of 150m. Actually it depends on several factors.
  Wi-Fi protocols test the quality of the signal between two devices by adjusting the data rate. The architecture of the WiFi is composed of several Access Points(AP) which communicate with clients (about 30) by broadcasting its network name (or Service Set Identifier) through packets.

- *Bluetooth Low Energy (BLE) :* is a low-power wireless standard in 2.5 GHz radio band. This band can be divided into 40 channels on 2 MHz. BLE technology supports very short data packets and it is suited to the transmission of data from compact wireless sensors. These sensors send a few bytes of data infrequently: their duty cycle tends to range from a few times per second to once every minute. The stand-alone BLE technology is optimized for low cost and low power consumption applications. In fact, it saves power by maximizing standby time and by using fast connections and low peak transmit/receive power. Typically, a BLE device spend only 1% of its time awake. This technology has a small form factor allowing an easier incorporation in small wearable devices. The communication is between a

master and a number of slaves. The slave communicates with the master in specific instants (determinated by the master). Respect to classic Bluetooth the BLE includes:
- The ability for a device to act as a "peripheral" and a "hub" at the same time
- Addition of a method to create a dedicated channel, which could be used for IPv6 communications
- Addition of the Internet Protocol Support Profile (IPSP) to allow Bluetooth low energy devices to communicate with any other IPv6 enabled device
- Higher strength security
- Increase in maximum transmit power
- Increase in packet length
- Increase in throughput
- Increase in transmission range

- *ZigBee :* is a low rate and low-power wireless communication protocol. It consumes less energy than traditional Bluetooth. ZigBee operates in the 2.4 GHz ISM band as well as in the 784-868-915 MHz bands. The supported network architectures are mesh, star and cluster. In a ZigBee network, all nodes share the same channel, and frequency agility is minimal. The maximum transmission range is about 75 m. The communication is protected by the use of the Advanced Encryption Standard (AES) algorithm which ensures privacy and message integrity. For this reason many medical applications use ZigBee technology. ZigBee network has two classes: Full-Function Devices (FFD) and Reduced-Function Devices (RFD). For every ZigBee network there is one coordinator that is a FFD and can route messages in mesh networks. The RFD are the ZigBee end devices (for example sensors or actuators) which can only communicate with one FFD in a star network setup.

- *LoRa :* is a long distance coverage wireless protocol [13]. LoRa modulates the signals in SUB-GHZ ISM band using a proprietary spread spectrum technique developed by Semtech Corporation. The overall network capacity is optmized by the Adaptive Data Rate (ADR) specification which enables the server to set the spread factor in order to best fit the requirements of each node. This feature allows also to reduce the power consuption. The range of the data rate is 290-50 kbps. It depends on the channel bandwidth and the spreading factor.

WiFi and Bluetooth Low Energy appear as the best technologies for the wireless communication of the prototype designed in this thesis. In fact, it is interesting to notice that almost all the wearable devices available on the market, both for industrial and consumer applications, use one or both of these protocols. The price of chipsets for WiFi continues to drop, making it an economical networking option. This protocol allows fast data rates but it has the drawback of a high energy consumption.
Several cheap solutions are commercially available. The choice of the components is

based on the following specifications: data rate transmission, operating frequency, output power sensitivity, memory size, input voltage, peak current and cost. Another feature very important for wearable application is the size and thickness of the wireless module. The table below summarizes some of the main features of the wireless protocols most used in wearable applications.

Wireless Protocol	Max Range	Max Data Rate	Power Consumption
Bluetooth (before version 4.0)	100 m	1–3 Mbps	2.5–100 mW
Bluetooth Low-Energy (BLE)	100 m	1 Mbps	10 mW
Wi-Fi	150–200 m	54 Mbps	1 W
ZigBee	100 m	250 kbps	35 mW
LoRa	50 km	700 bps	(customizable)

Figure 6.27. Main features of the wireless protocols used in wearable devices [68].

Chapter 7

Results and discussion

This section provides an explanation of the testing performed to ensure the correct behaviour of the implemented algorithms .
Tests on the firmware have been performed to verify the correct sending of the Start and End conditions during the data trasmission. Furthermore, particular attention was provided to the reception of the acknowledge (ACK) bit during the transimission of a sequence. The ACK bit is received if the address or data frame was successfully sent.
Once confirmed the right functioning of the I^2C communication between sensor and microcontroller, the processes of data reading and trasmission were analyzed. The firmware is based on the use of interrupts which enable the reading and sending of data packets. Once an interrupt from the sensor is generated, FIFO memory is read and data are sent. A careful debug stage of the microcontroller was carried out with Atmel Studio 7 platform. Each step of the code was analyzed in order to avoid errors which can compromise the final result. Particular attention was paid to the writing and reading processes from the sensors memory.
The most complex sensor is the MAX86150 because it incorporates a FIFO memory which contains all the data measured from the two LEDs of the pulse oximeter and from the ECG. So in this case, it is important performing the reading process with high accuracy in order to preserve the original configuration of the packets. Furthermore, errors in FIFO reading can result in loss of samples or having redundant data. Thus, during the debugging stage the position of the reading and writing pointers was analyzed.
Once completed the reading process, data are converted into the desired format. For example the ECG signal is expressed into a signed 32-bit integers. Thus, also the data conversion was analyzed in order to verify the correctness of the implemented functions.
After having checked that the firmware developed had a correct behaviour in all circumstances, algorithm testing is performed.

7.1 SpO_2 and HR testing

The SpO_2 and HR algorithms developed in this thesis were tested on 20 subjects of different age (between 25 and 55) and genders. To compare the results obtained from the MAX86150 sensor (PPG and ECG), it was considered as reference the PO30 pulse oximeter, already used during the calibration stage (see section 6.3.1 for further details). The reference sensor is a pulse oximeter based on transmittance technology. Instead, MAX86150 sensor used in this thesis is based on reflective technology, so photodetector and leds are positioned on the same side (see section 3.4.2). All the subjects selected for tests were in healthy and non-smoker. Furthermore, they were at rest condition in an environment with normal oxygen content. Each of the 20 subjects is assigned with a number to preserve confidentiality.
The parameter settings of the MAX86150 sensor had remained unchanged for all tests. A brief summary of the main settings is given as follows:

- Fs : 200 Hz
- Sample average: no averaging between samples
- ADC range: 32768 nA (full scale)
- IR and RED current: 50 mA
- Pulse width: 400 μs
- Active elements: three (ECG, IR led, RED led)
- Proximity function: not enabled

During tests, the subjects wore: PO30 pulse oximeter on a finger, ECG electrodes on the chest, and MAX86150 pulse oximeter on a finger of the opposite hand. The ECG recording was performed positioning two electrodes on the chest (differential measure) and a reference electrode on the abdomen. The test protocol consisted of the simultaneous measurement of reference sensor and MAX86150 sensor.
The output of the reference sensor was SpO_2 (in percentage) and HR (in bpm) measurements. The values shown on the sensor display were averaged in order to have a single value of reference. The output of the algorithm implemented in this thesis was the SpO_2 and HR calculated from both PPG and ECG signals. For each subject, one minute of recording was performed. At the end, all the measurements of each cardiac cycle were averaged in order to have only one parameter. Unfortunatly, the HR measurements extracted from ECG signal were not compared to an ECG reference. To improve the tests accuracy, tests should be performed using two sensors based on the same techonolgy.
During data recording particular sensor anomalies did not occur. The most frequent encountered problem was the noise superimposed on the ECG signals. Surely the movement

between electrodes and skin was the main causes of artifacts. In addition to the electrodes positioning, particular attention was provided also to the pressure exercised by fingers on the pulse oximeter. During the calibration step an important detail about the finger pressure has emerged. It is very important that the finger is well in contact with the sensor in order to avoid that the photodiode picks up the light coming from the environment. At the same time, the pressure exerted on the sensor should not be too high because it may result in noisy recording. An example of wrong performance is shown in Figure 7.1.
In this case, the subject had exercised too pressure on the sensor resulting in low signal quality. Consequently that recording was discarded in order to avoid wrong features extraction.

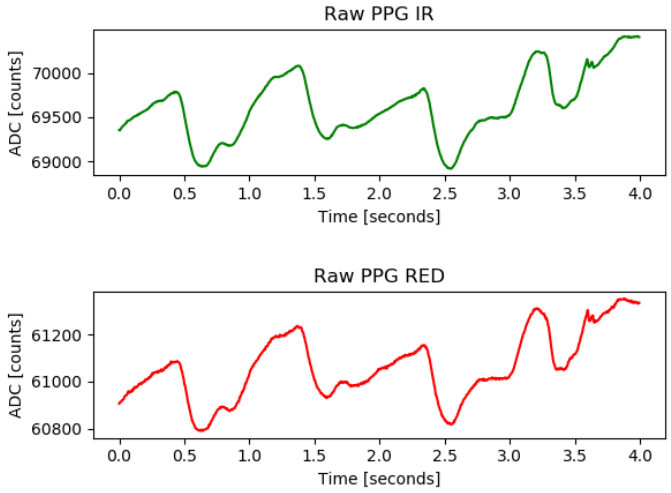

Figure 7.1. Errate PPG recording due to the too pressure applied to the MAX86150 sensor.

A clarification about the position of the pulse oximeter on the body it should be done. The calibration procedure was carried out considering the classic configuration of this technique, i.e. the finger placed on the pulse oximeter. Consequently, all tests were performed respecting that setup. Since this configuration is not suitable for wearable application, further tests should be carried out in order to study the sensor performance by varying the position on the body. Thus, a new calibration procedure should be done.
However, an example of a possible configuration and the resulting sensor performance is given as follows. Considering that the most widespread wearable devices are the wrist ones, the sensor was positioned on the wrist. The algorithm implemented was tested several times on the same subject in order to extract R values and compare them to the ones measured by the traditional configuration.
Figure 7.2 shows PPG waveforms obtained from the wrist. The shape of PPG_{wrist} was

similar to the PPG_{finger}. The amplitude of the DC components, for both RED and IR, was decreased. As a consequence, values of the Ratio parameter measured from these signals were changed. More in specific, the average of the R values was increased.
The subject had an oxygen saturation of 99% (measured by the reference pulse oximeter). The variation observed is summerized as follows:

- Finger : R_{mean}= 0.4
- Wrist : R_{mean}= 0.7

In both measurements, the SpO_2 value indicated by the reference sensor was 99%. The SpO_2 value measured from the algorithm implemented in this thesis (using the coefficients obtained from the calibration curve) was 98% for the PPG_{finger} and 86% for the PPG_{wrist}. This result is the evidence that the calibration procedure has to be repeated in order to extract new calibration coefficients and consequently right SpO_2 values.
The same consideration should be done for the chest positioning. Also in this case PPG features change thus requiring the repetition of the calibration process.

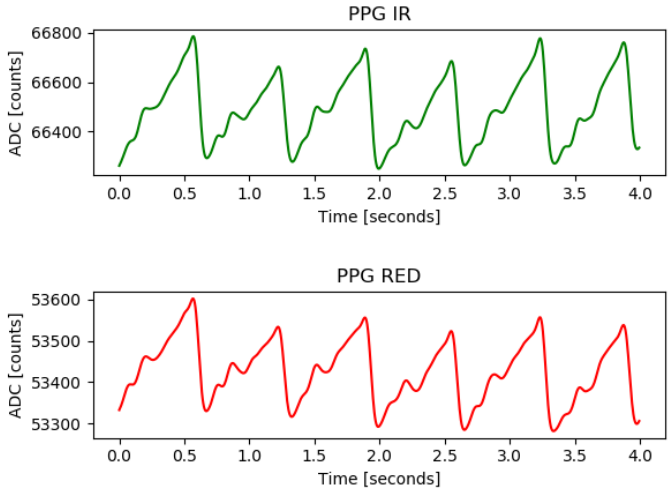

Figure 7.2. Filtered PPG IR and PPG RED waveforms obtained from the wrist.

The next paragraphs are dedicated to the discussion of the results obtained from the tests performed on 20 subjects with the traditional configuration. Results are compared with PO30 fingertip Pulse Oximeter and reported in the following table. Since from MAX86150 are extracted two HR values from two different signals, they are distinguished in: HR_{ppg} and HR_{ecg}.

Subject	PO30		MAX86150		
	SpO_2	HR	SpO_2	HR_{ppg}	HR_{ecg}
1	99	92	99	93	91
2	98	68	98	71	70
3	98	65	101	64	63
4	99	88	99	87	87
5	97	66	96	69	67
6	98	39	98	39	40
7	98	40	90	41	39
8	98	65	99	64	64
9	99	63	99	63	65
10	99	84	99	85	83
11	98	75	97	76	76
12	99	81	100	80	80
13	98	82	98	81	80
14	98	81	98	79	80
15	98	70	89	70	72
16	99	72	98	72	70
17	98	79	97	79	78
18	99	40	100	39	42
19	97	65	98	67	64
20	99	58	100	60	59

The results are also represented through histograms in order to better display differences. In fact, histograms report the error committed by the sensor used in this work compared to the reference.
Regarding the comparison between SpO_2 measurements, the range of SpO_2 values measured from the reference sensor is from 97 to 99%. The average error is about $\pm 1\%$. In particular, in 8 out of 20 subjects identical SpO_2 measurements are achieved. In 9 out of 20 subjects an error of $\pm 1\%$ is measured. In the three remaining cases, the measurement error exceed 3%. It should be remarked that the reference sensor is not a medical device used in hospital so it has an accuracy of $\pm 2\%$.
With regard to HR tests, the reference value is compared to the two HR measurements. The maximum error estimated for HR_{ppg} is 3 bpm in two subjects. The average error is about $\pm$ 1 bpm. In five cases no difference between HR_{ppg} and HR_{ref} is estimated. Instead, the maximum error stated for HR_{ecg} is $\pm$ 2 bpm in six subjects. The error value of both HR_{ecg} and HR_{ppg} that appears most often, i.e. the mode of the dataset, is -1 bpm.
Results shows good performance in therms of accuracy of the proposed algorithm. In order to have a broader vision to the system behaviour more tests should be performed.

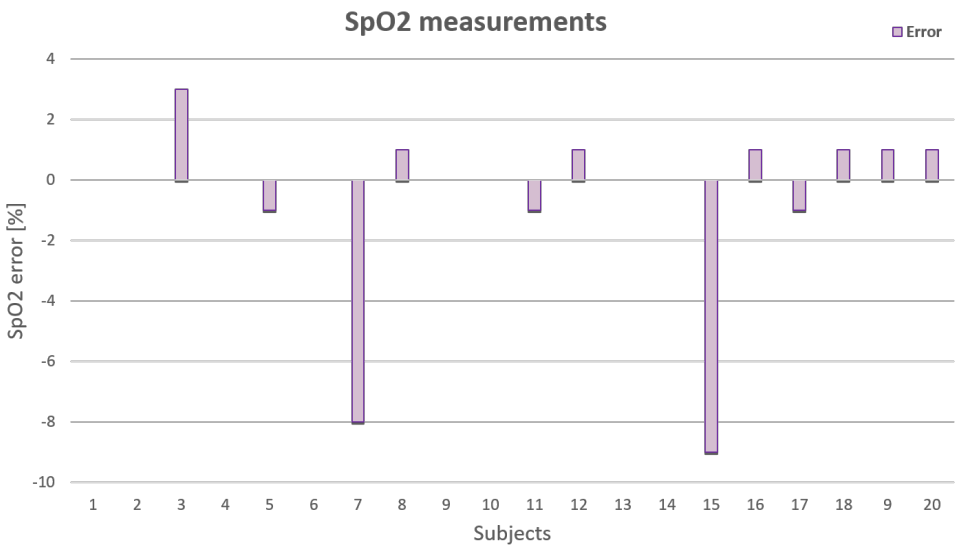

Figure 7.3. SpO_2 measurements on 20 subjects with the reference PO30 pulse oximeter and MAX86150 sensor. Errors are expressed as the difference between the two measurements.

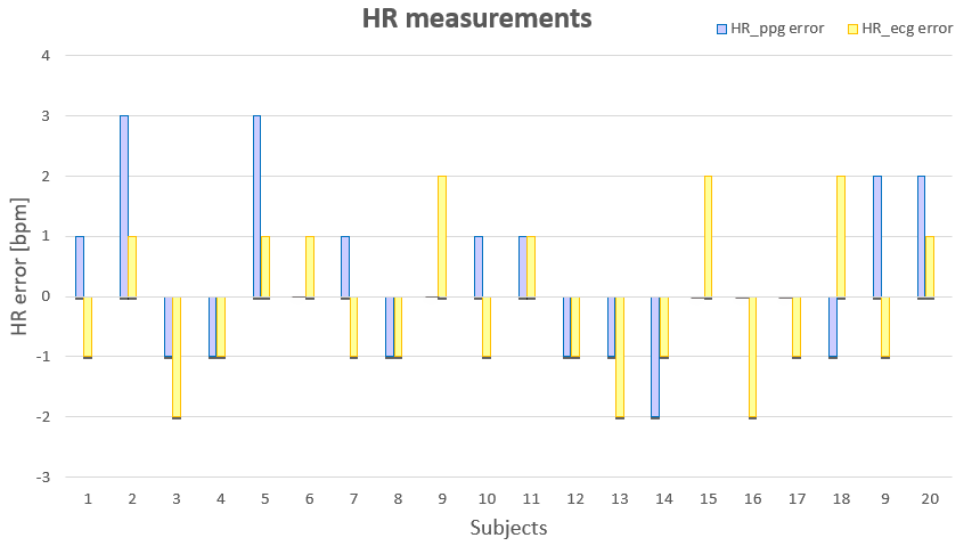

Figure 7.4. HR measurements on 20 subjects. Errors are expressed as the difference between HR measured from the reference sensor, HR extracted from ECG and PPG signals measured by MAX86150.

7.2 PTT measurement

Since the calibration step to determine calibration parameters has not been performed in this work, PTT measurements cannot be used to estimate blood pressure. Consequently, the algorithm implemented in this thesis to measure PTT cannot be tested. In general, the procedure to test the algorithm is based on the use of a reference sensor, such as an arm-cuff blood pressure device. The process is similar to that already explained in the previous section. Thus, two simultaneous measures should be taken in order to compare the results and to establish the accuracy of the measurement.
However, during the tests conducted for SpO_2 and HR measurements, PPG and ECG signals were also processed in order to calculate the pulse transit time value. The results obtained from the 20 subjects, are shown in figure 7.5. The range of PTT values is between 257 and 276 ms.
As already said, a calibration process is necessary to correlate these PTT values to the BP measurements taken from a reference device. In literature several efforts have been performed in order to find an accurate method to estimate blood pressure. The range of PTT values obtained in literature, varies according to the sensor setup and test subjects. An example of PTT values calculated from different points of the PPG waveform is given by [67].

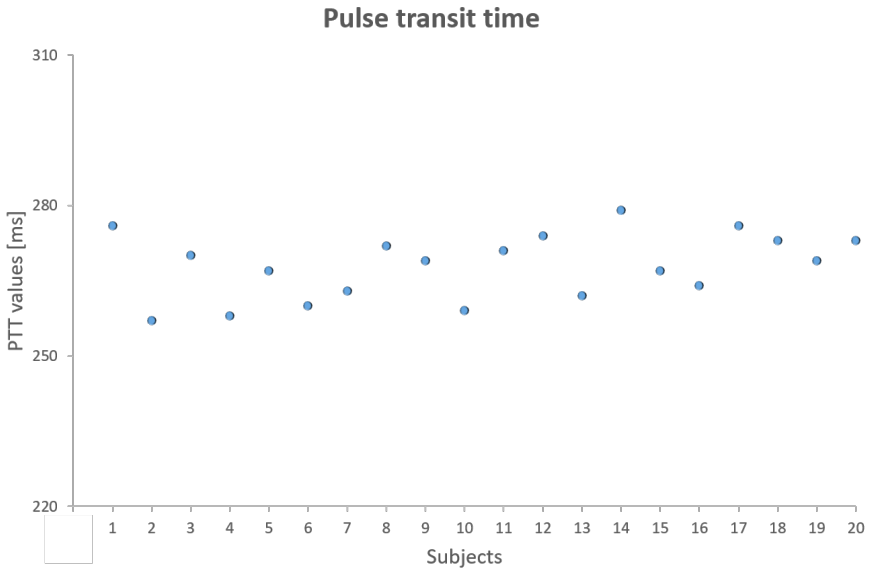

Figure 7.5. PTT measurements on 20 subjects in rest condition.

7.3 Stress detection testing

This section describes the test protocol and the results obtained from the GSR grove sensor. In order to analyze the performance of both sensor and algorithm, stress events were induced during the laboratory experiments. These experiments were conducted in a quiet room in order to avoid distractions. During the test, subjects were sitting in a relaxed position on a chair. All the subjects selected for tests were in healthy and their age ranges between 24 to 35. Regarding the sensor setup, subjects wore two electrodes on two fingers of the right hand. In figure 7.6 is shown the protocol used during tests.

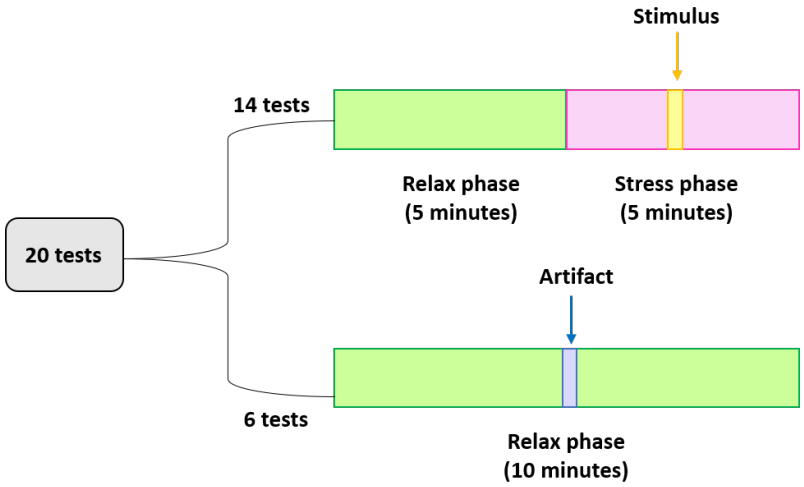

Figure 7.6. Protocol of the stress detection test.

In total 20 recordings have been performed. In order to understand more clearly the performance of both sensor and algorithm, the strategy adopted is the following:
- In 14 tests, auditory stimuli were induced;
- In 6 tests, no auditory stimuli were induced but motion artifacts were specifically introduced.
All the 14 tests, during which a stress event was simulated by the induction of a stimulus, were performed as follows.
The test started with a rest period of 5 minutes in order to calibrate the setup and identify the GSR baseline which is subject dependent. This period in Fig.7.6, is indicated as ”relax phase”. After that, a ”stress phase” with a duration of 5 minutes was performed. The test protocol was the induction of stress reactions through auditory stimuli. The sound was similar to an air-horn with the aim to ”scare” the subject. These moments of stress were induced one time at every session of recording. All the stimuli were identical in duration

and intensity. In the case of a test were repeated many times on the same subject, the auditory stimuli have been changed, with the hypothesis that a subject could become tolerant to the stimulus. Furthermore, for each test, the stimulus has been inducted randomly. In this way, subjects did not know when the auditory stimulus would arrive.
Regarding the 6 tests without stimuli, a premise should be done. It has been noted that during GSR recording, in addition to peaks due to arousal events, also other peaks were featured in the signal. These peaks could be the consequence of non-specific skin conductance responses (NS-SCRs). The NS-SCRs can happen spontaneously at a rate of 1-3 per minute [59]. Furthermore, motion artifacts might look like SCR events. In both cases, the algorithm could incorrectly classify these peaks as SCR event.
For this reason, to test the robustness of the algorithm, 6 tests without the induction of stimuli but with the introduction of artifacts have been considered. To introduce artifacts, it has been asked to the participants to move the fingers or the electrodes.
The results are represented in the form of a Confusion Matrix (CM) which allows the visualization of the performance of an algorithm. The classification of a test dataset produces four outcomes: true positive, false positive, true negative and false negative.
The CM allows to compare the real state (actual) with the output (predicted) of the system implemented in this thesis. If a stimulus has been induced, the actual value was positive. On the contrary, the actual value was negative.
The results obtained from the tests performed in this phase of the thesis are:

- On 7 out of the 20 cases the output of the algorithm was positive, i.e. a SCR event was detected
- On 13 out of the 20 cases the output of the algorithm was negative, i.e. no SCR event was detected.

In figure 7.7 is shown the typical structure of a CM and the resulting confusion matrix after the tests performed.

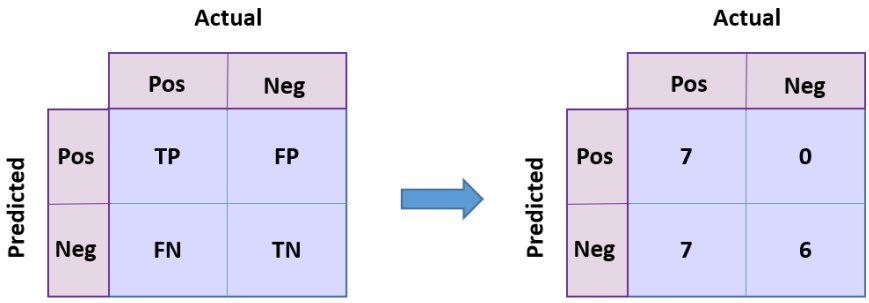

Figure 7.7. Confusion matrix of the stress detection tests.

Where:

- TP: A true positive is when the system recognises a stress event and really it happens.
- FP: A false positive is when by mistake it is classified as stress event when is not.
- TN: A true negative is when the system does not recognize a stress event and really it doesn't happen.
- FN: A false negative is when by mistake the system does not recognise a stress event and really it happens.

The CM allows to extract various measures which are useful to evaluate the performance of the system. System refers to the union of the hardware and software of the stress detection setup. In particular sensibility, specificity and accuracy are derived from the CM. These factors are calculated as follows:

$$\text{Sensitivity} = \frac{TP}{TP+FN} = \frac{7}{7+7} = 0.5 \rightarrow 50\% \tag{7.1}$$

$$\text{Specificity} = \frac{TN}{TN+FP} = \frac{6}{6+0} = 1 \rightarrow 100\% \tag{7.2}$$

$$\text{Accuracy} = \frac{TP+TN}{TN+FN+FP+TP} = \frac{13}{20} = 0.65 \rightarrow 65\% \tag{7.3}$$

The sensitivity of the system is 50% because in half of all cases the GSR signal had remained unchanged despite the induction of auditory stimuli. In the other half, a variation on the shape of the GSR signal had occurred. In particular, after the stimulus onset, a peak with the typical features of a SCR event was detected. Actually, not only one peak were present on the signal. As already explained, after a stress event, several GSR peaks can occur in direct succession instead of returning back to the baseline.
The specificity is 100% because the system had correctly identified all the actual negatives. Thus, all the 6 cases with only the introduction of artifacts were classified as cases without stress events. This means that the system has a good robustness to artifacts and NS-SCRs and none of them was mistaken for a stress event.
The accuracy, that is defined as the ratio of the correctly classified to the whole number of the dataset, is 65%. Thus, more of the half of cases were correctly classified.
The system performance is not so high because several variables come into play. First of all, in the 7 cases in which stress events did not detected, in the GSR signals no variation has been observed. Thus, it was not a problem of non-recognition of peaks related to the algorithm. Instead, it could be related to some kind of hardware problem such as the

insufficient sensitivity. Otherwise, might have happened that some of the subjects were impervious to the auditory stimulus. In fact, it should be emphasised that there is no guarantee that a subject reacts to a stimulation. It is important to note that the test results have shown that all the True Positives have been obtained from women. According to literature, women show stronger responses to a stressor than men [69].
The response to stimulus is not identical for all the subjects. It has been noted that the detected peaks were different in amplitude and duration. This aspect complicates the parameters setting, such as thresholds to detect stress events.
Another variable to take into account is the not perfect shape of the peaks. Despite filtering process, peaks can have irregularities which determine the wrong detection of the main SCR features.

7.4 Fall detection testing

The proposed fall detection algorithm (Section 6.3.5) was tested in order to evaluate its performance and effectiveness. The performance were investigated in normal activities and falling simulations. Tests were conducted by two young subjects with an average age of 25 years, average height of 170 cm and an average weight of 55 Kg. The sensor was placed on the upper trunk for all the tests.
The tasks designed in the experiment were based on the simulation of real activities. Each subject performed four kinds of falls (forward, backward, left side, right side) and different activities (sitting, walking, light running, taking objects, bending over, jumping). In total 60 tests were conducted: 40 tests with a fall event, 20 tests only with normal activities (Fig.7.8).

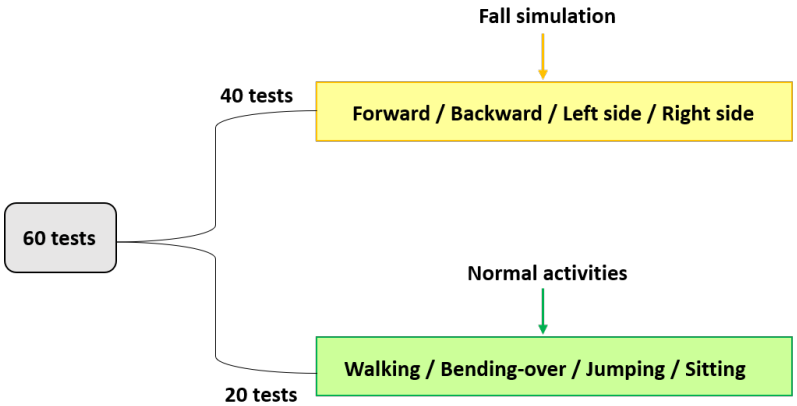

Figure 7.8. Protocol of the fall detection test.

It should be specified that during the 40 tests with simulated fall events also normal

tasks were performed by the subjects. The tasks were designed to verify whether the fall detection algorithm can evoke a fall alarm correctly. Ideally, normal activities should not be detected by the proposed algorithm as a fall event. However, in some cases, the parameters calculated may have the same features as falls and could be wrongly classified as falls. The fall simulations were not performed directly to the ground but to a mattress placed on the ground in order to alleviate the impact and avoid injuries. Fall detection systems present a binary output, either a fall event was recognized or it was not. Thus, the quality of a fall detection system cannot be evaluated through a single test, being necessary the application of statistical analysis on a series of tests. Thus, it has been used the same approach of the stress detection testing, i.e. CM (Fig.7.9). The actual value of the CM was positive if a fall event has been simulated. On the contrary was negative if only normal activities have been performed. The results obtained from the tests conducted to evaluate the robustness of the proposed algorithm are:

- On 42 out of 60 tests the output of the algorithm was positive, i.e. a fall event was detected
- On 18 out of 60 tests the output of the algorithm was negative, i.e. no fall event was detected.

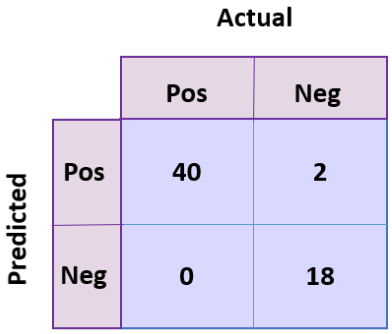

Figure 7.9. Confusion matrix of the fall detection tests.

Considering the output of the fall detection system and the user context there are four possible situations:

- TP: A true positive is when the system recognises a fall event and really it happens.
- FP: A false positive is when by mistake it is classified as fall event when is not.
- TN: A true negative is when the system does not recognize a falling and really it doesn't happen.

- FN: A false negative is when by mistake the system does not recognise a falling and really it happens.

In order to properly evaluate the fall detection system here proposed, the results are presented through sensitivity, specificity and accuracy:

$$\text{Sensitivity} = \frac{TP}{TP+FN} = \frac{40}{40+0} = 1 \rightarrow 100\% \tag{7.4}$$

$$\text{Specificity} = \frac{TN}{TN+FP} = \frac{18}{18+2} = 0.9 \rightarrow 90\% \tag{7.5}$$

$$\text{Accuracy} = \frac{TP+TN}{TN+FN+FP+TP} = \frac{58}{60} = 0.96 \rightarrow 96\% \tag{7.6}$$

The sensitivity represents the capacity to detect falls. The specificity is used to measure the algorithm's ability to mistake normal activities for falls. The accuracy represents the proportion of true results among the population. The results have demonstrated that all simulated falls were correctly identified, thus the sensibility is 100%. Furthermore, the algorithm had correctly reported the kind of fall simulated. The specificity is 90 % because two cases were incorrectly classified as falls. The activities performed by the subject were jumping, walking and sitting on a chair. The last movement was mistaken for a fall for two times. This action was classified as a fall on the right side because the subject had sat laterally (”on its side”) and it had remained in the same position for 2-3 seconds. The other false positive was due to a lie down on an armchair for 2-3s that it was exchanged for a fall backward.
The results in terms of accuracy are good, in fact its values is 96%.
At the basis of these simulations the results are satisfactory. However, further tests have to be done to evaluate if other motions during normal activities may be classified as falls. Surely, performing tests with higher accelerations will result in a variation of the accelerations measured. As a consequence the thresholds selected should be reviewed and tested again.

Chapter 8

Conclusions

The aim of this thesis is the experimentation of a wearable device including different types of sensors in order to obtain a complete health monitoring.
After a careful analysis of the state of the art, it has been noted that the market of WHD is mainly focused on the health montoring of a person in everyday life or during sport activities. Also WHD for elderly people and patients have drawn a lot of attention during the last years.
The purpose of this project is to shift the focus to other types of applications. In particular the aim was to develop a WHD prototype intended to be used by workers in hazardous environments such as Oil&Gas industries.
The risks associated to this type of work are of different nature: chemical exposure, temperature extremes, collision with moving parts, fatigue etc. Accidents happen frequently and the workers safety is not guaranteed. Several regulations exist to identify health hazards and decrease the health risks in workplace. Despite every standard and precaution, workers suffer injuries on the job every day. This evidence has brought to light the need of a WHD which can monitor continuously vital parameters of oilfield workers. The presence of allarm systems guarantee the fast response of the emergy services.
The prototyping process began with the scouting of technologies considered most suitable for this type of application. The sensors chosen to be included in the prototype allow to monitor several physiological parameters in order to have a complete picture of the health condition of a person.
All the data measured from each sensors are managed by the Atmega328 microcontroller. The firmware developed is based on the use of interrupts which are generated from events by hardware or software. The processor is sensible to an interrupt generation only in the IDLE state. A first interrupt is triggered when a command is inserted by the user. After the reception of a specific command several operations are executed. The I^2C communication between the microcontroller and the master (sensor) is enabled. The sensor configuration and activation are also performed. A second interrupt is generated when the pin of the sensor goes to low level. This triggers the data reading and trasmission processes.

The proposed firmware has been tested in order to evaluate its behaviour in all circumstances. Once confirmed the right functioning of the implemented firmware, a post-processing stage has been performed for each sensor in order to extract the parameters of interest.
The sensors included in the prototype are:

- MAX86150: it integrates both electrocardiogram and pulse oximeter sensors.
  Regarding the ECG signal, the algorithm performs basically three taks: filtering process, outliers removing and HR measuring. Filtering process includes detrending, LPF and Notch filter which reduce the typical interferences that affect the ECG signal. After that, possible outliers are removed using a statistical method based on the Z-score calculation. The output of this routine is the longer portion of signal without abnormal values. Finally, the HR parameter is measured by the recognition of R-peaks and the subsequent calculation of the distance between the peaks identified. If the HR measured is out of the range considered as normal (60-90 bmp), an allarm message is send.
  Regarding the PPG signal, the proposed algorithm extracts both SpO_2 and HR parameters. The first is useful to know the percentage of hemoglobin satured with oxygen. Also for the PPG signal, filtering and outliers removing stages are performed to improve the signal quality. After that, the main steps to measure the SpO_2 parameter are: individuation of the AC and DC components, R calculation and calibration procedure. The latter is implemented to find a relationship between R values calculated by the proposed algorithm and SpO_2 values read from a reference pulse oximeter. The method adopted in this work was to breath inside a bag with a mouthpiece. In this way the content of oxygen inside the bag is reduced incrementally. Using a regression method, a best curve was fitted to the data and the relationship between SpO_2 and R values was estimated. Actually, this procedure should be conducted using a mask gas which allows a precise control of the oxygen content inhaled by a subject. So, the calibration process should be rewieved in order to reach a more accurate control of the oxygen content inhaled. The number of partecipants should be higher in order to increase the accuracy of the calibration curve. Despite the highlighted limitations, the results obtained from the testing procedures performed on 20 subjects are good. In fact the average error is about $\pm 1\%$.
  The pulse oximeter used as reference performs also HR measurements. Thus, HR extracted from PPG and ECG during the 20 tests are compared to the HR of reference. The average error of both HR_{ecg} and HR_{ppg} is about ± 1 bpm. Future improvements, should include a comparison of HR_{ecg} with the HR measured by a professional electrocardiogram. Furthermore, other tests should be performed changing the pulse oximeter taken as reference and the position of the sensor on the body.

The MAX86150 sensor it has been chosen because allows to obtain the synchronization of the PPG and ECG signals. This feature is essential to calculate the PTT parameter. The idea was to develop a PTT-based method to estimate the blood pressure. In this thesis only the algorithm to extract PTT values is carried out. The PTT values calculated in 20 subjects are in the range of 257-276 ms. In future works a calibration procedure to find the relationship between PTT and BP should be done.

- Grove GSR: it measures the electrical variation of the skin after the onset of an emotional arousal. First of all, data read from the sensor are converted into conductance values and filtered with HPF and LPF. The result is the only SCR component. The second stage of the proposed algorithm performs the extraction of the most significant GSR features necessary to detect a ”stress event”.
  The procedure to recognize a SCR peak is based on the derivative method. In this method the sign of the first derivative is checked in order to identify the onset and off-set of a peak. Subsequently the features of interest are measured and thresholds are applied to recognize a stress event. The procedure to test the system (GSR sensor and implemented algorithm) is based on the induction of ”auditory stimuli” in order to trigger reactions. The results obtained from this experimental procedure are: 50% of sensitivity, 100% of specificity and 65% of accuracy. In half of the cases in which stimuli have been induced, the GSR signal had remained unchanged. Thus, it was not a problem of non-recognition of peaks related to the algorithm. Several variables could influence the system performance. Firstly, there is no guarantee that a subject reacts to a stimulation. Then, the false nagatives obtained might be involved in problems from the hardware point of view. Further studies should be performed changing the test protocol and also the sensor, in order to better understand the origin of the problem.

- MPU-9265 accelerometer: this sensor is included in order to monitor the motion of a person. The implemented fall detection algorithm is based on the use of thresholds. It has been chosen this approach because of its fast computational time and low energy consuption (compared to machine learning method). The algorithm processes the accelerations along three axis and calculates different parameters in order to recognize a fall. The falling event can be of different types: farward, backward, on the right or left side. Basing on which parameter exceeds the selected threshold, the algorithm distinguishes the type of fall. Testing are carried out in order to verify the robustness of the algorithm. The performance were investigated in normal activities (walking, jumping, taking objects, bend-over) and falling simulations. In total 60 tests were carried out, 40 with fall simulation and 20 with only normal movements. The results show: 100% of sensitivity, 90% of specificity, 96% of accuracy. Among all the 20 tests without fall events, only two cases were classified as false positive. The reason might be that the subjects had made a motion

similar to a fall.
Further tests have to be done to evaluate if other motions during normal activities may be classified as falls. Performing tests with higher accelerations and different motions could lead a variation of the sensor output. Consequently, the thresholds selected should be reviewed and other tests should be performed.

- MAX30205: it is used to measure the skin temperature. The temperatures values are simply averaged since the body temperature is quite constant during a brief time of observation.

A general architecture of a wearable system includes a portable unit (PU) which is responsible to collect data and trasmit them to a main device (smart-phone, PC). In this thesis a summary of the most widespread wireless standards in WHD is given. In order to complete the prototyping process of a wearable device, wireless communication system and battery should be included. With the implementation of these important features and considering the good performance obtained by the proposed system, the experimental process has solid basis to continue.

Bibliography

[1] *Anatomy of the human heart*, UOFM, 2017. Retrieved from: https://healthblog.uofmhealth.org/heart-health/anatomy-of-a-human-heart

[2] H. Lodish, A. Berk, *Molecular Cell Biology 4th ed. W.H. Freeman*, 2000.

[3] M. Joiner, *Blood Pressure Regulation: Every Adaptation is an Integration?*, Eur J Appl. Physiol., 2014.

[4] *Overview of the cardiovascular system*, Al for the common good. Retrieved from: http://data.allenai.org/tqa/overview-of-the-cardiovascular-system-L-0390/

[5] T. Nicolescu, *Data interpretation in Anesthesia*, Springer, 2017.

[6] P. Wagner, *The physiological basis of pulmonary gas exchange: implications for clinical interpretation of arterial blood gases*, Eur Respir J., 2015.

[7] A. Guyton, J. Hall, *Fisiologia Medica*, Elsevier, 2006.

[8] N. Pittman, *Regulation of tissue oxygenation*, Morgan & Claypool, 2016.

[9] *Oxygen dissociation curve*, AnaesthesiaUK, 2005. Retrieved from https://www.frca.co.uk/article.aspx?articleid=100345

[10] P.B. Thapa, *Oil Gas Offshore Safety Case (Risk Assessment)*, Memorial University.

[11] P.B. Thapa, *A Roadmap to Health Risk Assessment*, Ipieca.

[12] G. Bourbakis, *A Survey on Wearable Sensor-Based Systems for Health Monitoring and Prognosis*, IEEE, 2010.

[13] D. Duarte, *Wearable Health Devices—Vital Sign Monitoring, Systems and Technologies*, Sensors, 2018.

[14] A. Pantelopoulos, G. Bourbakis *A Survey on Wearable Sensor-Based Systems for Health Monitoring and Prognosis*, IEEE, 2010.

[15] K. Guk, G. Han, *Evolution of Wearable Devices with Real-Time Disease Monitoring for Personalized Healthcare*, nanomaterials, 2019.

[16] M. Sibanda, *Wearable devices and the global economy*,2019. Retrieved from: https://medium.com/@mandlahsibanda/wearable-devices-and-the-global-economy-9d6be53f33d1

[17] H. Banaee, M. Ahmed, *Data mining for wearable sensors in health monitoring systems: A review of recent trends and challenges*, Sensors, 2013.

[18] A. Kamisalic, I. Fister, *Sensors and Functionalities of Non-Invasive Wrist-Wearable Devices: A Review*, Sensors, 2018.

[19] D. Becker, *Fundamentals of Electrocardiography Interpretation*, Anesth Prog., 2006.

[20] N. Oliver, F. Mangas, *HealthGear: A Real-time Wearable System for Monitoring and Analyzing Physiological Signals*, Microsoft Research, 2006

[21] N. Bui, A. Nguyen, *PhO2: Smartphone based Blood Oxygen Level Measurement Systems using Near-IR and REDWave-guided Light*, SenSys, 2017.

[22] S. DeMeulenaere, *Pulse Oximetry: Uses and Limitations*, The journal for nurse practitioners, 2007.

[23] A. Hertzman, *The blood supply of various skin areas as estimated by the photoelectric plethysmograph*, Amer J Physiol,1938.

[24] F. Babiker, *Oxygen Level Measurement Techniques: Pulse Oximetry*, University of Khartoum, 2014.

[25] A. Bilgaiyan, *Optimizing performance of reflectance-based organic Photoplethysmogram (PPG) sensor*, Organic and Hybrid Sensors and Bioelectronics, 2018.

[26] O. Yossef Hay, M. Cohen, *Pulse Oximetry with Two InfraredWavelengths without Calibration in Extracted Arterial Blood*, Sensors, 2018.

[27] T. Tamura, *Wearable Photoplethysmographic Sensors—Past and Present*, Electronics, 2014.

[28] S. Sharmay, *A novel approach for IoT based wearable health monitoring and messaging system*, Journal of Ambient Intelligence and Humanized Computing, 2019.

[29] L. Antonelli, W. Ohley, *Dicrotic notch detection using wavelet transform analysis*, IEEE, 1994.

[30] T. Vandenberk, *Clinical Validation of Heart Rate Apps: Mixed-Methods Evaluation Study*, MSc, 2017.

[31] A. Choi, *Photoplethysmography sampling frequency: Pilot assessment of how low can we go to analyze pulse rate variability with reliability?*, Physiol Meas, 2017.

[32] *Calibration procedure Maximim integrated*, Retrieved from https://www.maximintegrated.com/en/design/technical-documents/app-notes/6/6845.html

[33] P. Kearney, M. Whelton, *Global burden of hypertension: Analysis of worldwide data*, Lancet, 2005.

[34] Q. Zhang, *Highly wearable cuff-less blood pressure and heart rate monitoring with single-arm electrocardiogram and photoplethysmogram signals*, BioMed Eng On-Line, 2017.

[35] Y. Choi, *Noninvasive cuffless blood pressure estimation using pulse transit time and Hilbert–Huang transform*, Computer and electrical engineering, 2013.

[36] S. Deb, *Cuff-less Estimation of Blood Pressure using Pulse Transit Time and Pre-ejection Period*, ITCSE, 2007.

[37] G. Fortino,R. Giannantonio, *Enabling effective programming and flexible management of efficient body sensor network applications*, IEEE, 2013.

[38] L. Peter, N. Noury, *A review of methods for non-invasive and continuous blood pressure monitoring: Pulse transit time method is promising?*, IRBM, 2014.

[39] LA. Geddes, P. Me, *Handbook of blood pressure measurement*, NJ: Humana Press Clifton, 1991.

[40] H. Xiang, Y. Liu, *Calibration of pulse wave transit time method in blood pressure measurement based on the korotkoff sound delay time.*, IUPESM,2013.

[41] J. Proenc, J. Muehlsteff, *Is pulse transit time a good indicator of blood pressure changes during short physical exercise in a young population?*, EMBC, 2010.

[42] M. Wong, Y. Zhang, *An evaluation of the cuffless blood pressure estimation based on pulse transit time technique: a half year study*, Cardiovasc Eng., 2009.

[43] C. Holz, J. Edward, *Glabella: Continuously Sensing Blood Pressure Behavior using an Unobtrusive Wearable Device*, ACM, 2017.

[44] M. Johnson, R. Jegan, *Performance Measures on Blood Pressure and Heart Rate Measurement from PPG Signal for Biomedical Applications, Melvin Johnson*, ICIEEIMT, 2017.

[45] A. Pielmus, *Novel computation of pulse transit time from multi-channel PPG signals by wavelet transform*, Material science, 2017.

[46] T. Tamura, *Current Developments in Wearable Thermometers*, Adv Biomed Eng., 2018.

[47] G. Liua, C. Hob*A wearable conductivity sensor for wireless real-time sweat monitoring*, Sensors and Actuators, 2016.

[48] A. Koh, D. Kang *A soft, wearable microfluidic device for the capture, storage, and colorimetric sensing of sweat*, Sci.Transl, 2016.

[49] W. Wolfenserger, *Relative effectiveness of Galvanic Skin Response Latency, Amplitude and Duration Scores as Measures of Arousal and Habituation in Normal and Retarded Adults*, Psychophysiology, 1967.

[50] K. Kytiakou, *Detecting Moments of Stress from Measurements of Wearable Physiological Sensors*, Sensors, 2019.

[51] B. Farnsworth, *Skin Conductance Response – What it is and How to Measure it*, Imotions, 2019. Available at: https://imotions.com/blog/skin-conductance-response/

[52] P. Gouverneur, *Classification of Physiological Data for Emotion Recognition*, ICAISC, 2017.

[53] W. Boucsein, *Electrodermal activity*, Springer, 2012.

[54] Y. Fang, *Accelerometer-based fall-portent detection algorithm for construction tiling operation*, Elsevier, 2017.

[55] Y. Fang, *A framework for real-time pro-active safety assistance for mobile crane lifting operations*, Autom. Constr., 2016.

[56] S. Khan, *Internet of things based multi-sensor patient fall detection system*, Healthc.Technol., 2019.

[57] *Equivital sensor belt*. Available at: https://www.adinstruments.com/products/equivital-sensor-belt

[58] *Il monitor indossabile QardioCore per l'ECG per iPhone*. Available at: https://www.getqardio.com/it/qardiocore-wearable-ecg-ekg-monitor-iphone

[59] M.J. Banet, M.J. Thompson, *Chest strap for measuring vital signs*, United Stated Patent US 2007/0142715, Triage Wireless, 2007.

[60] *The Biobeat wrist watch*. Available at: https://www.biobeat.cloud/products/

[61] *Protocentral MAX86150 PPG and ECG breakout with QWIIC*. Available at: https://www.protocentral.com/home/1338-protocentral-max86150-ppg-and-ecg-breakout-with-qwiic.html

[62] *I2C protocol explanation*. Available at: http://fastbitlab.com/stm32-i2c-lecture-3-i2c-protocol-explanation/

[63] *Grove-Galvanic skin response sensor*. Available at: http://wiki.seeedstudio.com/Grove-GSR-Sensor

[64] M.L. Mahon, W.G. Iacono, *Another look at the relationship of electrodermal activity to electrode contact area*, Psychophysiology, 1987.

[65] W. Boucsein, *Electrodermal activity*, Springer Science & Business Media, 2012.

[66] J. Schumm, *Effect of movements on the electrodermal response after a startle event*, Methods Inf. Med., 2008.

[67] S. Rajala, T. Ahmaniemi, *Pulse arrival time (PAT) measurement based on arm ECG and finger PPG signals – Comparison of PPG feature detection methods for PAT calculation*, IEEE, 2017.

[68] S. Majumder, T. Mondal, *Wearable sensors for remote health monitoring*, Sensors, 2017.

[69] F. Wilhelm, J. Rattel, *Attend or defend? Sex differences in behavioral, autonomic, and respiratory response patterns to emotion–eliciting films*, Biol. Psychol., 2017.